AD-A091 173 PENNSYLVANIA STATE UNIV UNIVERSITY PARK APPLIED RESE--ETC F/G 20/4
UNSTEADY PRESSURE DISTRIBUTIONS ON AIRFOILS IN CASCADE.(U)
APR 80 I SHEN N00024-79-C-6043
UNCLASSIFIED ARL/PSU/TM-80-45 NL

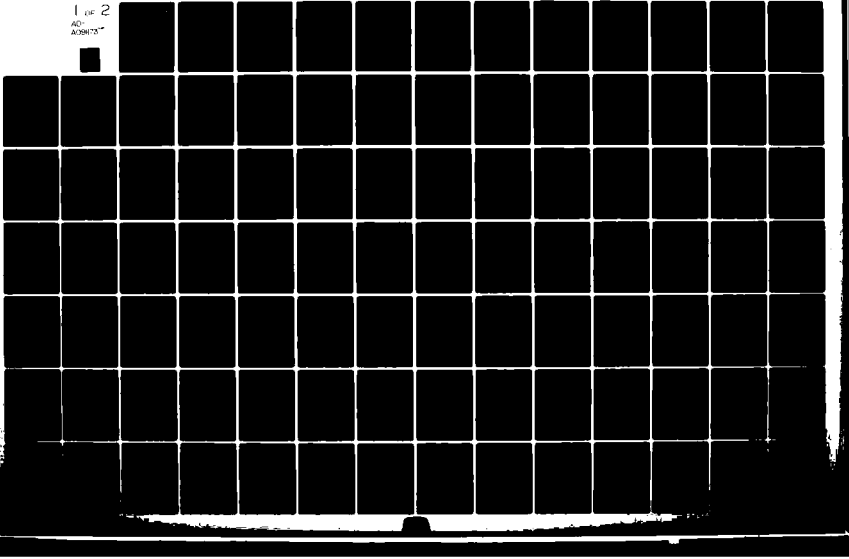

UNSTEADY PRESSURE DISTRIBUTIONS ON AIRFOILS IN CASCADE

I-Chung Shen

Technical Memorandum
File No. TM 80-45
1 April 1980
Contract No. N00024-79-C-6043

Copy No. 7

The Pennsylvania State University
APPLIED RESEARCH LABORATORY
Post Office Box 30
State College, PA 16801

NAVY DEPARTMENT

NAVAL SEA SYSTEMS COMMAND

UNCLASSIFIED

SECURITY CLASSIFICATION OF THIS PAGE (When Data Entered)

REPORT DOCUMENTATION PAGE		READ INSTRUCTIONS BEFORE COMPLETING FORM
1. REPORT NUMBER TM-80-45	2. GOVT ACCESSION NO. AD-A091173	3. RECIPIENT'S CATALOG NUMBER
4. TITLE (and Subtitle) UNSTEADY PRESSURE DISTRIBUTIONS ON AIRFOILS IN CASCADE		5. TYPE OF REPORT & PERIOD COVERED Technical Memorandum 6. PERFORMING ORG. REPORT NUMBER
7. AUTHOR(s) I-Chung Shen		8. CONTRACT OR GRANT NUMBER(s) N00024-79-C-6043
9. PERFORMING ORGANIZATION NAME AND ADDRESS Applied Research Laboratory Post Office Box 30 State College, PA 16801		10. PROGRAM ELEMENT, PROJECT, TASK AREA & WORK UNIT NUMBERS
11. CONTROLLING OFFICE NAME AND ADDRESS Naval Sea Systems Command Department of the Navy Washington, DC 20362		12. REPORT DATE 1 April 1980 13. NUMBER OF PAGES 148
14. MONITORING AGENCY NAME & ADDRESS(if different from Controlling Office)		15. SECURITY CLASS. (of this report) UNCLASSIFIED 15a. DECLASSIFICATION/DOWNGRADING SCHEDULE

16. DISTRIBUTION STATEMENT (of this Report)

Approved for Public Release. Distribution umlimited.
Per NAVSEA - April 21, 1980.

17. DISTRIBUTION STATEMENT (of the abstract entered in Block 20, if different from Report)

18. SUPPLEMENTARY NOTES

19. KEY WORDS (Continue on reverse side if necessary and identify by block number)

airfoils, blades, cascade, unsteady, pressure, distribution

20. ABSTRACT (Continue on reverse side if necessary and identify by block number)

The results of a study of unsteady pressure distributions in a two-dimensional cascade of blades caused by spatial inflow velocity variations are presented. An existing incompressible, inviscid theory which employs a simplified vortex model in conjunction with the assumptions of thin airfoil theory has been used by Henderson (16) and Bruce (17) to derive expressions for the unsteady response, which includes the cascade unsteady lift and pitching moment. An alternative way to obtain these unsteady response parameters is to establish the expression for the unsteady pressure distribution. The unsteady lift and pitching moment →

DD FORM 1 JAN 73 1473 EDITION OF 1 NOV 65 IS OBSOLETE

UNCLASSIFIED

SECURITY CLASSIFICATION OF THIS PAGE (When Data Entered)

are calculated by direct numerical integration over the unsteady pressure difference across the arifoil chord. Comparison of the computed theoretical results using these two approaches shows satisfactory agreement except when the wavelength of the velocity variations approaches the cascade blade spacing. Good agreement is also observed between the existing measured and predicted data. The effects of design parameters of a cascade, such as space-chord ratio, maximum blade camber, and mean incidence angle, on the unsteady response are presented and discussed.

ABSTRACT

The results of a study of unsteady pressure distributions in a two-dimensional cascade of blades caused by spatial inflow velocity variations are presented. An existing incompressible, inviscid theory which employs a simplified vortex model in conjunction with the assumptions of thin airfoil theory has been used by Henderson (16) and Bruce (17) to derive expressions for the unsteady response, which includes the cascade unsteady lift and pitching moment. An alternative way to obtain these unsteady response parameters is to establish the expression for the unsteady pressure distribution. The unsteady lift and pitching moment are calculated by direct numerical integration over the unsteady pressure difference across the airfoil chord. Comparison of the computed theoretical results using these two approaches shows satisfactory agreement except when the wavelength of the velocity variations approaches the cascade blade spacing. Good agreement is also observed between the existing measured and predicted data. The effects of design parameters of a cascade, such as space-chord ratio, maximum blade camber, and mean incidence angle, on the unsteady response are presented and discussed.

TABLE OF CONTENTS

LIST OF FIGURES

LIST OF TABLES

LIST OF SYMBOLS

Symbol	Definition
a	cascade parameter, $a = \frac{ce^{-i\xi}}{2s}$, constant
b	cascade parameter, $b = \frac{ce^{i\xi}}{2s}$, constant; width of the wake
B_1	cascade wake integral, $B_1 = \int_1^\infty \frac{e^{-i\omega\lambda^+}}{\sqrt{g_\lambda^2 - 1}} d\lambda^+$
B_2	cascade wake integral, $B_2 = \int_1^\infty \frac{e^{-i\omega\lambda^+}}{\sqrt{h_\lambda^2 - 1}} d\lambda^+$
c	blade chord
$\Delta\tilde{C}_p$	coefficient of unsteady pressure difference, $\Delta\tilde{C}_p = \frac{\overline{\Delta p}(\sigma^+)}{\rho W_m \hat{w}_d}$
C_1	cascade function, $C_1 = \sqrt{\frac{g_c + 1}{g_c - 1}}$
C_2	cascade function, $C_2 = \sqrt{\frac{h_c + 1}{h_c - 1}}$
$C(\omega)$	Theodorsen function

Symbol	Definition
$\tilde{C}_L$	unsteady lift coefficient, $\dfrac{\tilde{L}}{\pi c \rho W_m \hat{w}_d e^{i\nu t}}$
$\tilde{C}_m$	unsteady pitching moment coefficient, $\dfrac{\tilde{M}}{\pi c^2 \rho W_m \hat{w}_d e^{i\nu t}}$
D_1	cascade wake integral, $D_1 = \int_1^\infty \left(\sqrt{\dfrac{g_\lambda + 1}{g_\lambda - 1}} - 1 \right) e^{-i\omega\lambda^+} d\lambda^+$
D_2	cascade wake integral, $D_2 = \int_1^\infty \left(\sqrt{\dfrac{h_\lambda + 1}{h_\lambda - 1}} - 1 \right) e^{-i\omega\lambda^+} d\lambda^+$
E_1	cascade function, $E_1 = \dfrac{1}{g_c - \sigma^+} \sqrt{\dfrac{g_c + 1}{g_c - 1}}$
E_2	cascade function, $E_2 = \dfrac{1}{h_c - \sigma^+} \sqrt{\dfrac{h_c + 1}{h_c - 1}}$
f, g	functions in Söhngen inversion formula
g_c	cascade vortex function, $g_c = x^+_c + \dfrac{n}{ia}$
g_λ	cascade wake function, $g_\lambda = \lambda^+ + \dfrac{n}{ia}$

Symbol	Definition
g_1	cascade wake function evaluated at $\lambda^+ = 1$, $g_1 = 1 + \frac{n}{ia}$
$G(\omega,s/c,\xi)$	cascade lift function in Henderson's analysis
h	height of the wake
h_c	cascade vortex function, $h_c = x^+_c - \frac{n}{ia}$
h_λ	cascade wake function, $h_\lambda = \lambda^+ - \frac{n}{ib}$
h_1	cascade wake function evaluated at $\lambda^+ = 1$, $h_1 = 1 - \frac{n}{ib}$
$H_n^{(2)}(\omega)$	Hankel function of the second kind of order n
$J_n(\lambda)$	Bessel function of the first kind of order n
ℓ	wavelength of disturbance
ℓ_c	wavelength along blade chord
L	lift force
M	pitching moment about the midchord, positive for leading-edge up rotation

Symbol	Definition
M_c	cascade influence function, $$M_c = \left[\sum_{-\infty}^{-1} + \sum_{1}^{\infty}\right] e^{in\tau}(C_1 + C_2 - 2) - i\omega e^{i\omega} \left[\sum_{-\infty}^{-1} + \sum_{1}^{\infty}\right] e^{in\tau}(D_1 + D_2)$$
n	cascade blade number n = 0 for reference blade
p	pressure
Δp	pressure difference, $\Delta_p = p_{(-)} - p_{(+)}$
q	net chordwise velocity, $q = W_m + u_d$
r	radial distance, dummy variable
s	blade-to-blade spacing in cascade
$S(\omega)$	Sears' function; the airfoil response to a convected transverse disturbance
$S(\omega,\lambda)$	Kemp's function; the airfoil response to a nonconvected transverse disturbance
t	time
δt	infinitesimal increment of time

Symbol	Definition
$T(\omega)$	Horlock's function
u	chordwise velocity component
U	rotor blade rotational velocity
v	transverse velocity component
V	stator exit or circumferential-mean rotor inlet absolute velocity
w	magnitude of disturbance velocity or velocity deficit
W	blade relative velocity
W_1	circumferential-mean rotor inlet relative velocity
W_2	circumferential-mean rotor exit relative velocity
x	chordwise coordinate on reference blade
y	transverse coordinate on reference blade
y_m	maximum blade camber
$Z(\lambda,\sigma^+)$	function in the equation of unsteady pressure distribution for an isolated airfoil, $$Z(\lambda,\sigma^+) = \sum_{n=1}^{\infty} i^n J_n(\lambda) \sin\left(n(\pi - \cos^{-1}\sigma^+)\right)$$

Symbol	Definition
α	blade inlet incidence angle
β	relative flow angle measured from axial direction
γ	vorticity
Γ	circulation
Δ	circulation coefficient, $\Delta = \frac{\bar{\Gamma} e^{i\omega}}{c}$
ε	disturbance flow angle measured from the y-direction
$\theta(\chi^+_r)$	cascade function, $\theta(\chi^+_r) = \frac{2s}{ic} e^{in\tau} \left(\frac{1}{g_r - x^+} - \frac{1}{h_r - x^+} \right)$
λ	generalized reduced frequency or dummy variable
$\Lambda(\sigma,r)$	function, $\Lambda(\sigma,r) = 2 \tan^{-1} \left(\sqrt{\frac{1 - \sigma}{1 + \sigma} \frac{r + 1}{r + 1}} \right) - \pi$
μ	generalized disturbance frequency
ν	frequency
ξ	stagger angle of cascade measured from axial direction
ρ	mass density of fluid

Symbol	Definition
σ	arbitrary point on reference blade
τ	intra-blade phase angle, $\tau = \frac{2\pi s}{\ell}$
ϕ	phase angle or flow coefficient
Φ	angle defined by $\Phi = \pi - \beta - \xi$
$\Phi(\chi^+_r)$	cascade function, $\Phi(\chi^+_r) = \frac{2s}{ic} e^{in\tau} \left(\frac{1}{g_r - x^+} + \frac{1}{h_r - x^+} \right)$
ω	reduced frequency
$\Omega(\sigma^+, r)$	function, $\Omega(\sigma^+, r) = \frac{1}{2} \ln \left(\frac{1 - \sigma r + \sqrt{1 - r^2}\sqrt{1 - \sigma^2}}{1 - \sigma r - \sqrt{1 - r^2}\sqrt{1 - \sigma^2}} \right)$

Subscript

c	blade quarter-chord point
C.P.	center of pressure
d	disturbance
I	imaginary part of a complex quantity
k	related to the k^{th} Fourier component

Subscript	Definition
L	related to lift
m	circumferential mean value or maximum
M	related to moment
n	blade number in cascade, n = 0, ±1, ±2, ±3
o	quantity related to reference blade
p	point on the reference blade
r	dummy variable represents c or λ
R	real part of a complex quantity
s	steady
u	unsteady
w	wake
λ	arbitrary point in the wake
(+)	pressure side
(-)	suction side

Superscript	
+	quantities expressed in nondimensional coordinate system
-	amplitude of a hramonic function in time

Superscript	Definition
^	amplitude of a harmonic function of position and time
~	unsteady

ACKNOWLEDGEMENTS

The author would like to express his sincere appreciation to his research advisor, Dr. Robert E. Henderson, for both his guidance and his encouragement throughout the project. The assistance given by Dr. Frank S. Archibald and Mr. Robert F. Davis is also appreciated.

This research was supported by the Applied Research Laboratory at The Pennsylvania State University under contract with the Naval Sea Systems Command, Code 63R.

CHAPTER I

INTRODUCTION

1.1 State of the Art

The turbomachine is a significant component in today's technological society. For example, this device is used almost universally in power generation and in aircraft and marine propulsion.

In the real world, the flow in a turbomachine is time dependent; however, most designs and previous research in turbomachines have been conducted on a steady or time-mean basis. Dean (1) has shown that the flow relative to the casing of a turbomachine must be time dependent or unsteady if energy is to be transferred between the fluid and the rotating blades. Also, both spatial and temporal variations can occur in its inflow velocity as caused by the wakes of upstream blade rows, inlet flow distortions, wall boundary layers, etc. The motion of the rotating blades through these spatial and temporal velocity variations results in unsteady pressures with forces and moments being generated on the blades. The stator blades, which interact with the moving wakes of upstream rotor blades, also encounter an unsteady flow. The existence of these unsteady pressures leads to three undesired effects: blade vibration (2), radiated noise (3), and performance degradation (4).

These undesirable effects are a serious problem. The employment of large numbers of turbomachines with increasing power transmissions has resulted in intolerable noise and vibration levels. Considerable effort has been and continues to be devoted to the understanding of such flows

and to provide methods with which the turbomachinery designer can predict the unsteady response of the blades as a function of the design parameters. One aspect of this effort is the study of unsteady response of a turbomachine to spatial velocity variations. Various mathematical models are employed to obtain the theoretical solutions. These models usually replace the airfoils by a distribution of vorticity on the blades and in their wakes. The strength of the vorticity and the resulting induced velocities are then determined to satisfy the boundary conditions on the surface of the airfoils. This specifies the unsteady pressure distribution and, hence, the unsteady lift and moment. Similar solutions are also obtained by representation of blades by distribution of potential flow sources and sinks and doublets (5, 6). The earliest unsteady analyses are performed for an isolated airfoil. Von Kármán and Sears (7) and Sears (8) determine the unsteady lift of an isolated flat plate airfoil subjected to a small sinusoidal velocity disturbance normal to the chord. The solution of this problem results in the familiar Sears response function. Kemp and Sears (9, 10) extend the original Sears analysis for an isolated airfoil to calculate the unsteady lift of the rotors and stators in turbomachines. This method considers only the unsteady interaction of the other airfoils in the cascade. The unsteady interaction and, hence, the effect of cascade spacing are neglected by Kemp and Sears.

Although the response of an airfoil to a chordwise disturbance is usually of second order compared to that of a normal disturbance, there are situations in which the configuration of a turbomachine blade row is such that the response of the airfoil to the chordwise disturbance is nearly equivalent to that of the normal disturbance. Horlock (11)

reported a solution for the unsteady lift and moment of an isolated flat plate airfoil subjected to a disturbance having components both parallel and normal to the chord. The solution results in the Horlock response function and has a form similar to that of the Sears function for a normal disturbance.

Holmes (12) and Naumann and Yeh (13) extend the previously developed isolated airfoil analyses to consider the effects of blade camber. Nauman and Yeh present a series of design charts which show the variation of unsteady lift as a function of blade camber, stagger angle, and reduced frequency and assume the turbomachine blade can be represented by a single airfoil. Holmes further summarizes these results and extends them by solving the generalized disturbance case for the pressure distribution and the pitching moment.

These analyses are of questionable validity for representation of a turbomachine since they do not account for the effect on a given blade of fluctuations occurring on other blades of the same blade row. This cascade effect has an influence on the unsteady force acting on a blade row, particularly at low values of space-chord ratio, that is, high solidity, and low values of reduced frequency. The analysis of a cascade of airfoils has been performed in a manner similar to that of an isolated airfoil, but it includes the effects of adjacent blades and their wakes. Several theoretical analyses, Whitehead (14), Schorr and Reddy (15), Henderson and Daneshyar (16), and Smith (17), have been formulated to predict the unsteady response of a thin, two-dimensional cascade of airfoils operated in an inviscid, incompressible, spatially varying flow.

The analyses of References (14) and (16) use different representations of the blade in the cascade. In Reference (14), a finite number of vortices, five to eight, are placed on each airfoil, whereas in Reference (16) a continuous distribution of vorticity is used on the reference airfoil, that is, the one on which the unsteady lift is calculated, and a single vortex is used on the adjacent airfoils. In both analyses, a continuous distribution of wake vorticity is used for each airfoil. The results of References (14) and (17) produce identical results but assume the cascade to be composed of flat plate airfoils; that is, the effects of camber and angle of incidence are neglected. The analysis presented in Reference (16) can account for the effects of camber and angle of incidence.

Henderson's analysis (18) predicts a resonance effect, that is, a sharp change in the unsteady lift when the disturbance wavelength equals the blade spacing. Bruce (19) further extends this theory to give an expression for unsteady pitching moment.

In recent years, with the development of instrumentation to conduct dynamic measurements, some experimental results have become available for isolated airfoils to check the validity of the predicted results. However, very few direct experimental results, such as unsteady pressure distribution or lift, have been available to check the existing theoretical analyses of a cascade of airfoils. The lack of experimental data is attributed to the complexity in producing a suitable flow and the measurement of unsteady parameters.

An experimental result has recently been published by Gallus et al. (20) for the measurements of fluctuating pressures on the midspan profile surfaces of a compressor blade row. The shapes of the wakes or

inflow distortions produced by upstream stage are also measured. Another typical experiment has been conducted by Satyanarayana (30). An instrumented two-dimensional cascade was mounted in a gust tunnel which produced a sinusoidal flow onto the blades. This enables the fluctuating lift to be measured. The results of these two experimental studies can be an indirect check of the validity of the present analysis.

1.2 Relevance of This Study

Using the theory developed by Henderson (18), the present study undertakes to solve the problem of unsteady response of a turbomachine to spatial velocity variations. In Henderson's analysis, the unsteady response of a cascade of airfoils is described in terms of unsteady lift. Mathematically, this is accomplished by evaluating the integrals that result from the integration of the unsteady pressures over the entire airfoil chord. Similar procedures have been used by Bruce (19) to determine the unsteady moment. The expression for unsteady pressure distribution, however, is left in implicit form in both of these studies.

The unsteady lift and pitching moment occurring on a turbomachine blade row can be determined if the unsteady pressure differences across the airfoil chord are known. Development of an expression for unsteady pressure distributions is needed and is reflected in the recent comment by Sisto (2):

> "What is still needed, at the present time, is a general treatment that handles both chordwise and transverse gust components and outputs the unsteady pressure distribution

from which the lift and moment may subsequently be obtained by quadratures."

Such pressure distributions are also required for the prediction of turbomachine radiated noise.

1.3 Objective of This Study

The objective of the present study is to develop an explicit solution for pressure fluctuations on the surface of a turbomachinery blade row operating in a spatially varying disturbance flow field, for example, one which is caused by an upstream stationary blade row or inlet distortions. This is to be accomplished by considering an inviscid, incompressible flow through a two-dimensional cascade with motion relative to the disturbance flow. A thin airfoil model which neglects the influence of airfoil thickness is used, but the effects of airfoil camber and angle of incidence are included.

The results calculated from the corresponding expressions in References (18) and (19) for unsteady lift and moment are compared with those obtained from the present study. Comparisons with other available experimental results are made and discussed.

CHAPTER II

THEORETICAL ANALYSIS OF UNSTEADY PRESSURE DISTRIBUTIONS FOR A CASCADE OF AIRFOILS

In order to develop an expression for the unsteady pressure distribution and, hence, the unsteady response of a cascade to an inflow disturbance, including unsteady lift and moment, a thin airfoil theory is employed. Since a cascade of airfoils is considered, the contribution of the cascade effect or blade-to-blade interaction must be included along with the effect of camber and angle of incidence.

As stated in Section 1.2, the method of analysis and the mathematical model employed in this study have been used to predict the unsteady lift and moment (18, 19). The contributions of the present study will be the development of the expression for unsteady pressure distributions and the subsequent calculations. However, the complete analysis in obtaining this solution is presented for the sake of completeness.

2.1 Flow Model and Method of Analysis

As stated in Chapter I, the problem to be studied is the unsteady pressure distribution on the blades of a cascade when the blade row experiences a spatial velocity variation in the inflow, for example, the nonuniform flow caused by the wakes of upstream blade row. The flow model and method that will be employed in this analysis is a Singularity Vortex Method which has been broadly used in the thin airfoil theory.

It is necessary that the disturbance flow field be considered before the problem can be analyzed. The flow field is assumed to be two-dimensional, inviscid, and incompressible and represents a development of a cylindrical surface, as shown in Figure 1. This general disturbance flow field represents the passage of a rotor through the wakes of an upstream stator blade with a swirling mean flow. These wakes have a maximum velocity deficit of $2w_d$ and are transported over the rotor by the velocity W_m, the average time-mean velocity between the inlet and exit of the rotor, relative to the rotor blades with the wake present. The velocity deficit w_d represents the perturbation about the mean velocity W_m. The description of the wake deficits shown in Figure 1 can be accomplished using Fourier series representation. From this analysis, the contribution of each harmonic of the velocity variation and subsequently its contribution to the unsteady response of the blade can be determined.

The disturbance flow shown in Figure 2 represents a particular case in which the rotor inlet absolute velocity is axial and varies sinusoidally with wavelength ℓ in the direction which the blade row moves. This flow model represents the fundamental harmonic of the Fourier representation of wakes from upstream stationary blades and can therefore be extended to the general disturbance flow field. The disturbance flow is transported through the machine by the circumferential-mean axial velocity C_x and is fixed with respect to solid boundaries. The blade row moves with a constant rotational velocity U. The circumferential-mean velocities relative to the blades at the inlet and exit are shown in Figure 2 as W_1 and W_2 with W_m being their mean value. The geometry of the cascade is described by the

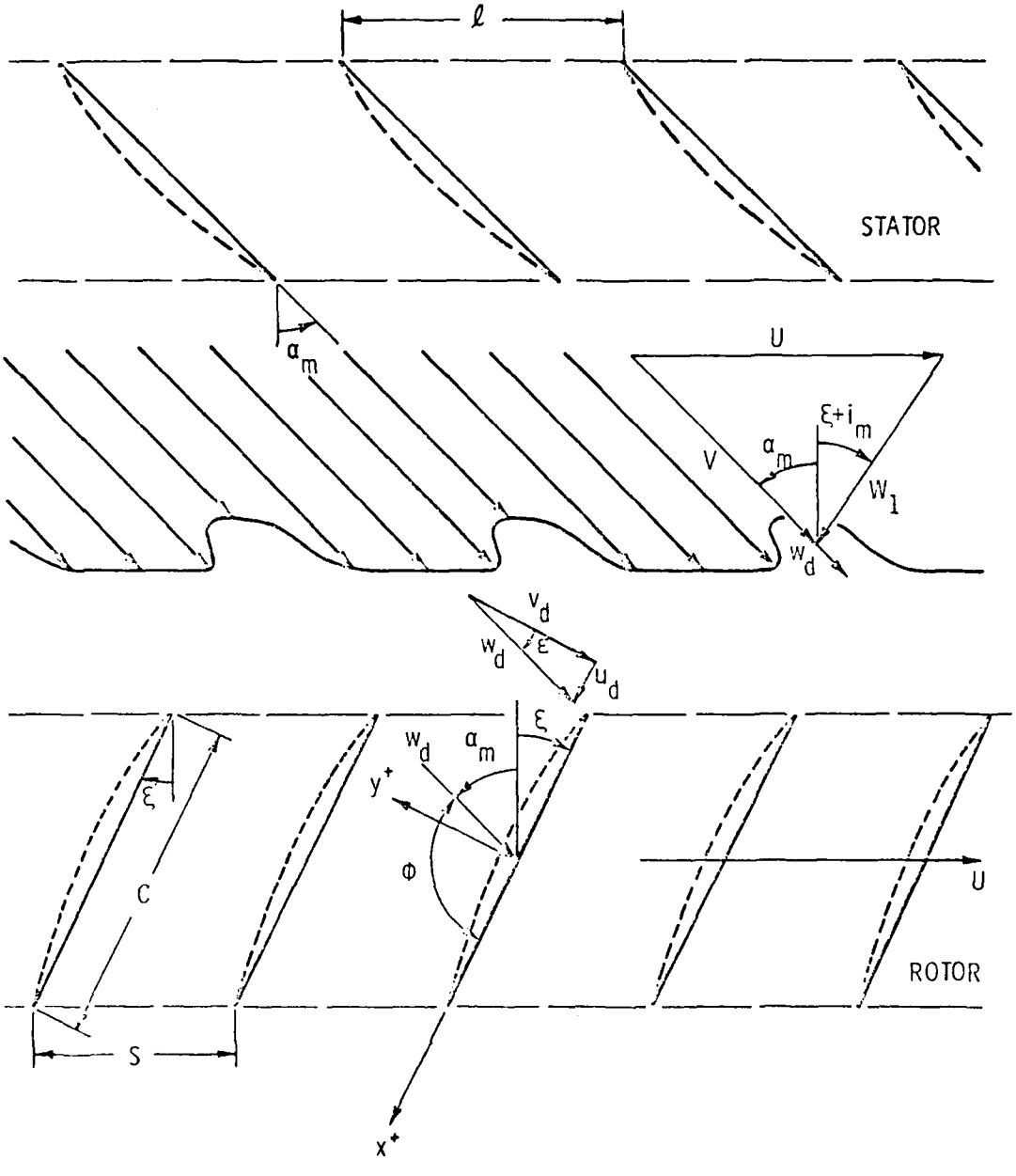

Figure 1. General Disturbance Flow Field.

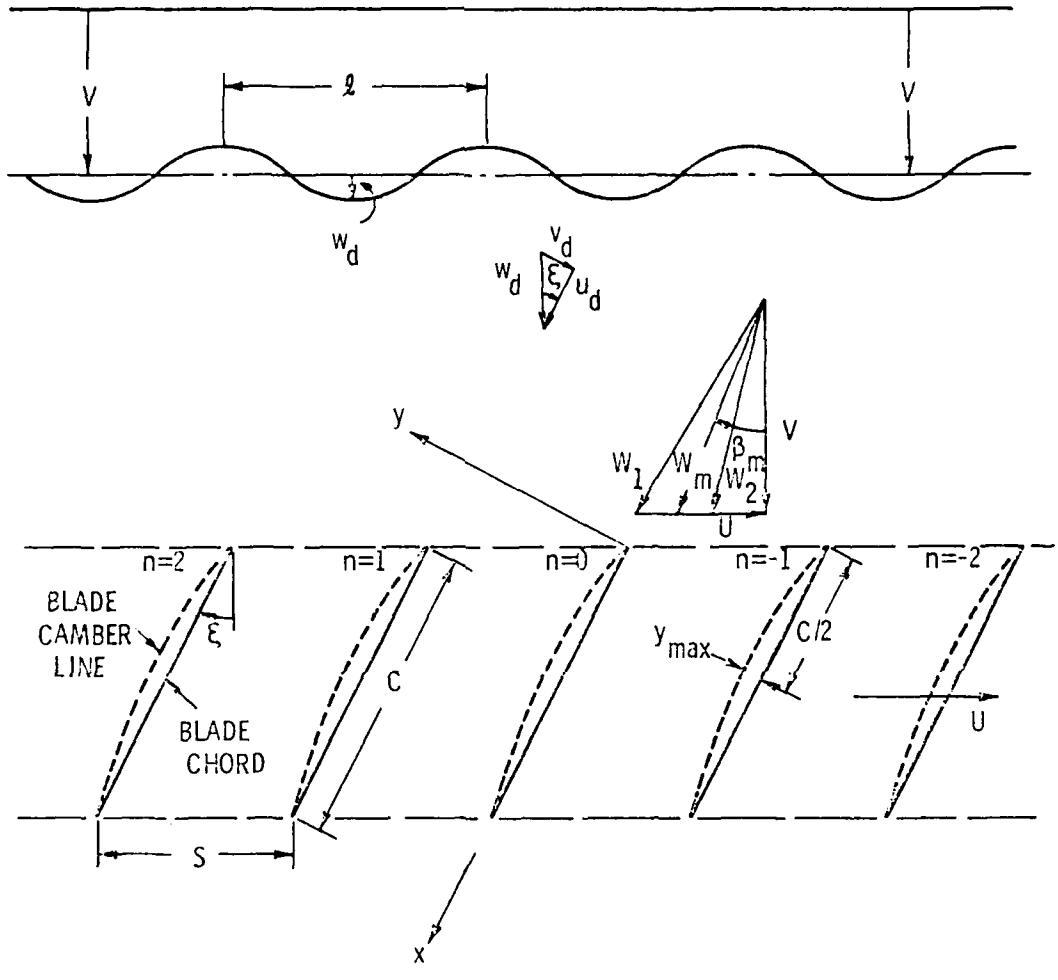

Figure 2. Cascade of Airfoils Moving Through a Disturbance Flow Field.

parameters commonly used in turbomachine design, the stagger angle ξ, spacing or pitch s, chord length c, and maximum camber y_m. The characteristics of the disturbance flow are described by the reduced frequency ω and λ which will be discussed in Section 2.2.

By considering the velocity relative to the blades, either a stator or a rotor can be analyzed. However, the presented case will be for a rotor. The relative motion of the disturbance or velocity variation and the cascade consequently causes the unsteady response on the blade. In this analysis, the disturbance is considered as a perturbation around the time-mean or steady velocity. By virtue of this assumption, the analysis becomes linear and therefore makes the solution linearized and suitable for summation.

According to the Singularity Vortex Method in the thin airfoil theory, each blade in a cascade is represented by a vortex sheet, that is, by a series of vortex lines with a continuous distribution of vorticity. Because of the nonuniformity of the inflow and the effects of neighboring blades, each blade leaves a wake composed of continuously distributed vortex sheets extending from its trailing edge to far downstream. However, the present analysis employs a simplified model which is shown in Figure 3. The vorticity on the reference blade on which the unsteady pressure distribution is to be calculated is considered to be continuously distributed along its chord, whereas that of the adjacent [illegible] at their quarter chord points. The shed or [illegible] considered as a continuous sheet [illegible] blades to [illegible].

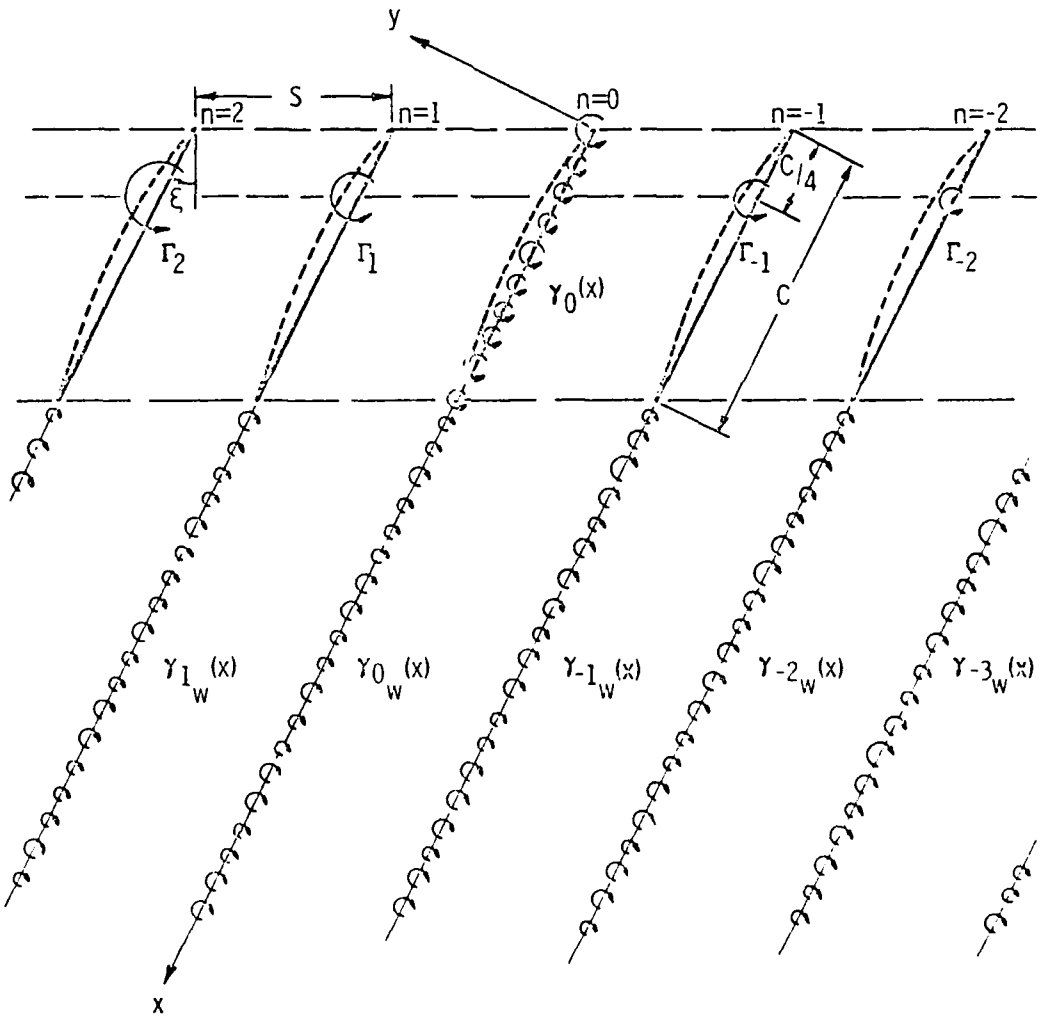

Figure 3. Vortex Representation of a Cascade.

This flow representation greatly simplifies the subsequent mathematics and is justified on the basis of results obtained by Tanabe and Horlock (21), who use a similar model for the steady flow case.

To obtain a solution to the problem studied, the following assumptions concerning the flow field are made. These are similar to those often employed in isolated airfoil theory for the unsteady flow problem. They are:

(1) The flow is two-dimensional, inviscid, and incompressible.

(2) The blades are represented as thin airfoils by placing bound vortex sheets along their camber lines. The lift is small so that the boundary condition can be satisfied on the chord line rather than on the camber line of the airfoils.

(3) The perturbation disturbance velocities u_d and v_d parallel and normal to the chord, respectively, are small as compared with mean velocity W_m past the airfoils.

(4) The circulation of the whole flow system remains zero at any instant of time. This is a statement of Helmholtz's Vortex Theorem which says that a fluid which is initially irrotational will remain irrotational unless acted upon by an external rotational force.

(5) The free or wake vorticity which is shed from the trailing edge of airfoils travels with the mean relative velocity W_m of the flow and forms a vortex sheet along the chord direction.

(6) All quantities representing the unsteadiness vary as harmonic functions of time.

While these are very strict assumptions when compared to the actual case, it is possible to use the results of the analysis to establish trends which demonstrate the variation of the unsteady response with various geometrical parameters. Thus, the present analysis can be employed as a design tool.

The mathematical analysis then follows the procedure utilized by Blisplinghoff et al. (22) for the case of isolated airfoil, but it is more complicated because of the presence of the additional blades in the cascade.

2.2 Representative Description of the Disturbance Flow Field

To obtain a solution for unsteady pressure distribution on a cascade, it is necessary that relations between the disturbance velocities and inlet flow, the mathematical expressions for flow disturbances and definitions of the frequency parameters, be established.

From the geometrical considerations in the general disturbance flow field, Figure 1, the resulting components of the disturbance velocity w_d normal and parallel to the chord can then be expressed as

$$v_d = -w_d \cos \varepsilon$$

and

$$u_d = w_d \sin \varepsilon \quad .$$

The negative sign arises due to the selected coordinates. In addition,

$$\varepsilon = \phi - 90^\circ \quad ,$$

where $\gamma = 180^{o} - \beta - \xi$, β being the exit flow angle from the stator row and ξ being the stagger angle of the rotor blade row. Thus,

$$v_d = -w_d \sin \gamma$$

and

$$u_d = -w_d \cos \gamma \quad . \tag{1}$$

If $\beta = 0$,

$$v_d = -w_d \sin \xi$$

and

$$u_d = w_d \cos \xi \quad . \tag{2}$$

The consideration of the disturbance velocity w_d as components parallel and normal to the chord facilitates the solution of this problem, and it is possible to add the respective solutions since the model employed is linear.

Following assumption (6) in the previous section, which states that fluctuating quantities are assumed harmonic with time, it is practical to employ a complex representation of these quantities. The disturbance velocity relative to the moving rotor blade is then harmonic with respect to time t and can be written as $w_d = w_d e^{i\nu t}$. The normal component of the disturbance velocity along the blade $v_d(x^+,t)$ occurs with the same frequency ν as w_d and can be written as

$$v_d(x^+,t) = v_d(x^+)e^{i\nu t} \quad . \tag{3}$$

The variation of disturbance velocity along the chord, the x^+ direction ($-1 \leq x^+ \leq 1$), can be expressed as

$$\bar{v}_d(x^+) = \hat{v}_d e^{-i\mu x^+/W_m} \quad , \tag{4}$$

where μ is a complex number, $\mu = \alpha + i\delta$. For example,

(1) if $\delta = 0$, the disturbance has a constant amplitude over the airfoil;

(2) if $\delta < 0$, the disturbance amplitude decays over the airfoil;

(3) if $\alpha = \nu$, the disturbance is termed convected and is transported over the airfoils with a velocity W_m; and

(4) if $\alpha \neq \nu$, the disturbance is termed nonconvected and is transported over the airfoil with a velocity different from W_m.

A frequency parameter λ is then defined as

$$\lambda = \frac{\omega c}{2W_m}$$

and represents a ratio of the chord to the disturbance wavelength along the chord. Equation (3) can then be written as

$$v_d(x^+,t) = \hat{v}_d e^{i(\omega t - \lambda x^+)} \quad . \tag{5}$$

If $\mu = \nu$, that is, $\alpha = \lambda$ and $\delta = 0$, the disturbance is convected and has a constant amplitude. Thus,

$$v_d(x^+,t) = \hat{v}_d e^{i\nu\left(t - \frac{cx^+}{2W_m}\right)}$$

$$= \hat{v}_d e^{i(\nu t - \omega x^+)} \quad , \tag{6}$$

where $\omega = \nu c/2W_m$ is the reduced frequency. Most studies of unsteady flows consider the disturbance to be of this form. In this analysis, however, the general expression for a nonconvected disturbance of constant amplitude will be considered, that is,

$$\omega = \frac{\nu c}{2W_m} \quad .$$

Similarly, the chordwise component of the disturbance velocity u_d can also be written as

$$u_d(x^+,t) = \hat{u}_d e^{i(\nu t - \omega x^+)} \quad . \tag{7}$$

Equations (5) and (7), respectively, can therefore be used to depict the disturbance flow velocities normal to and parallel to the rotor blades as illustrated in Figure 1.

The generalized reduced frequency ω can be related to the wavelength of the disturbance along the chord λ_c, the wavelength of the disturbance an observer will see on the moving blade row. From the geometry of Figure 1,

$$\lambda_c = \frac{2\pi c}{\omega \lambda_x} \quad , \tag{8}$$

where ℓ is the stator spacing or wavelength in the direction in which the rotor blades move. Thus, the generalized reduced frequency λ becomes

$$\lambda = \frac{\omega c}{2W_m} = \frac{2\pi W_t}{\ell_c} \frac{c}{2W_m}$$

$$= \frac{2\pi}{\ell} \frac{W_t}{W_m} \frac{\sin \beta}{\cos \beta} \frac{c}{2} \quad , \tag{9}$$

where W_t is the velocity at which disturbance is transported over the blade. The reduced frequency ω, that is, when $W_t = W_m$, is then

$$\omega = \frac{\nu c}{2W_m} = \frac{2\pi W_m}{\ell_c W_m} \frac{c}{2} = \frac{\pi c}{\ell_c} \tag{10}$$

from Equation (9), where ℓ_c is related to ℓ by Equation (8).

An additional frequency parameter occurs in a cascade and is the so-called intra-blade frequency τ.

$$\tau = -\frac{2\pi s}{\ell} \quad . \tag{11}$$

This frequency parameter accounts for the variation of the flow from blade to blade in the cascade. An extreme situation occurs when the spacing s of the cascade is some integer multiple of the wavelength of the disturbance velocity, the intra-blade frequency for this case is an integer multiple of 2π; each blade will then experience the same disturbance velocity at a given time. As will be discussed in Chapter IV, this corresponds to a resonance point where the unsteady effect contributed from each blade in a cascade accumulates and becomes

significant. In a vibrating blade, τ expresses the relative motion of adjacent blades in the cascade. The negative sign appears as a result of the coordinate system chosen in Figure 3.

The relationship between the intra-blade and the reduced frequency for a nonvibrating cascade can be found by substituting Equations (8) and (10) into Equation (11). Thus,

$$\tau = - \frac{2\omega \cos \beta}{\sin \phi} \frac{s}{c} \tag{12}$$

or, when $\beta = 0$, that is, $\phi = 180^{\circ} - \xi$, the relation in Equation (12) becomes

$$\tau = - \frac{2\omega}{\sin \xi} \frac{s}{c} \quad . \tag{13}$$

Thus, the intra-blade frequency τ is proportional to the reduced frequency ω provided that the cascade is rigid and nonvibrating.

2.3 Mechanics of the Flow Field

Since the present analysis employs an approach similar to that in the thin airfoil theory, where the flow situation is generally simulated by an appropriate distribution of vorticity, the unsteady pressure distribution on airfoils can be determined only when the vorticity distribution or circulation is established. This is accomplished by, first, a formulation of the induced velocities on the reference blade using the Law of Biot and Savart (23) for the cascade geometry and then the application of Söhngen inverse formula (24) to obtain the expression for vorticity distribution or circulation in terms of induced velocity. With the use of the inviscid Euler's equation of motion or the momentum

equation together with the vorticity distribution, the unsteady pressure difference along a blade chord can be written as a function of the induced velocity.

When the induced velocity obtained from satisfying the boundary condition for the reference blade, which in this analysis is a nonvibrating or rigid airfoil with camber and angle of incidence, is inserted into the expression, a closed-form solution for unsteady pressure distribution can finally be derived as a function of the disturbance characteristics and the geometrical parameters considered in a cascade.

2.3.1 Formulation of Induced Velocities

From the Law of Biot and Savart and the cascade configuration as specified in Figure 4, the induced velocity dw_o at a point x_p on the reference blade, due to an element of circulation $(\gamma_n dx_n)$ on the n^{th} blade of the cascade at time t, can be expressed as

$$dw_o(x_p,t) = \frac{1}{2\pi} \frac{\gamma_n(x_n,t)dx_n}{\sqrt{(ns\cos\xi)^2 + (x_n - x_p + ns\sin\xi)^2}} \quad .$$

This can be decomposed into the normal and chordwise induced velocities dv_o and du_o with respect to the chosen coordinate:

$$du_o(x_p,t) = -\frac{1}{2\pi} \frac{\gamma_n(x_n,t)ns\cos\xi\, dx_n}{(ns\cos\xi)^2 + (x_n - x_p + ns\sin\xi)^2}$$

and

$$dv_o(x_p,t) = \frac{1}{2\pi} \frac{\gamma_n(x_n,t)(x_n - x_p + ns\sin\xi)dx_n}{(ns\cos\xi)^2 + (x_n - x_p + ns\sin\xi)^2} \quad .$$

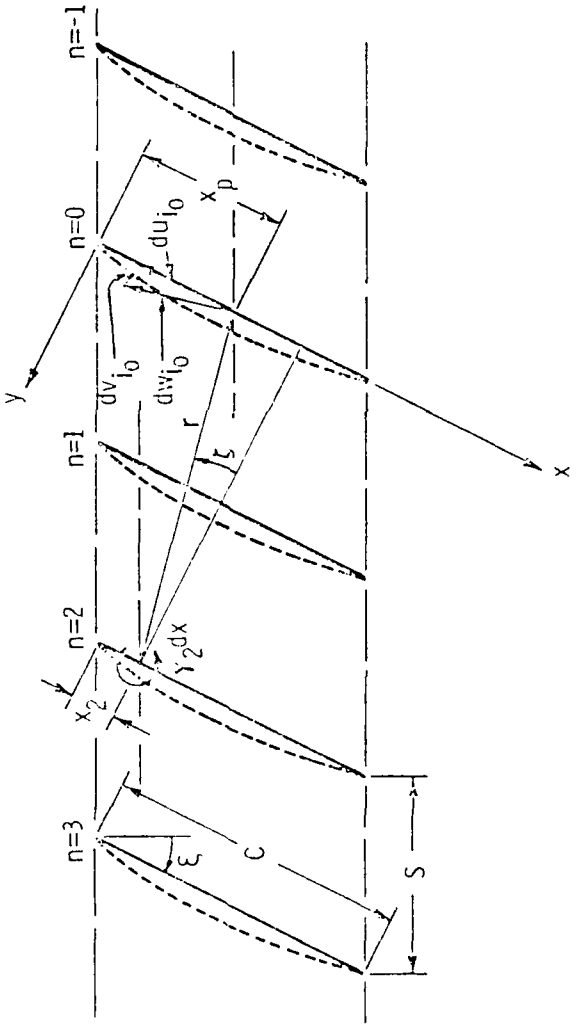

Figure 4. Induced Velocity in a Cascade.

From Figure 4, it can be assumed that the vorticity at a fixed distance from the leading edge of each blade in the cascade is of the same amplitude but with a constant phase difference τ from blade to blade. Also, utilizing the assumption that unsteady quantities vary harmonically with time,

$$\gamma_n(x_n,t) = \gamma_o(x,t)e^{in\tau} = \bar{\gamma}_o(x)e^{i(\nu t + n\tau)} \quad ,$$

$$du_o(x_p) = \bar{du}_o(x_p)e^{i\nu t} \quad ,$$

and

$$dv_o(x_p) = \bar{dv}_o(x_p)e^{i\nu t} \quad , \tag{14}$$

where $\tau = -(2\pi s/c)$. Thus,

$$\bar{du}_o(x_p) = -\frac{1}{2\pi}\frac{\bar{\gamma}_o(x)e^{in\tau}ns\cos\xi\, dx_n}{(ns\cos\xi)^2 + (x_n - x_p + ns\sin\xi)^2} \tag{15a}$$

and

$$\bar{dv}_o(x_p) = \frac{1}{2\pi}\frac{\bar{\gamma}_o(x)e^{in\tau}(x_n - x_p + ns\sin\xi)dx_n}{(ns\cos\xi)^2 + (x_n - x_p + ns\sin\xi)^2} \quad . \tag{15b}$$

These expressions give the velocity induced at a point x_p on the reference blade by an element of circulation located at a point x_n on the n^{th} blade and can be integrated from the leading edge and along the wake of the n^{th} blade to obtain the total velocity induced at x_p. Before this

can be done, however, it is necessary to relate the wake vorticity to the circulation on the blade.

Consider an element of wake vorticity of the reference blade of strength $\gamma_{o_w}(x,t) = \overline{\gamma_{o_w}}(x)e^{i\nu t}$ which, from assumptions (5) and (6), is harmonic with time and is transported away from the blade with velocity W_m in a direction parallel to the chord. Then, for any location $x > c$ downstream of the trailing edge,

$$\gamma_{o_w}(x,t) = \gamma_{o_w} e^{i\nu\left(\frac{t - x}{W_m}\right)} \quad . \tag{16}$$

During an interval of time δt, the total circulation on the blade changes its strength by

$$\frac{d\Gamma_o}{dt}\delta t = \frac{d}{dt}(\bar{\Gamma}_o e^{i\nu t})\delta t = i\nu\bar{\Gamma}_o e^{i\nu t}\delta t \quad ,$$

where

$$\Gamma_o(t) \int_o^c \gamma_o(x,t)dx \quad .$$

This change in total circulation results in an element of wake circulation which is shed at $x = c$ and moves downstream a distance $W_m\delta t$ in time t. The wake circulation is of opposite sign to the change in circulation on the blade by the Helmholtz's Vortex Theorem as stated in assumption (4). Therefore,

$$\frac{-i\nu\bar{\Gamma}_o e^{i\nu t}\delta t}{W_m \delta t} = \hat{\gamma}_{o_w} e^{i\nu\left(\frac{t-\zeta}{W_m}\right)} \quad .$$

Thus, the amplitude constant $\hat{\gamma}_{o_w}$ in Equation (16) is found and leads to an expression for the strength of the wake vorticity:

$$\gamma_{o_w}(x,t) = -\frac{i\nu}{W_m}\Gamma_o e^{i\nu(c-x)/W_m} \quad . \tag{17}$$

From the statement of the model employed, the vorticity on the n^{th} blade is concentrated at a chordwise point x_{cn}, while the vorticity in its wake is continuously distributed as shown in Figure 2. The circulation on the n^{th} blade is related to that on the reference blade by $\Gamma_n = \Gamma_o e^{in\tau}$ from Equation (14). At this point, the coordinate axes are transformed to midchord of the reference blade by $x^+ = (2x/c) - 1$, where x^+, the dimensionless coordinate for the reference blade, varies from -1 to 1.

Substituting these relations into Equation (15) and integrating from the leading edge to infinity far downstream gives the total velocity induced by the n^{th} blade at the point x^+_p as

$$u_o(x^+_p) = -\frac{\Gamma_o}{4\pi s}\,\vartheta(\lambda^+_c) + \frac{i\omega}{4\pi}\frac{c}{s}\int_1^\infty e^{-i\omega\lambda^+}\vartheta(\lambda^+_\lambda)d\lambda^+ \quad , \tag{18.a}$$

and

$$\bar{v}_o(x^+_p) = -\frac{\bar{\Gamma}_o}{4\pi s}\,\vartheta(\chi^+_c) + \frac{i\omega}{4\pi}\frac{c}{s}\int_1^\infty e^{-i\omega\lambda^+}\vartheta(\chi^+_\lambda)\,d\lambda^+ \quad , \qquad (18b)$$

where

Δ = circulation coefficient $\left(= \frac{\bar{\Gamma}_o}{c}\, e^{i\omega}\right)$;

ω = reduced frequency $\left(= \frac{\nu c}{2W_m}\right)$;

$\vartheta(\chi^+_c)$, $\vartheta(\chi^+_c)$ = functions relating the location of the blade vorticity and the point x^+_p ;

and

λ^+ = dummy variable along wake .

The total velocity induced at the point x^+_p by all of the blades can be found by taking summation of Equation (18) from $n = -\infty$ and $n = \infty$. It is assumed that the vorticity on the reference blade is continuously distributed rather than a concentrated vortex of strength Γ_o. Thus, by writing x^+_p as x^+, Equation (18) becomes

$$u_o(x^+) = -\frac{\Gamma_o}{4\pi s}\left[\sum_{-\infty}^{-1} + \sum_{1}^{\infty}\right]\vartheta(\chi^+_c) + \frac{i\omega}{4\pi}\frac{c}{s}\left[\sum_{-\infty}^{-1} + \sum_{1}^{\infty}\right]\int_1^\infty e^{-i\omega\lambda^+}\vartheta(\chi^+_\lambda)\,d\lambda^+$$

and

$$\bar{v}_o(x^+) = \frac{1}{2\pi} \oint_{-1}^{1} \frac{\bar{\gamma}_o(x^+_1)dx^+_1}{(x^+_1 - x^+)} + \frac{\omega\Delta}{i\pi} \int_{1}^{\infty} \frac{e^{-i\omega\lambda^+}d\lambda^+}{(\lambda^+ - x^+)}$$

$$- \frac{\bar{\Gamma}_o}{4i\pi s} \left(\sum_{-\infty}^{-1} + \sum_{1}^{\infty} \right) \Phi(\chi^+_c)$$

$$+ \frac{\omega\Delta}{4\pi} \frac{c}{s} \left(\sum_{-\infty}^{-1} + \sum_{1}^{\infty} \right) \int_{1}^{\infty} e^{-i\omega\lambda^+} \Phi(\chi^+_\lambda)d\lambda^+ \quad .$$

2.3.2 Unsteady Vorticity Distribution and Circulation

To determine the vorticity distribution $\bar{\gamma}_o(x^+)$ and the total circulation $\bar{\Gamma}_o$, the Söhngen inverse formula is employed, which states that, if

$$g(\sigma) = -\frac{1}{2\pi} \oint_{-1}^{1} \frac{f(\xi)d\xi}{\xi - \sigma} \quad ,$$

then

$$f(\sigma) = -\frac{2}{\pi} \sqrt{\frac{1-\sigma}{1+\sigma}} \oint_{-1}^{1} \sqrt{\frac{1+\xi}{1-\xi}} \frac{g(\xi)}{(\sigma - \xi)} d\xi \quad ,$$

where $f(\sigma)$ is the desired unknown function. This leads to the following expression for $\bar{\gamma}_o(x^+)$:

$$\bar{\gamma}_o(x^+) = \frac{2}{\pi}\sqrt{\frac{1-x^+}{1+x^+}}\oint_{-1}^{1}\sqrt{\frac{1+x^+_1}{1-x^+_1}}\,\frac{\bar{v}_o(x^+_1)dx^+_1}{(x^+-x^+_1)}$$

$$-\frac{2\omega\Lambda}{i\pi^2}\sqrt{\frac{1-x^+}{1+x^+}}\oint_{-1}^{1}\sqrt{\frac{1+x^+_1}{1-x^+_1}}\int_1^{\infty}\frac{e^{-i\omega\lambda^+}d\lambda^+}{(\lambda^+-x^+_1)(x^+-x^+_1)}\,dx^+_1$$

$$+\frac{2}{\pi}\sqrt{\frac{1-x^+}{1+x^+}}\left(\sum_{-\infty}^{-1}+\sum_{1}^{\infty}\right)\oint_{-1}^{1}\sqrt{\frac{1+x^+_1}{1-x^+_1}}\,\frac{\bar{\Gamma}_o}{4i\pi s}\,\phi(\chi^+_c)\,\frac{dx^+_1}{(x^+-x^+_1)}$$

$$-\frac{2}{\pi}\sqrt{\frac{1-x^+}{1+x^+}}\left(\sum_{-\infty}^{-1}+\sum_{1}^{\infty}\right)\int_{-1}^{1}\sqrt{\frac{1+x^+_1}{1-x^+_1}}\,\frac{\omega\Lambda}{4\pi}\,\frac{c}{s}\int_1^{\infty}e^{-i\omega\lambda^+}\psi(\chi^+_\lambda)$$

$$\cdot\,\frac{d\lambda^+}{(x^+-x^+_1)}\,dx^+_1\quad . \tag{19}$$

Only the normal induced velocity $\bar{v}_o(x^+)$ is considered in this expression for $\bar{\gamma}_o(x^+)$ because the influence of the chordwise induced velocity $\bar{u}_o(x^+_1)$ is of a higher order and is therefore neglected [18].

By interchanging the order of integration in Equation (19) and introducing the functions $\phi(\chi^+_c)$ and $\psi(\chi^+_\lambda)$, $\bar{\gamma}_o(x^+)$ becomes

$$\bar{\gamma}_o(x^+) = \frac{2}{\pi}\sqrt{\frac{1-x^+}{1+x^+}}\oint_{-1}^{1}\sqrt{\frac{1+x^+_1}{1-x^+_1}}\,\frac{\bar{v}_o(x^+_1)dx^+_1}{(x^+-x^+_1)} - \frac{2\omega\Lambda}{i\pi^2}\sqrt{\frac{1-x^+}{1+x^+}}$$

$$\cdot\int_1^{\infty}e^{-i\omega\lambda^+}\oint_{-1}^{1}\sqrt{\frac{1+x^+_1}{1-x^+_1}}\,\frac{dx^+_1}{(\lambda^+-x^+_1)(x^+-x^+_1)}\,d\lambda^+$$

$$- \frac{\bar{\Gamma}_o}{\pi^2 c} \sqrt{\frac{1 - x^+}{1 + x^+}} \left[\sum_{-\infty}^{-1} + \sum_{1}^{\infty} \right] e^{in\tau} \oint_{-1}^{1} \sqrt{\frac{1 + x^+_1}{1 - x^+_1}} \left\{ \frac{1}{(g_c - x^+_1)} \right.$$

$$\left. + \frac{1}{(h_c - x^+_1)} \right\} \frac{dx^+_1}{(x^+ - x^+_1)} - \frac{\omega \Delta}{i\pi^2} \sqrt{\frac{1 - x^+}{1 + x^+}} \left[\sum_{-\infty}^{-1} + \sum_{1}^{\infty} \right]$$

$$\cdot e^{in\tau} \int_{-1}^{\infty} e^{i\omega\lambda^+} \oint_{-1}^{1} \sqrt{\frac{1 + x^+_1}{1 - x^+_1}} \left\{ \frac{1}{g_\lambda - x^+_1} + \frac{1}{h_\lambda - x^+_1} \right\}$$

$$\cdot \frac{dx^+_1}{(x^+ - x^+_1)} d\lambda^+ \quad , \tag{20}$$

where the quantities g_c and h_c represent the position of the concentrated vortices of the adjacent blades and g_λ and h_λ describe the positions of their shed vorticity.

The products of the form $\left((r - x^+_1)(x^+ - x^+_1)\right)^{-1}$, which occur in Equation (20), can be written as

$$\frac{1}{(r - x^+_1)(x^+ - x^+_1)} = \frac{1}{(r - x^+)} \left\{ \frac{1}{(x^+ - x^+_1)} - \frac{1}{(r - x^+_1)} \right\} \quad .$$

Substitution of this relation into Equation (20) allows the integrals with respect to x^+_1 to be evaluated using integral relations listed in Appendix B. However, the complex quantities g_c, h_c, g_λ, and h_λ, which have the form

$$g_p = p + \frac{n}{ia} = p - i\,\frac{2ns}{c}\,e^{i\xi} = (p + \frac{2ns}{c}\sin\xi) - i(\frac{2ns}{c}\cos\xi)$$

and

$$h_p = p - \frac{n}{ib} = p + i\,\frac{2ns}{c}\,e^{-i\xi} = (p + \frac{2ns}{c}\sin\xi) + i(\frac{2ns}{c}\cos\xi) \quad ,$$

where p represents x^+_{cn} or ξ^+_n, must be examined to assure that they fulfill the mathematical restriction that $|g_p|^2$ and $|h_p|^2 > 1$, that is

$$|g_p|^2 = |h_p|^2 = p^2 + 4pn\,\frac{s}{c}\sin\xi + 4n^2\,\frac{s}{c} > 1 \quad . \qquad (21)$$

This condition requires that the magnitudes of g_p and h_p on the complex plane be larger than unity as illustrated by Figure 5.

For $p = x^+_{cn} = -\frac{1}{2}$, that is, considering g_c and h_c, Equation (21) becomes

$$\frac{1}{4} - 2n\,\frac{s}{c}\sin\xi + 4n^2(\frac{s}{c})^2 > 1 \quad .$$

The solution for this inequality is

$$\frac{s}{c} > \frac{1}{4n}\,(\sin\xi + \sqrt{\sin^2\xi + 3}) \quad \text{for } n = 1, 2, 3, \ldots$$

$$> \frac{1}{-4n}\,(\sin\xi - \sqrt{\sin^2\xi + 3}) \quad \text{for } n = -1, -2, -3, \ldots$$

For $p = \xi^+_n$, that is, considering g_ξ and h_ξ,

$$\xi^{+2}_n + 4n\,\frac{s}{c}\sin\xi\,\xi^+_n + 4n^2\,\frac{s}{c} > 1 \quad .$$

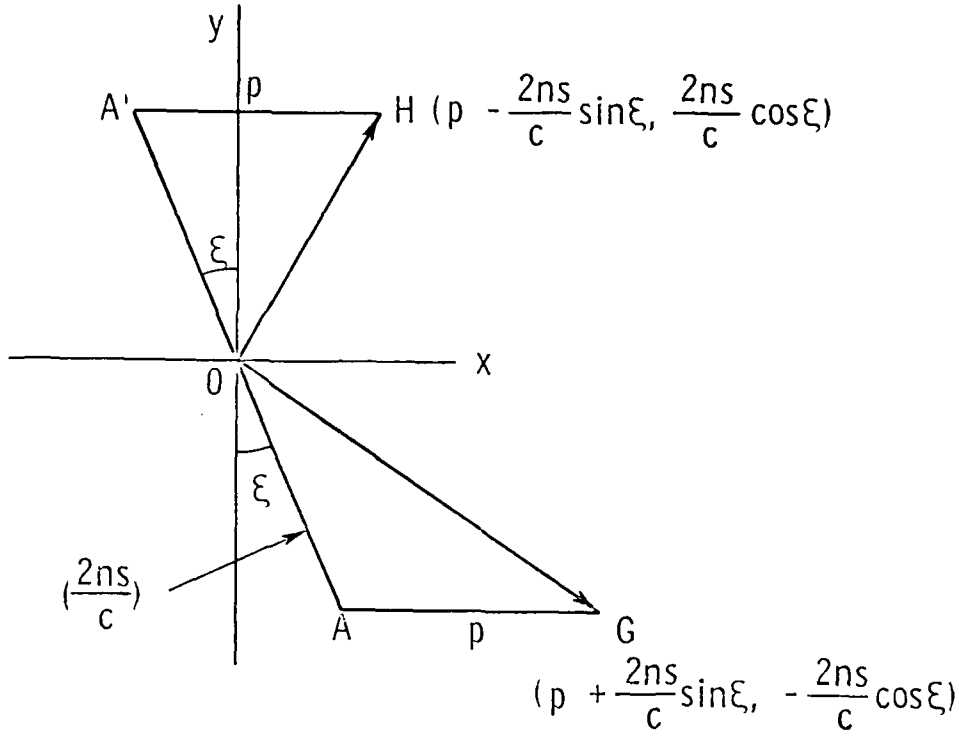

Figure 5. Complex Representation of Cascade Functions g_p and h_p.

This is always true for $n \geq -1$. The inequality gives

$$\frac{s}{c} \geq \frac{1}{2\pi} \left\{ \lambda_n^+ \sin^{-1} + \sqrt{1 - \lambda_n^{+2}} \left(1 - \sin^{-2} \right) \right\} \quad \text{for } n = -1, -2, -3, \ldots ,$$

where values of λ_n^+ vary from one to infinity.

Bruce [19] has obtained the overall region of validity of the theoretical model by combining the result for the $n = +1$ case from the analysis of g_c and h_c and the result for $n = -1$ case from the analysis of g_s and h_s. His result and the approximate region of validity defined by Henderson [20] is shown in Figure 6. The restriction requires that the space-chord ratio becomes infinite when the stagger angle of cascade is very close to 90°. However, this does not heavily restrict the range of application of the analysis since such a value of stagger angle is not of practical importance for turbomachines.

With the above condition imposed, Equation (20) becomes

$$\bar{v}_o(x^+) = \frac{2}{\pi} \sqrt{\frac{1 - x^+}{1 + x^+}} \int_{-1}^{1} \sqrt{\frac{1 + x^+_1}{1 - x^+_1}} \frac{\bar{v}_o(x^+_1) dx^+_1}{(x^+ - x^+_1)}$$

$$- \frac{2i\lambda}{\pi} \sqrt{\frac{1 - x^+}{1 + x^+}} \int_{1}^{\infty} \sqrt{\frac{\lambda^+ + 1}{\lambda^+ - 1}} \frac{e^{-i\lambda x^+}}{(\lambda^+ - x^+)} d\lambda^+$$

$$+ \frac{\Gamma_o}{\pi c} \sqrt{\frac{1 - x^+}{1 + x^+}} \left[\sum_{-\infty}^{-1} + \sum_{1}^{\infty} \right] \left\{ \frac{1}{\lambda_n^+ - x^+} + \sqrt{\frac{\lambda_n^+ + 1}{\lambda_n^+ - 1}} \right.$$

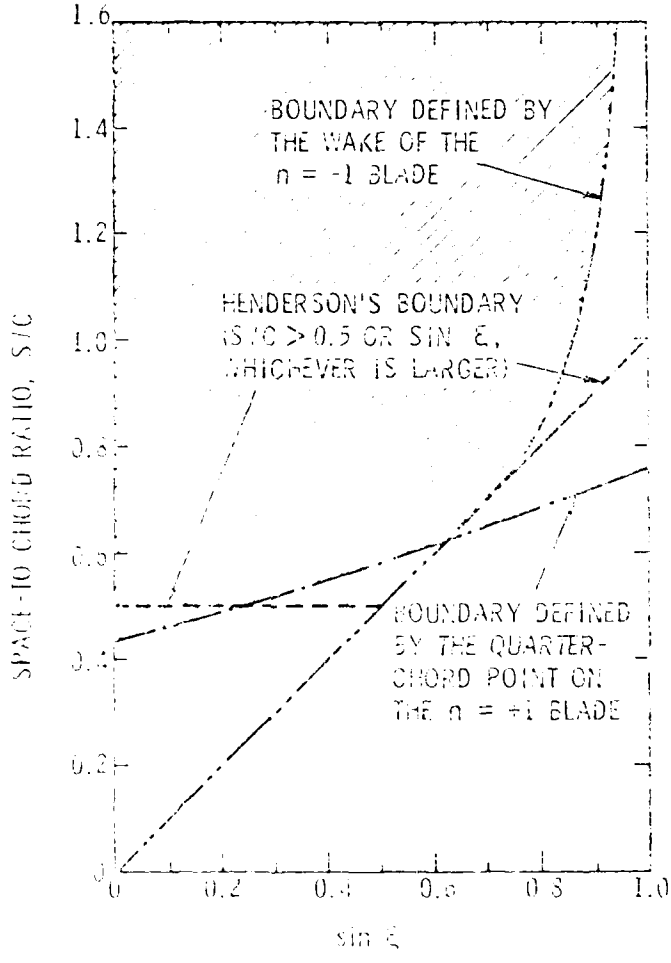

Figure 5. Region of Validity of the Theoretical Model.

$$+ \frac{1}{h_c - x^+}\sqrt{\frac{h_c + 1}{h_c - 1}}\Bigg\} - \frac{i\omega A}{\pi}\sqrt{\frac{1 - x^+}{1 + x^+}}\left\{\sum_{-\infty}^{-1} + \sum_{1}^{\infty}\right\}$$

$$\cdot\, e^{in\pi}\left\{\int_1^\infty \sqrt{\frac{g_\lambda + 1}{g_\lambda - 1}}\,\frac{e^{-i\omega\lambda^+}}{(g_\lambda - x^+)}\,d\lambda^+\right.$$

$$\left. + \int_1^\infty \sqrt{\frac{h_\lambda + 1}{h_\lambda - 1}}\,\frac{e^{-i\omega\lambda^+}}{(h_\lambda - x^+)}\,d^+\lambda\right\} \quad . \tag{21}$$

From this expression, the total circulation on the reference blade Γ_o can be obtained by integration from the leading to the trailing edge of the airfoil. Thus,

$$\frac{2\Gamma_o}{c} = -2\int_{-1}^{1}\sqrt{\frac{1 + x^+_1}{1 - x^+_1}}\,\bar{v}_o(x^+_1)dx^+_1$$

$$+ e^{i\omega}\left\{\left[\sum_{-\infty}^{-1} + \sum_{1}^{\infty}\right] e^{in\pi}(C_1 + C_2 - 2)\right.$$

$$- 2i\omega e^{-i\omega}\int_1^\infty\left\{\sqrt{\lambda^+ + 1} - 1\right\} e^{i\omega\lambda^+}d\lambda^+$$

$$\left. - i\omega e^{i\omega}\left[\sum_{-\infty}^{-1} + \sum_{1}^{\infty}\right] e^{in\pi}(D_1 + D_2)\right\} \quad , \tag{22}$$

where the terms C_1, C_2, D_1, and D_2 are cascade functions defined as

$$C_1 = \sqrt{\frac{g_c + 1}{g_c - 1}} \quad ,$$

$$C_2 = \sqrt{\frac{h_c + 1}{h_c - 1}} \quad ,$$

$$D_1 = \int_1^\infty \left(\sqrt{\frac{g_c + 1}{g_c - 1}} - 1 \right) e^{-i\omega\lambda^+} d\lambda \quad ,$$

and

$$D_2 = \int_1^\infty \left(\sqrt{\frac{h_c + 1}{h_c - 1}} - 1 \right) e^{-i\omega\lambda^+} d\lambda^+ \quad .$$

Rearranging this equation gives the total circulation $\bar{\Gamma}_0$ on the reference blade:

$$\bar{\Gamma}_0 = \frac{\int_{-1}^{1} \sqrt{\frac{1 + x^+_1}{1 - x^+_1}} \, \bar{v}_0(x^+_1) dx^+_1}{1 - e^{-i\omega} \left[H_1^{(1)}(\omega) + i H_0^{(2)}(\omega) \right] + H_c} \quad , \tag{23}$$

where M_c is the cascade function:

$$M_c = \left[\sum_{-\infty}^{-1} + \sum_{1}^{\infty}\right] e^{in\gamma}(C_1 + C_2 - 2) - i\omega e^{i\omega} \left[\sum_{-\infty}^{-1} + \sum_{1}^{\infty}\right] e^{in\gamma}(D_1 + D_2) \quad .$$

The steady part or time average of the vorticity distribution and circulation which will be needed to solve the problem can be found by making use of the linear properties of the analysis. Thus, by letting $\omega = 0$, the steady vorticity distribution $\gamma_{o_s}(\sigma^+)$ is found from Equation (21):

$$\gamma_{o_s}(\sigma^+) = \frac{2}{\pi}\sqrt{\frac{1-\sigma^+}{1+\sigma^+}}\int_{-1}^{1}\sqrt{\frac{1+x_1}{1-x_1}}\frac{v_{o_s}(x_1)}{(\sigma^+ - x_1)}\,dx_1$$

$$+\frac{\Gamma_{o_s}}{\pi c}\sqrt{\frac{1-\sigma^+}{1+\sigma^+}}\left[\sum_{-\infty}^{-1} + \sum_{1}^{\infty}\right]$$

$$\cdot\left\{\frac{1}{g_c - \sigma^+}\sqrt{\frac{g_c+1}{g_c-1}} + \frac{1}{h_c - \sigma^+}\sqrt{\frac{h_c+1}{h_c-1}}\right\} \quad , \quad (24)$$

where the induced velocity $v_o(x_1)$ and the total circulation Γ_o have been replaced by their steady components $v_{o_s}(x_1)$ and Γ_{o_s}, respectively.

Following the same procedure in obtaining Equation (23), that is, by integration from leading edge to trailing edge of the airfoil, the steady total circulation can then be obtained. Hence,

$$\Gamma_{o_s} = \frac{4 \int_{-1}^{1} \sqrt{\frac{1 + x_1}{1 - x_1}}\, v_{o_s}(x_1)\, dx_1}{\left[\sum_{-\infty}^{-1} + \sum_{1}^{\infty}\right]\left\{\sqrt{\frac{g_c + 1}{g_c - 1}} + \sqrt{\frac{h_c + 1}{h_c - 1}} - 2\right\} - 2} \quad . \tag{25}$$

2.3.3 Unsteady Pressure Distribution

From the assumption (2) made in Section 2.1 and the Euler's momentun equation which links the kinematic flow with dynamic conditions, the basic relation between the flow velocity and pressure for the flow field is found to be

$$\frac{\partial q}{\partial t} + q \frac{\partial q}{\partial x} = - \frac{1}{\rho} \frac{\partial p}{\partial x} \quad .$$

Since the thin airfoil theory is employed in the anaiysis and since the unsteady response of the airfoils to the flow condition as stated is of ultimate concern, the expression for unsteady pressure along the airfoil is given in a form of pressure difference. The pressure difference Δp is defined as the difference between the static pressure on the suction and pressure surfaces of the airfoil, $p_{(-)}$ and $p_{(+)}$, respectively.

The distribution of the pressure difference can then be determined by subtraction of the equations written for suction and pressure surfaces. Thus,

$$\frac{\partial}{\partial t}\left(q_{(-)} - q_{(+)}\right) + \frac{1}{2} \frac{\partial}{\partial x}\left(q_{(-)}^2 - q_{(+)}^2\right) = \frac{1}{\rho} \frac{\partial}{\partial x}\left(p_{(-)} - p_{(+)}\right) \quad ,$$

(26)

where the velocity q is the sum of all the velocities in the x direction, that is, the instantaneous chordwise velocity. Therefore,

$$q_{(-)} = W_m + u_d + \frac{\gamma_{o_t}(x,t)}{2}$$

and

$$q_{(+)} = W_m + u_d - \frac{\gamma_{o_t}(x,t)}{2} \quad ,$$

where u_d is the disturbance velocity of order ϵ parallel to the chord as described in Section 2.2, $\gamma_{o_t}(x,t)$ is the total vorticity distribution, and W_m is the steady mean velocity. Equation (26) then becomes

$$\frac{\partial}{\partial t}\gamma_{o_t}(x,t) + \frac{\partial}{\partial x}\left\{(W_m + u_d)\gamma_{o_t}(x,t)\right\} = -\frac{1}{\rho}\frac{\partial}{\partial x}\Delta p(x,t) \quad .$$

Taking the origin of the coordinate system at the airfoil midchord with its chord length c equal to two and integrating this expression from the leading edge of the airfoil to any location x^+, $-1 \leq x \leq x^+$, permits the pressure difference to be given in terms of the vorticity distribution on the airfoil,

$$-\Delta p(x^+,t) = \rho(W_m + u_d)\gamma_{o_t}(x^+,t) + \rho\frac{\partial}{\partial t}\int_{-1}^{x^+}\gamma_{o_t}(x^+,t)dx^+ \quad .$$

Assuming the total vorticity γ_{o_t} to be composed of a steady vorticity γ_{o_s} plus an unsteady vorticity γ_{o_u}, that is, γ_o of order ϵ, the linearized form of unsteady pressure difference becomes

$$-\Delta\tilde{p}(\sigma^+) = \rho W_m \gamma_o(\sigma^+,t) + \rho u_d \gamma_{o_s}(\sigma^+) + \rho \frac{\partial}{\partial t}\int_{-1}^{\sigma^+} \gamma_o(x^+,t)dx^+ \quad ,$$

where only the unsteady contribution to pressure difference is considered. Again, using the assumption that all the unsteady quantities are harmonic with time,

$$\Delta\tilde{p}(\sigma^+,t) = \bar{\Delta p}(\sigma^+)e^{i\nu t} \quad ,$$

$$\gamma_o(\sigma^+,t) = \bar{\gamma}_o(\sigma^+)e^{i\nu t} \quad ,$$

and

$$u_d(\sigma^+,t) = \bar{u}_d(\sigma^+)e^{i\nu t} \quad ,$$

the unsteady distribution of pressure difference can be written in terms of its amplitude. Thus,

$$-\Delta p(\sigma^+) = \rho W_m \bar{\gamma}_o(\sigma^+) + \rho u_d(\sigma^+)\gamma_{o_s}(\sigma^+) + \rho \frac{\partial}{\partial t}\int_{-1}^{\sigma^+} \bar{\gamma}_o(x^+)dx^+ \quad . \tag{27}$$

The integral in Equation (26) can be determined by integration of Equation (21) between the limits -1 and σ^+. With the relations from Appendix B, Equations (B-4) and (B-5), this integral can be written as

$$\int_{-1}^{\sigma^+} \bar{\gamma}_o(x^+)dx^+ = -\frac{2}{\pi}\int_{-1}^{1}\left\{\sqrt{\frac{1+x^+_1}{1-x^+_1}}\left(\frac{\pi}{2}+\sin^{-1}\sigma^+\right)\right.$$

$$\left.+\,\Omega(\sigma^+,x^+_1)\right\}\bar{v}_o(x^+_1)dx^+_1$$

$$-\frac{2i\omega\Lambda}{\pi}\int_{1}^{\infty}\left\{\sqrt{\frac{\lambda^+ + 1}{\lambda^+ - 1}}\left(\frac{\pi}{2}+\sin^{-1}\sigma^+\right)\right.$$

$$\left.+\,\Lambda(\sigma^+,\lambda^+)\right\}e^{-i\omega\lambda^+}d\lambda^+ + \frac{\bar{\Gamma}_o}{\pi c}\left\{\sum_{-\infty}^{-1}+\sum_{1}^{\infty}\right\}e^{in\tau}\left\{\left(\frac{\pi}{2}+\sin^{-1}\sigma^+\right)\right.$$

$$\left.\cdot\left\{\sqrt{\frac{g_c+1}{g_c-1}}+\sqrt{\frac{h_c+1}{h_c-1}}\right\}+\Lambda(\sigma^+,g_c)+\Lambda(\sigma^+,h_c)\right\}$$

$$-\frac{i\omega\Lambda}{\pi}\left\{\sum_{-\infty}^{-1}+\sum_{1}^{\infty}\right\}e^{in\tau}\left\{\int_{1}^{\infty}\left\{\sqrt{\frac{g_\lambda+1}{g_\lambda-1}}\left(\frac{\pi}{2}+\sin^{-1}\sigma^+\right)\right.\right.$$

$$\left.+\,\Lambda(\sigma^+,g_\lambda)\right\}e^{-i\omega\lambda^+}d\lambda^+ + \int_{1}^{\infty}\left\{\sqrt{\frac{h_\lambda+1}{h_\lambda-1}}\left(\frac{\pi}{2}+\sin^{-1}\sigma^+\right)\right.$$

$$\left.\left.+\,\Lambda(\sigma^+,h_\lambda)\right\}e^{-i\omega\lambda^+}d\lambda^+\right\} \quad .$$

Subtracting the product of Equation (22) and the quantity $1/2 + 1/\pi \sin^{-1}\sigma^+$ from this expression leads to

$$\int_{-1}^{\sigma^+} \bar{\gamma}_o(x^+)dx^+ = -\frac{2}{\pi}\int_{-1}^{1} \bar{v}_o(x^+_1)\Omega(\sigma^+,x^+_1)dx^+_1 - \frac{2i\omega\Delta}{\pi}\int_{1}^{\infty} e^{-i\omega\lambda^+}\Lambda(\sigma^+,\lambda^+)d\lambda^+$$

$$+ \frac{\Delta e^{-i\omega}}{\pi}\left[\sum_{-\infty}^{-1} + \sum_{1}^{\infty}\right] e^{in\tau}\left(\Lambda(\sigma^+,g_c) + \Lambda(\sigma^+,h_c)\right)$$

$$- \frac{i\omega\Delta}{\pi}\left[\sum_{-\infty}^{-1} + \sum_{1}^{\infty}\right] e^{in\tau}\left\{\int_{1}^{\infty} e^{-i\omega\lambda^+}\Lambda(\sigma^+,g_\lambda)d\lambda^+\right.$$

$$\left. + \int_{1}^{\infty} e^{-i\omega\lambda^+}\Lambda(\sigma^+,h_\lambda)d\lambda^+\right\} \quad . \tag{28}$$

Substitution of Equations (21) and (28) into Equation (27) results in a general expression for unsteady pressure difference $\Delta\bar{p}$ at a position σ^+ along the blade chord. From the integral relations, Equation (B-6) given in Appendix B, and the definitions of terms in Reference [27], $\Delta p(\sigma^+)$ can be written as

$$-\frac{\Delta\bar{p}(\sigma^+)}{\rho W_m} = \frac{2}{\pi}\sqrt{\frac{1-\sigma^+}{1+\sigma^+}}\int_{-1}^{1}\sqrt{\frac{1+x^+_1}{1-x^+_1}}\,\frac{\bar{v}_o(x^+_1)dx^+_1}{(\sigma^+ - x^+_1)}$$

$$-\frac{2i\omega}{\pi}\int_{-1}^{1}\bar{v}_o(x^+_1)K(\sigma^+,x^+_1)dx^+_1 - \omega\Delta H_o^{(2)}(\omega)\sqrt{\frac{1-\sigma^+}{1+\sigma^+}}$$

$$+\frac{i\omega\Delta e^{-i\omega}}{\pi}\left\{\sum_{-\infty}^{-1}+\sum_{1}^{\infty}\right\}e^{in\pi}\left(A(\sigma^+,g_c)+A(\sigma^+,h_c)-A(\sigma^+,g_1)\right.$$

$$\left.-A(\sigma^+,h_1)\right)+\frac{\Delta e^{-i\omega}}{\pi}\sqrt{\frac{1-\sigma^+}{1+\sigma^+}}\left\{\sum_{-\infty}^{-1}+\sum_{1}^{\infty}\right\}$$

$$\cdot\, e^{in\pi}\left\{\frac{1}{(g_c-\sigma^+)}\sqrt{\frac{g_c+1}{g_c-1}}+\frac{1}{(h_c-\sigma^+)}\sqrt{\frac{h_c+1}{h_c-1}}\right.$$

$$\left.-i\omega e^{-i\omega}\left(\int_1^{\infty}\frac{e^{-i\omega\lambda^+}}{\sqrt{g_\lambda^2-1}}\,d\lambda^+ + \int_1^{\infty}\frac{e^{-i\omega\lambda^+}}{\sqrt{h_\lambda^2-1}}\,d\lambda^+\right)\right\}$$

$$+\frac{u_d(\sigma^+)\tau_{o_s}(\sigma^+)}{W_m}, \qquad (29)$$

where $\tau_{o_s}(\sigma^+)$ is derived in Section 2.3, Equation (24). This expression is equivalent to that derived in Reference [18] except for the fourth term which is in error in Reference [16].

The first two terms and the third term in Equation (29) represent the unsteady pressure contributed from the bound vorticity of the reference blade and its shed vorticity, respectively. The last term $\bar{u}_{d'o_s}(x^+)/W_m$ is the contribution from the interactions between the chordwise disturbance and the bound vorticity on the reference blade. Other terms having infinite summations include the effect from the concentrated vortices of the adjacent blades and that from their wake vorticity.

Equation (29) can finally be solved when the induced velocity $\bar{v}_o(x^+_1)$, known from the given boundary condition, is inserted.

2.4 Determination of Unsteady Pressure Distribution

To obtain a solution of Equation (29) for the unsteady pressure distribution, the total normal induced velocity $\bar{v}_o(x^+_1)$ must be specified along the entire chord length of the reference blade. This is possible when the boundary condition on the reference blade is specified.

2.4.1 Specification of Unsteady Boundary Condition

The boundary condition on the blade requires that the resultant flow (mean flow plus disturbance plus any induced flow) be tangent to the blade contour. Following the assumptions made in Section 2.1 where the blade is assumed to be infinitely thin and the camber small, this boundary condition can be fulfilled on the blade chord line and is similar to that in the analysis for isolated airfoil with camber and

angle of incidence as illustrated in Figure 7. The kinematic flow condition is then

$$\frac{dy^+}{dx^+} = \frac{W_m \sin \alpha_m + v_d + v_o}{W_m \cos \alpha_m + u_d + u_o} \quad .$$

If the incidence angle α_m is assumed small, the equation can be written as

$$v_o(x^+) = \frac{dy^+}{dx^+} (W_m + u_d) - \alpha_m W_m - v_d \quad , \tag{30}$$

where u_o is neglected as discussed in Section 2.3. For the specific case where flat plate and zero angle of incidence is considered, Equation (30) reduces to $v_o(x^+) = -v_d$.

The linear nature of the present analysis enables the boundary condition to be separated into two parts: a steady boundary condition and an unsteady boundary condition. The normal induced velocity v_o is then composed of a steady part v_{o_s} and an unsteady part v_{o_u}, that is, $v_o = v_{o_s} + v_{o_u}$. Thus, the steady boundary condition becomes, from Equation (30),

$$v_{o_s}(x^+) = \left(\frac{dy^+}{dx^+} - \alpha_m\right) W_m \tag{31}$$

and the unsteady boundary condition is

$$v_{o_u}(x^+) = \frac{dy^+}{dx^+} u_d - v_d \quad . \tag{32}$$

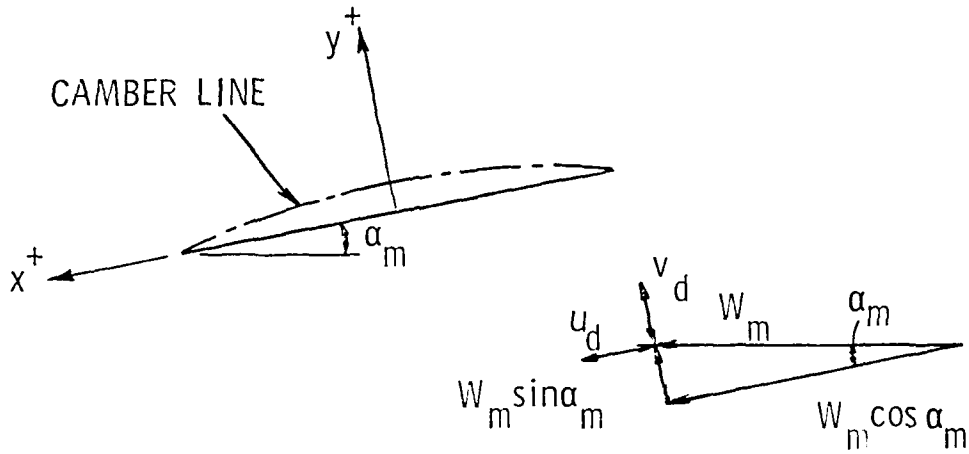

Figure 7. Velocities in Boundary Condition.

In this analysis, a parabolic arc camber line representing the airfoil is considered and can be described as

$$y^+ = y^+_m(1 - x^{+2}) \quad , \tag{33}$$

where y^+_m is the ratio of maximum camber to the chord. For the general disturbance velocity, Equations (31) and (32) can combine with Equations (33) and (5) and (7) in Section 2.2 to obtain the following relations:

$$v_{o_s}(x^+) = -(2y^+_m x^+ - \alpha_m)W_m \tag{34a}$$

and

$$v_{o_u}(x^+,t) = v_{o_u}(x^+)e^{i\nu t} = (2y^+_m x^+ u_d + v_d)e^{i(\nu t - \beta x^+)} \quad . \tag{34b}$$

2.3.2 General Expression for Unsteady Pressure Distribution

Equation (29) gives an expression for unsteady pressure distribution on airfoils of a cascade which interacts with a disturbance in the inlet flow fields. This expression is written in terms of the induced velocity $\bar{v}_o(x^+)$ on the blade surface and is directly related to the disturbance flow by the boundary condition which is discussed in the previous section. The steady vorticity distribution and total circulation must also be determined before the complete solution can be obtained. With the substitution of induced velocity derived from the boundary condition into Equations (29), (33), and (34), the unsteady

pressure distribution can finally be determined as a function of inlet flow disturbance and cascade geometry.

In order to solve the first two terms in Equation (C9), it is possible to consider the isolated airfoil case in which the expression for unsteady pressure distribution has been determined. The details are contained in Appendix A. Thus, by substitution of the result from Equation (A-6),

$$
\begin{aligned}
&\frac{2}{\sqrt{1+\bar{x}_1^+}\,\bar{c}^+}\int_{-1}^{1}\sqrt{\frac{1+\bar{x}_1}{1-\bar{x}_1}}\,\frac{-(iv_m^+ x_1 u_d + v_d)e^{i\bar{x}_1}}{(\bar{x}^+ - \bar{x}_1)}\,d\bar{x}_1 \\
&-\frac{2}{\sqrt{1+\bar{x}^+}\,\bar{c}^+}\int_{-1}^{1}(-(iv_m^+ x_1 u_d + v_d)e^{-i\bar{x}_1}+(\bar{x}^+ - \bar{x}_1)\,\cdots\,d\bar{x}_1 \\
&\quad -iv_m^+ u_d\sqrt{\frac{1-\bar{x}^+}{1+\bar{x}^+}}\,(1+\bar{x}^+)J_0(\bar{x}^+) - iJ_1(\bar{x}^+) - 2^+\sqrt{\frac{1-\bar{x}^+}{1+\bar{x}^+}}\,\cdots(\bar{x}^+,\bar{x}^+) \\
&\quad +iv_d\sqrt{\frac{1}{1-\bar{x}^+}}\,J_0(\bar{x}^+) - 2\sqrt{\frac{1+\bar{x}^+}{1-\bar{x}^+}}\,\cdots(\bar{x}^+,\bar{x}^+) \\
&\quad -\cdots v_m^+ u_d\sqrt{1-\bar{x}^+}\,\cdots_0(\bar{x}^+) + \cdots(\bar{x}^+ + i)\Sigma(\bar{x}^+,\bar{x}^+) \\
&\quad +\cdots v_d(\bar{x}^+,\bar{x}^+) \quad .
\end{aligned}
$$

When the terms are rearranged into two parts, those with the coordinate and transverse disturbance u_d and x_1, the right-hand side of the equation becomes

$$= 4v^{+}_{m} u_d \left\{ -\sqrt{\frac{1-\zeta^{+}}{1+\zeta^{+}}}\, i J_1(\alpha) - i \frac{2}{\alpha} Z(\alpha, \zeta^{+}) \right.$$

$$\left. + \left(\frac{2}{\alpha} - 1\right) \left[2\zeta^{+} Z(\alpha, \zeta^{+}) - \sqrt{1-\zeta^{+2}}\, J_0(\alpha) \right] \right\} \quad , \qquad (35)$$

where

$$Z(\alpha, \zeta^{+}) = \sum_{k=1}^{\infty} i^{k} J_k(\alpha) \sin k\gamma \quad ; \quad \gamma = \pi - \cos^{-1} \zeta^{+} \quad .$$

For a convected flow, $M_\infty > 0$, Equation (35) reduces to

$$= 4v^{+}_{m} u_d \left\{ -\sqrt{\frac{1-\zeta^{+}}{1+\zeta^{+}}}\, i J_1(\alpha) - i \frac{2}{\alpha} Z(\alpha, \zeta^{+}) \right\} + 2v_d \sqrt{\frac{1-\zeta^{+}}{1+\zeta^{+}}}\, J_0(\alpha) \quad .$$

To find the steady vorticity distribution $\gamma_{o_s}(\zeta^{+})$, Equation (25), the steady circulation Γ_{o_s} must be determined. Substituting the steady boundary condition, Equation (36a), and integral relations from Appendix A into Equation (34) gives

$$\gamma_{o_s} = \frac{4 \int_{-1}^{1} \sqrt{\frac{1+x_1}{1-x_1}} \left\{-W_m(2y^+_m x_1 + \alpha_m)\right\} dx_1}{\left[\sum_{-\infty}^{-1} + \sum_{1}^{\infty}\right] \left\{\sqrt{\frac{g_c+1}{g_c-1}} + \sqrt{\frac{h_c+1}{h_c-1}} - 2\right\} - 2}$$

$$= \frac{-\pi W_m(y^+_m + \alpha_m)}{\left[\sum_{-\infty}^{-1} + \sum_{1}^{\infty}\right] (C_1 + C_2 - 2) - 2} \quad .$$

The steady vorticity distribution is therefore

$$\gamma_{o_s}(x^+) = \frac{2}{\pi} \sqrt{\frac{1-x^+}{1+x^+}} \int_{-1}^{1} \sqrt{\frac{1+x_1}{1-x_1}} \frac{\left\{-W_m(2y^+_m x_1 + \alpha_m)\right\} dx_1}{(x^+ - x_1)}$$

$$+ \frac{\gamma_{o_s}}{\pi c} \left[\sum_{-\infty}^{-1} + \sum_{1}^{\infty}\right] \left\{\frac{1}{g_c - x^+} \sqrt{\frac{g_c+1}{g_c-1}} + \frac{1}{h_c - x^+} \sqrt{\frac{h_c+1}{h_c-1}}\right.$$

$$= 2W_m \sqrt{\frac{1 - \xi^+}{1 + \xi^+}} \left\{ 2\gamma_m (1 + \xi^+) + \epsilon_m \right.$$

$$\left. + \frac{(\gamma_m + \epsilon_m) \left[\left(\sum_{-\infty}^{-1} + \sum_{1}^{\infty} \right) (E_1 + E_2) \right]}{2 - \left[\left(\sum_{-\infty}^{-1} + \sum_{1}^{\infty} \right) (C_1 + C_2 - 2) \right]} \right\} . \qquad (37)$$

The total unsteady circulation on the blade is also obtained by substituting unsteady boundary condition, Equation (36b), and employing the integral relations presented in Appendix B. Hence,

$$\Gamma_0 e^{i\omega t} = 2e^{i\omega t} \int_{-1}^{1} \sqrt{\frac{1 + x_1}{1 - x_1}} \left\{ -(2\gamma_m \hat{n}_d x_1 + \nu_d) e^{-i\omega x_1} \right\} dx_1$$

$$\frac{-1}{i\omega e^{i\omega t} \left\{ iH_1^{(2)}(\omega) + iH_0^{(2)}(\omega) \right\} + M_c}$$

$$\cdot 2\pi e^{i\omega t} \left\{ \gamma_m \hat{n}_d \left[J_0(\omega) - J_2(\omega) - iJ_1(\omega) \right] + \nu_d \left[J_0(\omega) - iJ_1(\omega) \right] \right\}$$

$$i\omega e^{i\omega t} \left\{ iH_1^{(2)}(\omega) + iH_0^{(2)}(\omega) \right\} + M_c$$

(38)

The results in Equations (35), (37), and (38) lead to the final expression for unsteady pressure distribution for a blade in a cascade of parabolic arc blades operating at a nonzero mean angle of incidence in a velocity field that contains both transverse and chordwise disturbance velocities.

$$
-\frac{\Delta\bar{p}(\sigma^+)}{\rho W_m} = 4\gamma^+_m \hat{u}_d \left\{ -\sqrt{\frac{1-\sigma^+}{1+\sigma^+}}\, iJ_1(\lambda) - i\frac{2\omega}{\lambda^2} Z(\lambda,\sigma^+) \right.
$$

$$
\left. + \left(\frac{\omega}{\lambda} - 1\right)\left[2\sigma^+ Z(\lambda,\sigma^+) - \sqrt{1-\sigma^+}\, J_0(\lambda)\right] \right\}
$$

$$
+ 2\hat{v}_d \left\{ \sqrt{\frac{1-\sigma^+}{1+\sigma^+}}\, J_0(\lambda) + 2\left(\frac{\omega}{\lambda} - 1\right) Z(\lambda,\sigma^+) \right\}
$$

$$
- \omega\pi H_0^{(2)}(\omega) \sqrt{\frac{1-\sigma^+}{1+\sigma^+}} + \frac{i\omega e^{-i\omega}}{\pi} \left\{ \sum_{-\infty}^{-1} + \sum_{1}^{\infty} \right\}
$$

$$
\cdot e^{in\omega} \left[\lambda(\sigma^+, B_c) + \lambda(\sigma^+, h_c) - \lambda(\sigma^+, g_1) - \lambda(\sigma^+, h_1) \right]
$$

$$
+ \frac{\omega e^{-i\omega}}{\pi} \sqrt{\frac{1-\sigma^+}{1+\sigma^+}} \left\{ \sum_{-\infty}^{-1} + \sum_{1}^{\infty} \right\} e^{in\omega} \left(E_1 + E_2 \right.
$$

$$
\left. - i\omega e^{i\omega}(B_1 + B_2) \right] + \frac{\hat{u}_d}{W_m} e^{-i\lambda\sigma^+} \gamma_{o_s}(\sigma^+) \quad , \tag{39}
$$

where λ and $\gamma_{o_s}(\sigma^+)$ are as described in Equations (37) and (38).

The Kutta flow condition, which requires that the pressure difference at the trailing edge of the airfoil is zero, $\Delta p(TE) = 0$, is demonstrated by substituting $\sigma^+ = 1$ into the equations for unsteady pressure difference. The unsteady pressure difference is found to vanish since

terms such as $\sqrt{1 - \sigma^{+}/1 + \sigma^{+}}$, $\sqrt{1 - \sigma^{+2}}$, $Z(\sigma,\sigma^{+})$, and $\Lambda(\sigma,\sigma^{+})$ all equal zero when $\sigma^{+} = 1$.

The correctness of this expression can also be checked by examining the isolated airfoil case, Appendix A, in which the blade-to-blade spacing in cascade becomes infinity. For this condition, the expression of unsteady pressure distribution, Equation (39), reduces to one which is identical to that obtained by Naumann [26] since the terms containing infinite summations in Equations (29), (23), and (24) must vanish as shown in Appendix C.

CHAPTER III

CALCULATION OF UNSTEADY PRESSURE DISTRIBUTION AND OTHER UNSTEADY PARAMETERS

The theoretical analysis in the previous chapter provides a solution of unsteady pressure distribution for a cascade of airfoils in an inviscid, incompressible, distorted inflow. Specifically, this solution is expressed in terms of the general parameters - the cascade geometry: space-chord ratio s/c, stagger angle γ, blade camber y_m, mean angle of incidence α_m, and the reduced frequency ν or σ.

Equations (39), (37), and (38) contain several quantities expressing the unsteady contribution of the blades in a cascade which are adjacent to the reference blade. Each of these quantities is an infinite summation as listed in Table I. The evaluation of these summations is discussed in the following sections.

3.1 Cascade Functions and Infinite Summations

The infinite summations listed in Table I consist of so-called cascade functions, some of which have been defined in Appendix IV of Reference [18]. These terms will be examined prior to obtaining their solutions:

(1) The cascade summations required to determine the steady vorticity, Equation (38), are

Table 1

INFINITE SUMMATIONS FOR UNSTEADY EFFECT IN CASCADE

	Cascade Summations	Main Program Eq. (39)	Y_{o_s} Eq. (37)	$\dot{z}$ Eq. (38)	Remarks
1	$\sum_{-\infty}^{-1} + \sum_{1}^{\infty} e^{-i\pi(C_1 + C_2 - 2)}$		X		REAL
2	$\sum_{-\infty}^{-1} + \sum_{1}^{\infty} e^{-i\pi(C_1 + C_2 - 2)}$			X	COMPLEX
3	$\sum_{-\infty}^{-1} + \sum_{1}^{\infty} e^{-i\pi(B_1 + B_2)}$	X			COMPLEX
4	$\sum_{-\infty}^{-1} + \sum_{1}^{\infty} e^{-i\pi(D_1 + D_2)}$			X	COMPLEX

5	$\sum_{-\infty}^{-1} + \sum_{1}^{\infty} e^{in\theta}\{\Lambda(\sigma^+,g_e) + \Lambda(\sigma^+,h_e) - \Lambda(\sigma^+,g_1) - \Lambda(\sigma^+,h_1)\}$	X			COMPLEX
6	$\sum_{-\infty}^{-1} + \sum_{1}^{\infty} (E_1 + E_2)$		X		REAL
7	$\sum_{-\infty}^{-1} + \sum_{1}^{\infty} e^{in\theta}(E_1 + E_2)$	X			COMPLEX

$$\left(\sum_{-\infty}^{-1} + \sum_{1}^{\infty}\right) (C_1 + C_2 - 2)$$

and

$$\left(\sum_{-\infty}^{-1} + \sum_{1}^{\infty}\right) (E_1 + E_2) \quad .$$

$$C_1 + C_2 - 2 = \sqrt{\frac{g_c + 1}{g_c - 1}} + \sqrt{\frac{h_c + 1}{h_c - 1}} - 2$$

and

$$E_1 + E_2 = \frac{1}{g_c - c} + \sqrt{\frac{g_c + 1}{g_c - 1}} + \frac{1}{h_c - c} + \sqrt{\frac{h_c + 1}{h_c - 1}} \quad ,$$

where

$$g_c = x_c + 2n \frac{s}{c} \sin \delta - i2n \frac{s}{c} \cos \delta$$

and

$$h_c = x_c + 2n \frac{s}{c} \sin \delta + i2n \frac{s}{c} \cos \delta \quad .$$

The quantities g_c and h_c are conjugate numbers. It can be shown that the values of $\sqrt{r + 1/r - 1}$, where r represents g_c or h_c, respectively, are also conjugates.

The quantity $C_1 + C_2 - 2$, as a result, is a real number. This is also true for E_1 and E_2. The steady vorticity $\gamma_{o_s}(\sigma^+)$, Equation (38), therefore, has no imaginary component and no phase lag with the steady lift. This agrees with the result from steady flow theory for thin airfoil (21).

(2) The infinite summations having the forms

$$\left(\sum_{-\infty}^{-1} + \sum_{1}^{\infty}\right) e^{int}(C_1 + C_2)$$

and

$$\left(\sum_{-\infty}^{-1} + \sum_{1}^{\infty}\right) e^{int}(E_1 + E_2)$$

are complex, since a phase difference factor e^{int} multiplies each of the real quantities discussed above.

(3) Equation (39) contains a special infinite summation:

$$\left(\sum_{-\infty}^{-1} + \sum_{1}^{\infty}\right) e^{int}\left(\lambda(\sigma^+, g_c) + \lambda(\sigma^+, h_c)\right.$$

$$\left. - \lambda(\sigma^+, g_1) - \lambda(\sigma^+, h_1)\right) \quad .$$

where λ is defined as

$$\lambda(\sigma^+,r) = 2 \tan^{-1} \sqrt{\frac{1 + \sigma^+ \; r + 1}{1 - \sigma^+ \; r - i}} - \pi \quad .$$

The quantities g_1 and h_1 are identical to g_c and h_c except that the position of the concentrated vortex for the adjacent blades x^+_c is replaced by one, that is

$$g_1 = 1 + 2n \frac{s}{c} \sin \xi - i2n \frac{s}{c} \cos \xi$$

and

$$h_1 = 1 + 2n \frac{s}{c} \sin \xi + i2n \frac{s}{c} \cos \xi \quad .$$

It can also be shown that $\lambda(\sigma^+,g_c)$ and $\lambda(\sigma^+,h_c)$, together with $\lambda(\sigma^+,g_1)$ and $\lambda(\sigma^+,h_1)$, are pairs of conjugates. The value for $\lambda(\sigma^+,g_c) + \lambda(\sigma^+,h_c) - \lambda(\sigma^+,g_1) - \lambda(\sigma^+,h_1)$ is therefore real and can be found by using the trigonometric identity which relates the sum of two arc tangents:

$$\tan^{-1} a + \tan^{-1} b = \tan^{-1} \frac{a + b}{1 - ab} \quad .$$

(...) the infinite summations

$$\sum_{l=-\infty}^{-1} + \sum_{l=1}^{\infty} e^{in\xi}(B_1 + B_2)$$

and

$$\left[\sum_{-\infty}^{-1} + \sum_{1}^{\infty}\right] e^{int}(D_1 + D_2)$$

contain the improper integral $B_1 + B_2$ and D_1 and D_2, that is,

$$B_1 + B_2 = \int_1^{\infty} \left\{ \frac{1}{\sqrt{g_1^2 - 1}} + \frac{1}{\sqrt{h_1^2 - 1}} \right\} e^{-i\alpha x^+} d\alpha^+ \qquad (40a)$$

and

$$D_1 + D_2 = \int_1^{\infty} \left\{ \sqrt{\frac{g_1^2 + 1}{g_1^2 - 1}} + \sqrt{\frac{h_1^2 + 1}{h_1^2 - 1}} - 2 \right\} e^{-i\alpha x^+} d\alpha^+ \qquad (40b)$$

where

$$g_1 = \alpha^+ + 2n\frac{s}{c}\sin\xi - i2n\frac{s}{c}\cos\xi$$

and

$$h_1 = \alpha^+ + 2n\frac{s}{c}\sin\xi + i2n\frac{s}{c}\cos\xi \quad .$$

By the same manner as discussed above, the terms within the brackets in Equation (40) are real numbers. The imaginary term in Equation (40) arising from $e^{-i\alpha x^+}$

permits it to be easily separated into the real and imaginary components and a numerical integration performed. Some are also functions of the position x^+ along the reference blade chord or a function of the reduced frequency ω. For example, terms such as $L_1 + iL_2$ must first be evaluated at the location x^+ where the unsteady pressure difference is to be found and then summed over different values of n which represent the adjacent blades of the cascade.

3.3 Unsteady Response Parameters

The unsteady pressure difference on a cascade blade, Equation (39), can be considered in two parts: the part with chordwise disturbance u_d and that with the transverse disturbance v_d. When the relation for disturbance velocity and inlet flow obtained in Section 2.2, Equation (1), is applied, the disturbances u_d and v_d can be replaced by $-\hat{w}_d \sin\gamma$ and $-\hat{w}_d \cos\gamma$ where the angle γ describes the relative position between the stator wakes and the rotor.

The coefficient of unsteady pressure difference is introduced at this point:

$$\hat{C}_p(x^+) = \frac{\hat{\Delta p}(x^+)}{\rho W_m \hat{w}_d e^{i\omega t}} \quad \text{or} \quad = \frac{\hat{\Delta p}(x^+)}{\rho W_m \hat{w}_d} \quad , \tag{41}$$

which is a dimensionless complex quantity suitable for analysis. This quantity can be expressed alternatively by its magnitude and phase angle: the magnitude is defined as its absolute value, that is,

$$|\Delta C_{p'}| = \sqrt{(\Delta C_{p_R})^2 + (\Delta C_{p_I})^2} \quad ,$$

and the phase angle is defined as

$$\phi_p = \tan^{-1} \frac{(\Delta C_p)_I}{(\Delta C_p)_R}$$

which represents the amount by which the unsteady pressure difference vector at a location x^+ on the airfoil chord lags the vector of oscillation velocity w_g. In order to observe the unsteady effect due to chordwise or transverse disturbance, the coefficient of unsteady pressure difference can be separated into two parts, that is, the term multiplied by $\sin$ which represents the response to the disturbance parallel to the blade and the term multiplied by $-\cos$ which represents a transverse gust. As discussed in Reference [22], the unsteady response generated by the interaction of an upstream disturbance with a moving cascade of thin, slightly cambered airfoils can be considered as two acoustic problems whose solutions are additive. Thus,

$$\Delta C_p = \Delta C_{p_{u_d}} + \Delta C_{p_{v_d}} \quad .$$

The term $\Delta C_{p_{u_d}}$ contributed by the chordwise disturbance is generally of second order and vanishes completely only when the blades in cascade are represented by flat plates, that is, zero camber, and the mean incidence angle of the flow is zero. This is justified by Equation (30) with the substitution of $v_g = \sin \omega t$.

The unsteady lift can be determined by direct numerical integration of the unsteady pressure difference over the airfoil chord:

$$L = \int_0^c (-\Delta p(x))\,dx \quad .$$

Since the coordinates have been transformed into a dimensionless system whose origin is located at midchord on the reference blade by $\xi = x/c - 1$, the present analysis uses an alternative expression.

$$L = \int_{-1}^{1} (-\Delta p(\xi))\,d\xi \quad .$$

The unsteady lift coefficient can then be expressed as

$$C_L = \frac{1}{\frac{1}{2}\rho V_a^2} \int_{-1}^{1} \Delta p(\xi)\,d\xi \quad , \qquad (6.2)$$

where V_a is the axial velocity used in the unsteady airfoil theory.

In a similar manner, the unsteady pitching moment about an axis through the midchord position,

$$M = \int_0^c (x - \tfrac{c}{2})(-\Delta p(x))\,dx \quad ,$$

$$M = \int_{-1}^{1} \Delta p(x^+) x^+ dx^+$$

in the dimensionless coordinate system. Thus, the coefficient of unsteady pitching moment is

$$\tilde{C}_M = -\frac{1}{\rho U^2 c} \int_{-1}^{1} \left(\frac{\partial \tilde{p}(x^+)}{\partial \tilde{w}_m} \right) x^+ dx^+ \quad . \tag{43}$$

The unsteady lift and pitching moment coefficients as expressed by Equations (4.5) and (4.3) are also complex quantities. Thus, they can be expressed as

$$\tilde{C}_L = (C_L)_R + i(C_L)_I$$

and

$$\tilde{C}_M = (C_M)_R + i(C_M)_I$$

An alternative form for expressing these quantities also uses magnitude and phase relationships:

$$C_L = \sqrt{(C_L)_R^2 + (C_L)_I^2} \quad , \quad \tan^{-1} \frac{(C_L)_I}{(C_L)_R}$$

$$|C_M| = \sqrt{(C_M)_R^2 + (C_M)_I^2} \quad , \quad \phi_M = \tan^{-1} \frac{(C_M)_I}{(C_M)_R} \quad .$$

The above magnitude-phase relationships for unsteady pressure distribution, lift and moment, are employed to present the results obtained from this analysis.

The location of the unsteady center of pressure $x_{C.P.}$ measured from the leading edge of the airfoil is given by

$$\frac{x_{C.P.}}{c} = \frac{1}{2} - \frac{C_M}{C_L} \quad . \tag{44}$$

3.3 Computer Programming

Theoretical results given by Equations (39), (37), and (38) include Bessel functions, Hankel functions, the special complex functions $\Xi(\nu^+, \ )$, and the infinite summations composing the so-called cascade function as discussed in Section 3.1. A computer program [27] has been developed to permit the calculation of these functions and, hence, the unsteady pressure distribution.

The improper integrals $S_1 + S_{-1}$ and D_1 and D_2 which appear in the expression of unsteady pressure distribution have been evaluated numerically by Simpson's [28] when programming the cascade unsteady lift function $C(\ , \ , \ )$. It is observed that these integrals which originate from the mathematical continuation of the wake shed by adjacent blades can be expressed in terms of the Hankel functions having complex arguments and the Hankel function of the second kind which is still the solution of the wake vorticity of the reference

blade. It can then be argued that the convergence of the numerical integration of these integrals is assured by their similarity with Hankel functions. Henderson's programming of the solution for $B_1 + B_2$ and $D_1 + D_2$ is retained in the present analysis.

The infinite cascade summations listed in Table 1 can then be evaluated by summing them over their arguments, which are usually complex numbers, for positive and negative pairs of n, that is, n = +, ±2, and so forth. Physically, this is equivalent to considering the addition of neighboring blades in the cascade. The summation is continued until the averaged value of the individual sums computed from n = +3 to n = +k differs from the averaged value of the individual sums computed from n = +3 to n = +(k + 1) by less than a specified factor, usually 0.001. This criterion is adequate since, as this factor is reduced further, the number of pairs of arguments needed increases in an exponential manner while the sums, which are characterized by a damped, oscillatory behavior, approach a constant value [27].

A subroutine for calculating the infinite summations for cascade has been written and is capable of performing the summation of these improper into proper [27]. This permits the unsteady pressure difference coefficient, defined by Equation (39), to be evaluated.

The coefficients of unsteady lift and moment, Equations (41) and (42), can be calculated by direct numerical integrations. However, a typical integration scheme will not be sufficient to obtain the solutions since a mathematical singularity exists at the leading edge of the airfoil chord, $\frac{1}{\sin(\phi/2)}$, where $\sin(\phi/2) = 0$. This singularity was eliminated analytically in the analyses for unsteady lift and moment [28], so that, hence, did not represent a problem.

A Gauss-Legendre quadrature method, which is recommended [28] for the numerical evaluation of integrals with the presence of singularity, is introduced. As a demonstration of the validity of this integration technique, the simple case of an isolated flat-plate airfoil is considered. For example, the improper integral

$$\int_{-1}^{1} \sqrt{\frac{1 - \sigma^{+}}{1 + \sigma^{+}}}\, d\sigma^{+} \quad ,$$

whose analytical exact solution is π, is used in evaluating unsteady lift for this case. The present integration scheme gives a numerical value within a significant accuracy of four decimal points. Consequently, the computer program developed in Reference [27] can be employed to calculate the unsteady lift and pitching moment in addition to the unsteady pressure distribution.

CHAPTER IV

THEORETICAL PREDICTIONS AND COMPARISONS WITH EXPERIMENTAL RESULTS AND OTHER SOLUTIONS

4.1 Introduction

To demonstrate the validity of the present solution, comparisons will be made with other solutions and with available measured data describing the unsteady pressure difference distribution or unsteady response of a cascade whose geometry is specified. The theoretical results obtained in Chapter II are presented herein as the magnitudes and phase angles of the unsteady pressure difference, unsteady lift and pitching moment coefficients, $\Delta C_p(\bar{x}^+)$, $\bar{C}_L$, and $\bar{C}_M$, as defined by Equations (41), (42), and (43), respectively. The dimensionless location of unsteady center-of-pressure $x_{C.P.}/c$, Equation (44), is also presented. After establishing the validity of the present theoretical model by comparing predicted and measured cascade response, this theoretical model will be used to predict cascade response over a range of values of reduced frequencies, mean incidence angle, and blade camber that can be helpful for turbomachine designs.

4.2 Comparisons of Theoretical Predictions and Measured Data

As stated in Section 2.1, the present analysis employs a theoretical model identical to that developed by Henderson [18]. The results of the unsteady lift and moment coefficients $\bar{C}_L$ and $\bar{C}_M$, which were calculated using the present analysis, are compared with those obtained in References [13] and [19], respectively.

Of all the theoretical developments of unsteady cascade response, the unsteady analysis of Whitehead [14] is the one which can provide the most exact comparison. While developed primarily for the vibration analysis of a cascade, a special solution can be obtained for the interaction of rigid blades with upstream disturbances. It is based on the vortex representation of thin, zero-camber airfoils, whereas each airfoil in the cascade is represented by an odd number of equally spaced bound vortices with continuously varying strength. Smith's theory [17], which is a modification of Whitehead's, to include compressibility effects gives Whitehead's solution for $M = 0$ and is actually used in the following computations. These results are referred to as the Whitehead-Smith theory.

The present analysis employs a reference point at the midchord of the airfoil by virtue of the coordinate system employed with its origin at the airfoil midchord. Thus, the equations described above are referred to that point, that is, the phase angle ζ is measured with respect to the disturbance velocity occurring at the blade midchord. As discussed by Whitehead [14] and demonstrated by Geising [29], this reference point can be moved to other different positions on the airfoil. The transformation of the reference point from the midchord to any other position on the airfoil can be accomplished using the following relationship:

$$L_{x^+} = L_0 e^{i\zeta x^+} , \qquad (65)$$

where

L_o = unsteady lift referenced to midchord ,

L_{x^+} = unsteady lift referenced at another location x^+ ,

x^+ = location on airfoil ($-1 \leq x \leq 1$) ,

and

κ = reduced frequency .

For example, the relation $L_{x^+} = L_o e^{-i\kappa x^+}$ will be used when comparing this analysis with the Whitehead-Smith theory, which is referenced to the leading edge of an airfoil.

In order to conduct a meaningful comparison of the results, it is necessary to select a flow and cascade configuration which is compatible with each method. For this purpose, a disturbance flow field, which represents a special case of Figure 2, was selected in which $\beta = 0$. The disturbance is defined as that which would exist in the absence of the cascade and is convected by the mean axial velocity C_x with no attenuation in its amplitude as it passes through the cascade.

Bruce [18] has conducted a series of experiments in a large axial flow fan to measure the unsteady lift and moment on a rotor based on this disturbance flow field. He employed screens to provide a variety of rotor inlet flows having a sinusoidally varying axial velocity component similar to that shown in Figure 2. The rotor response during operation in the wake flows is measured by a strain-gaged sensing element on one rotor blade. He varied the cascade stagger angle and space-chord ratio and the flow characteristics, mean incidence angle and reduced

frequency, to obtain results for various operating conditions. Bruce's measured data are suitable for comparison with the unsteady lift predicted by the present analysis. However, experimental data describing the unsteady pressure difference distribution are not available from Bruce's experiment. As a result, the values of unsteady pressure difference coefficient $\Delta\tilde{C}_p$ predicted by the present analysis are presented to compare only with the Whitehead-Smith theoretical solutions.

Utilizing the computer program developed in Reference (27), the quantities $|\Delta\tilde{C}_p|$, $\tilde{\ell}_p$, $|\tilde{C}_L|$, $\tilde{\ell}_L$, $|\tilde{C}_M|$, $\tilde{\ell}_M$, and $\bar{x}_{C.P.}/c$ are computed for values of $\gamma = 35^\circ$, 45° and 55° at s/c = 0.076, 1.353, and 2.029 covered in Bruce's experiment with $\epsilon_m = y^+_m = 0$ and $\kappa = 0.2$, 0.4, ... 2.0, and 2.2. A typical result of the theoretical prediction of $\Delta\tilde{C}_p$ is the series of calculations for $\gamma = 45^\circ$ with s/c = 1.353 over a range of reduced frequency of 0.5, 1.0, 1.5, and 2.0, which are presented in Figures 8 through 11, in terms of its magnitude and phase angle referenced to the leading edge of the airfoil. The results of computations for $\tilde{C}_L$, $\tilde{C}_M$, and $\bar{x}_{C.P.}/c$ are presented in Figures 12 through 20 where they are compared with Bruce's measured data, with computations based on the Whitehead-Smith theory, and with theoretical analysis by Henderson and Bruce. As shown in Figure 8, the present theoretical model is not valid for $\gamma = 45^\circ$ and 55° at s/c = 0.076. However, these cases are calculated for the purpose of comparison and can demonstrate the applicability of the present theory.

From the variations of $\Delta\tilde{C}_p$ demonstrated in Figures 8 through 11 and the corresponding integrated result $\tilde{C}_L$ in Figures 13 and 16, it is found that these comparisons between the present analysis and the Whitehead-Smith theory show good agreement except in the range where the

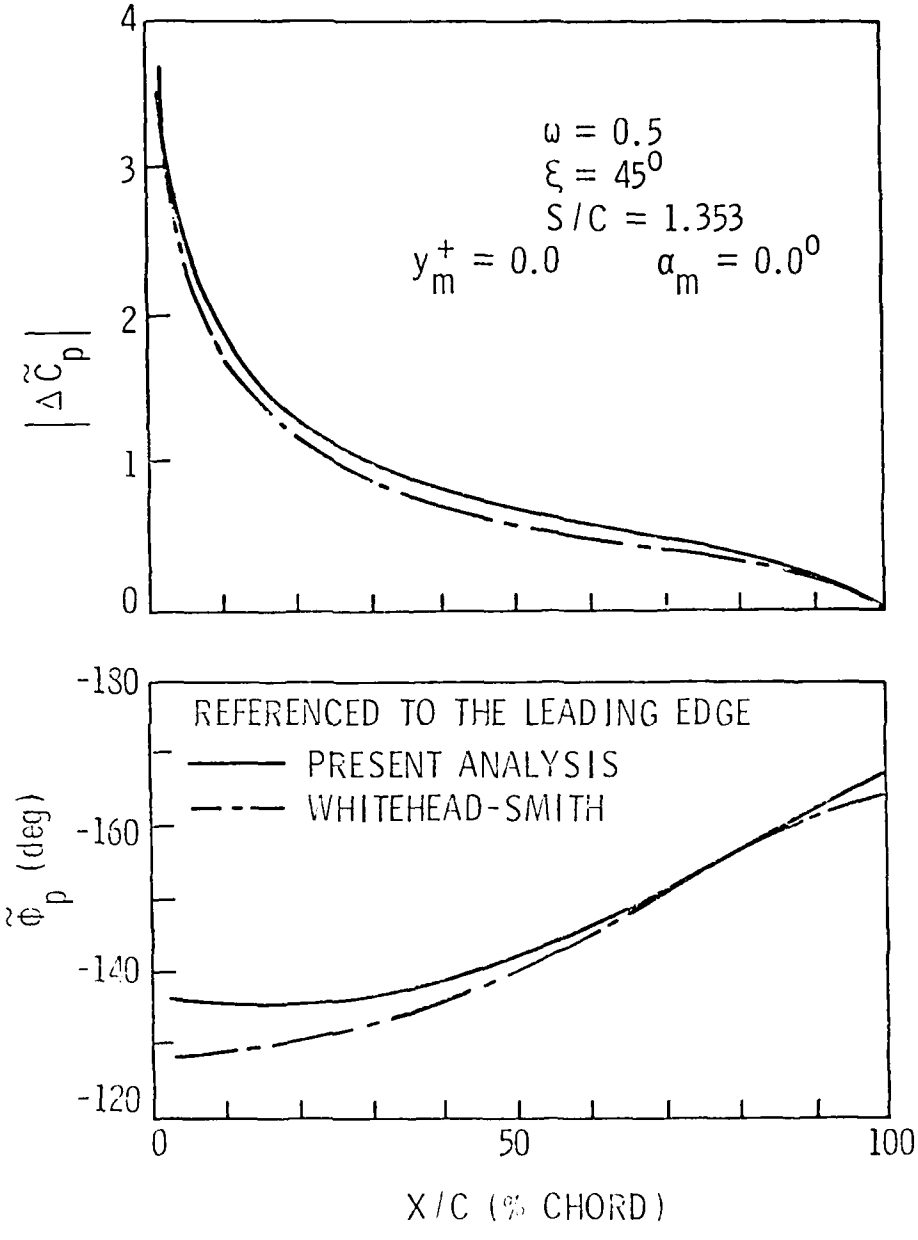

Figure 8. Comparison of Theoretical Unsteady Pressure Distribution with $\xi = 45°$, s/c = 1.353, and $\omega = 0.5$.

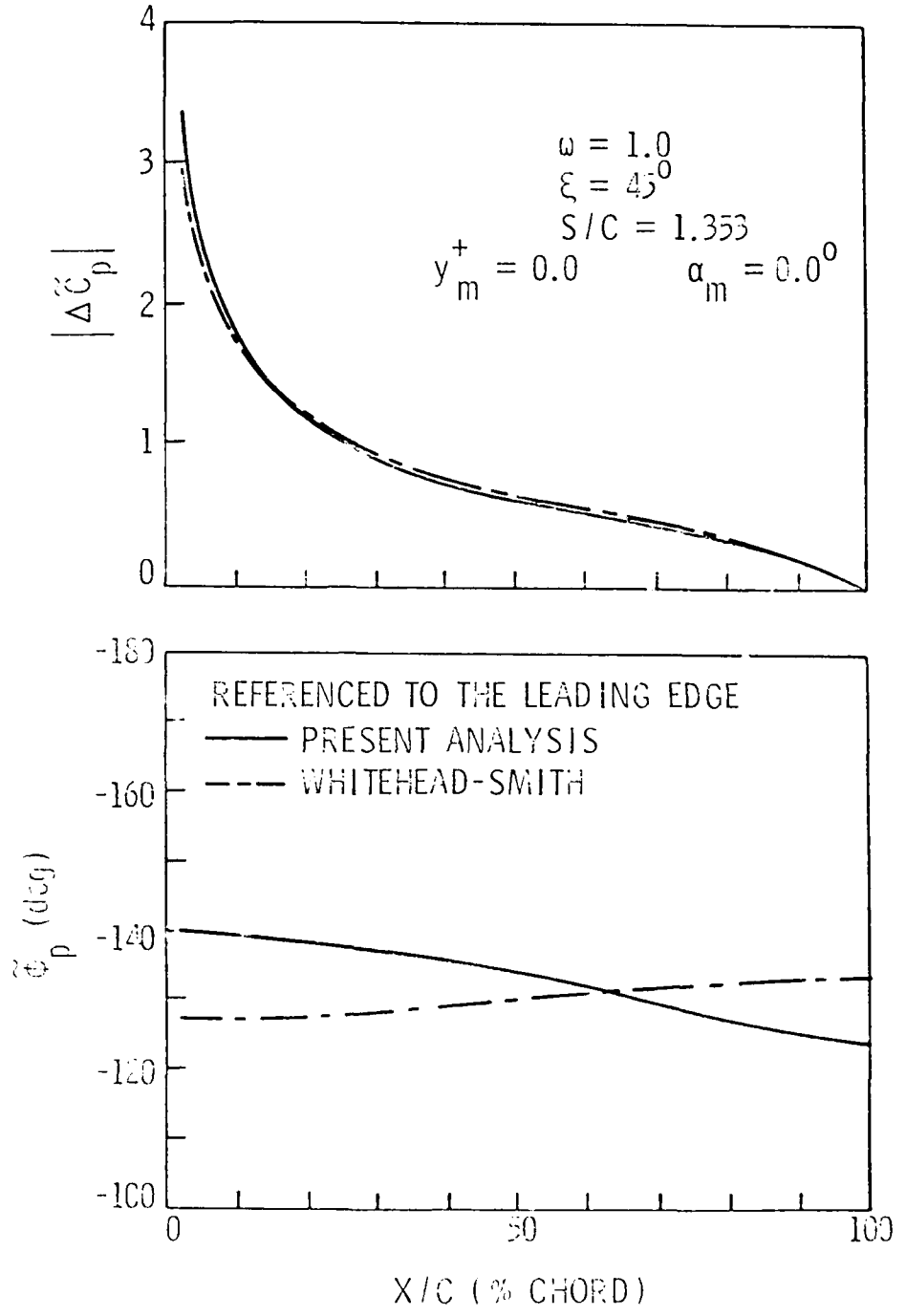

Figure 9. Comparison of Theoretical Unsteady Pressure Distribution with $\xi = 45^\circ$, S/C = 1.353, and ω = 1.0.

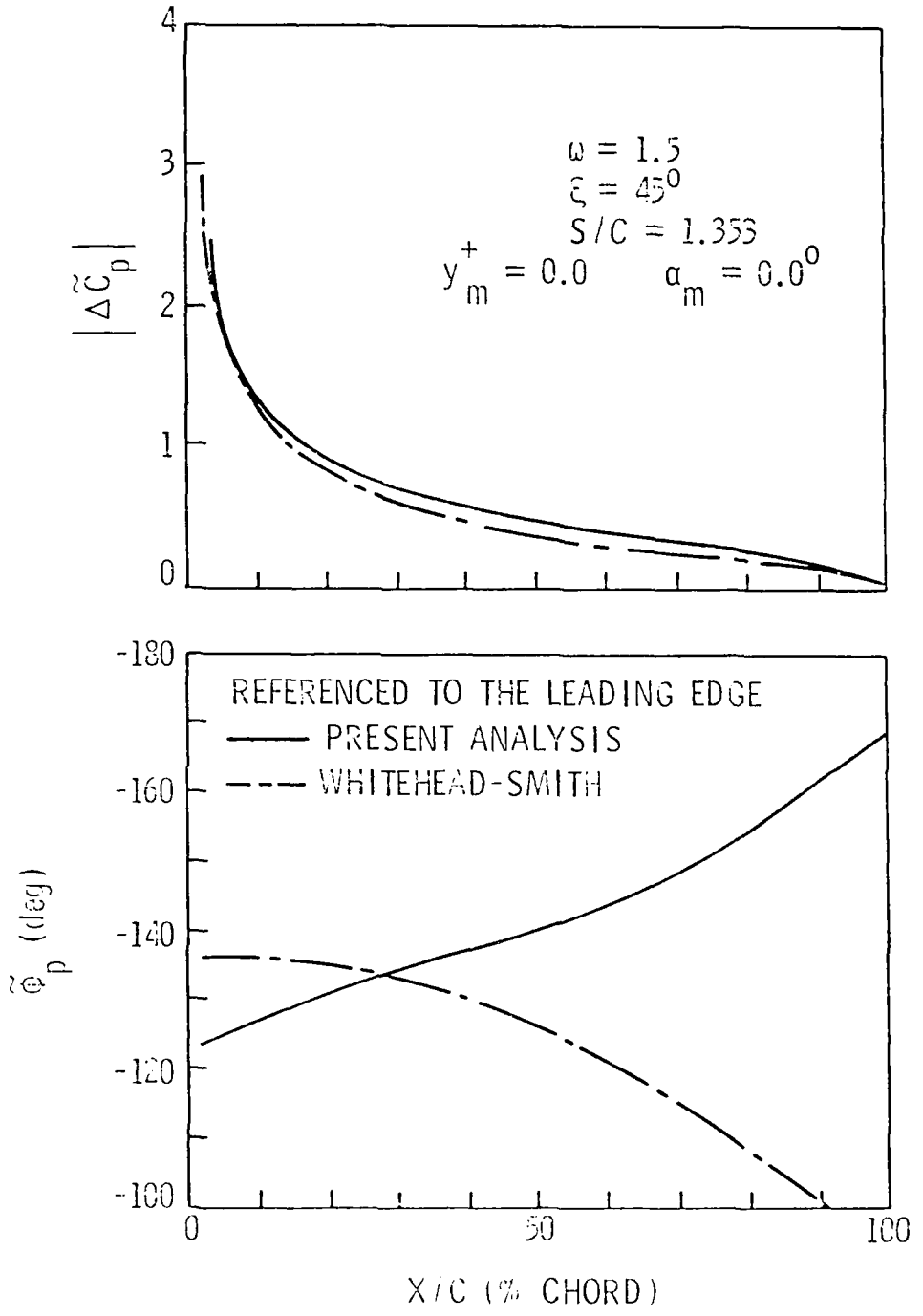

Figure 13. Comparison of Theoretical Unsteady Pressure Distribution with ξ = 45°, s/c = 1.353, and ω = 1.5.

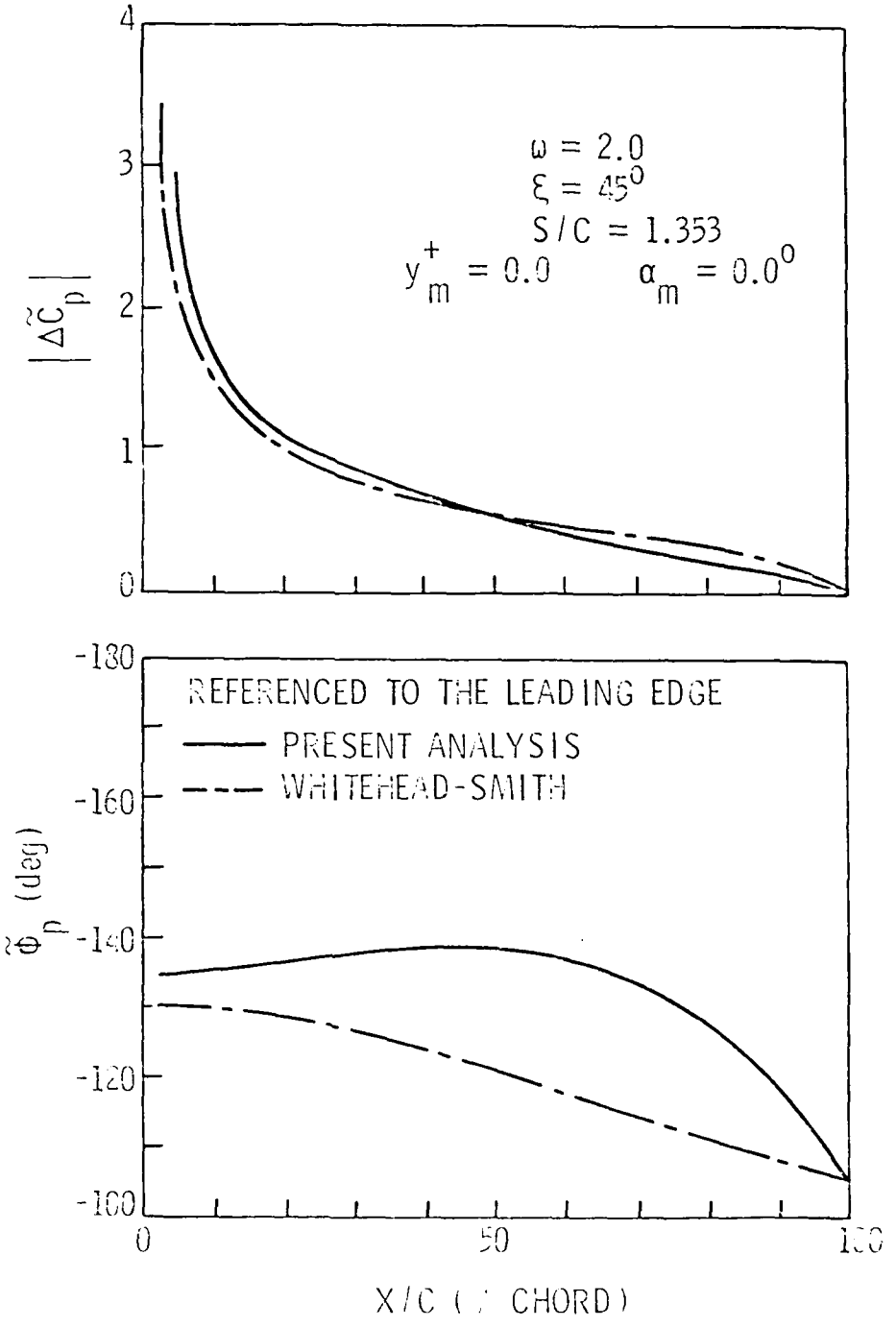

Figure 11. Comparison of Theoretical Pressure Distribution with [illegible]

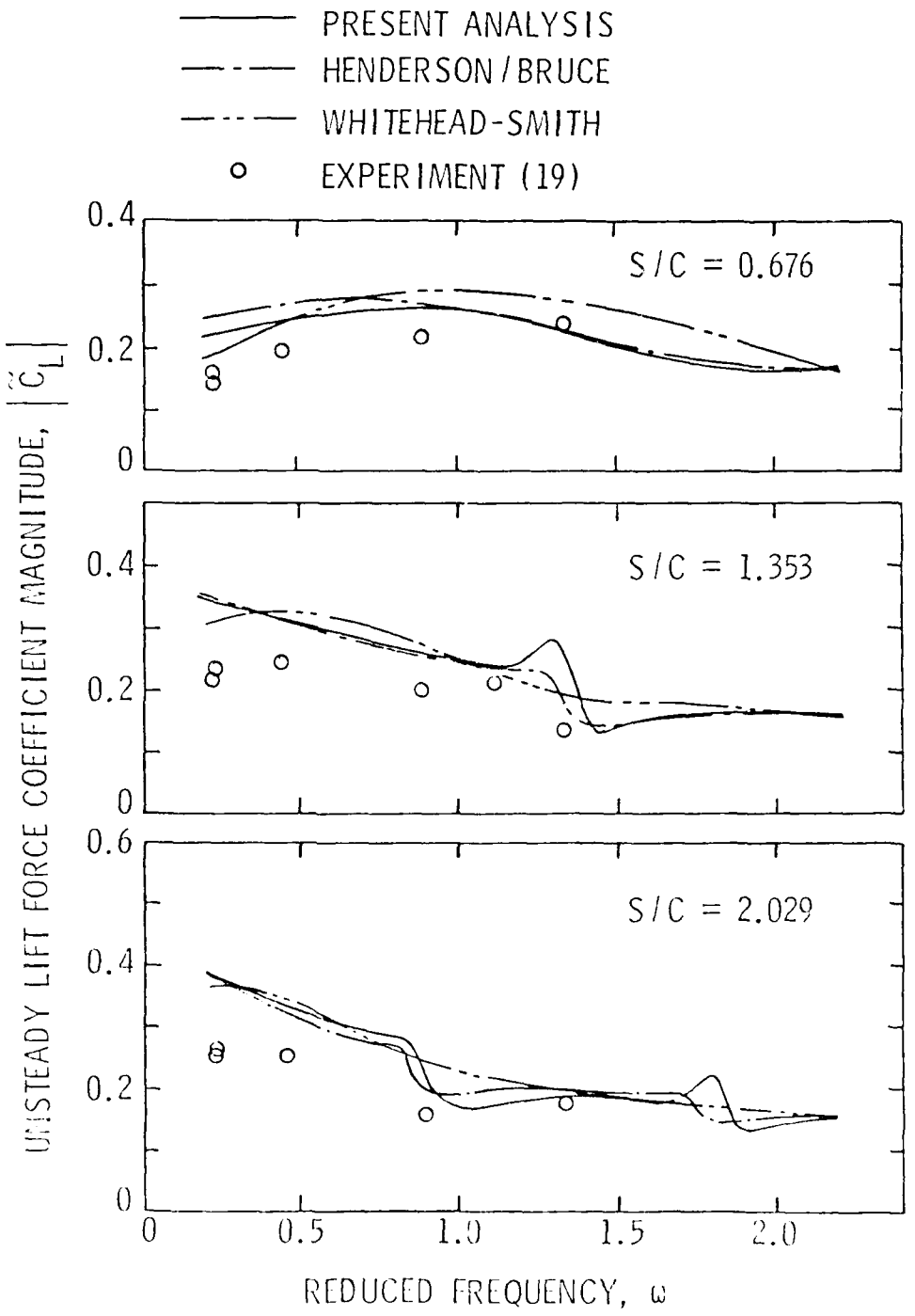

Figure 7. Comparison of Experimental and Theoretical Unsteady Lift Force Coefficients with $\epsilon_m = \psi_m^+ = 0$ and $\beta = 45^\circ$.

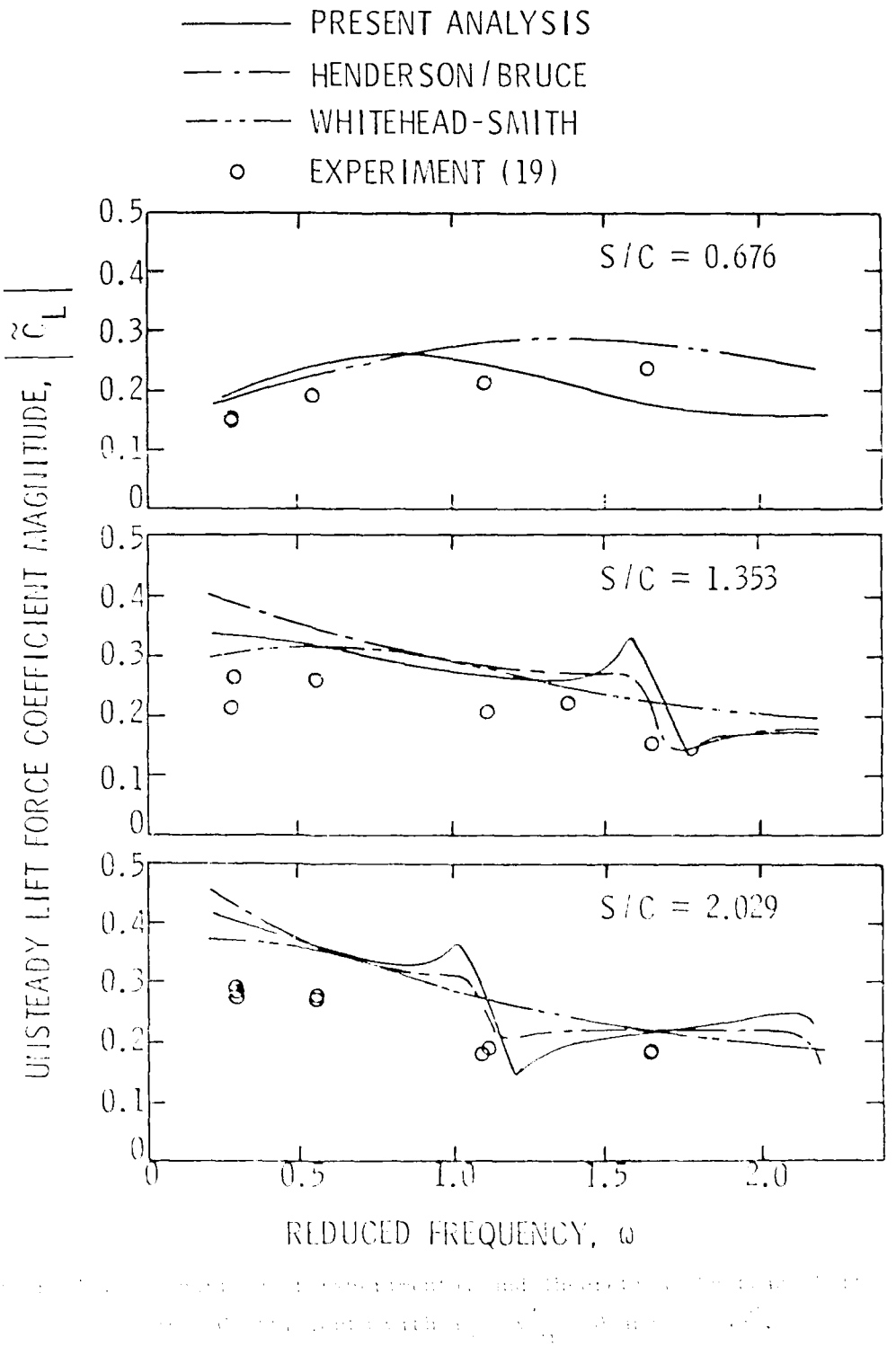
PRESENT ANALYSIS
HENDERSON / BRUCE
WHITEHEAD-SMITH
EXPERIMENT (19)
S/C = 0.676
S/C = 1.353
S/C = 2.029
UNSTEADY LIFT FORCE COEFFICIENT MAGNITUDE, $|\tilde{C}_L|$
REDUCED FREQUENCY, ω
0
0.1
0.2
0.3
0.4
0.5
0.5
1.0
1.5
2.0

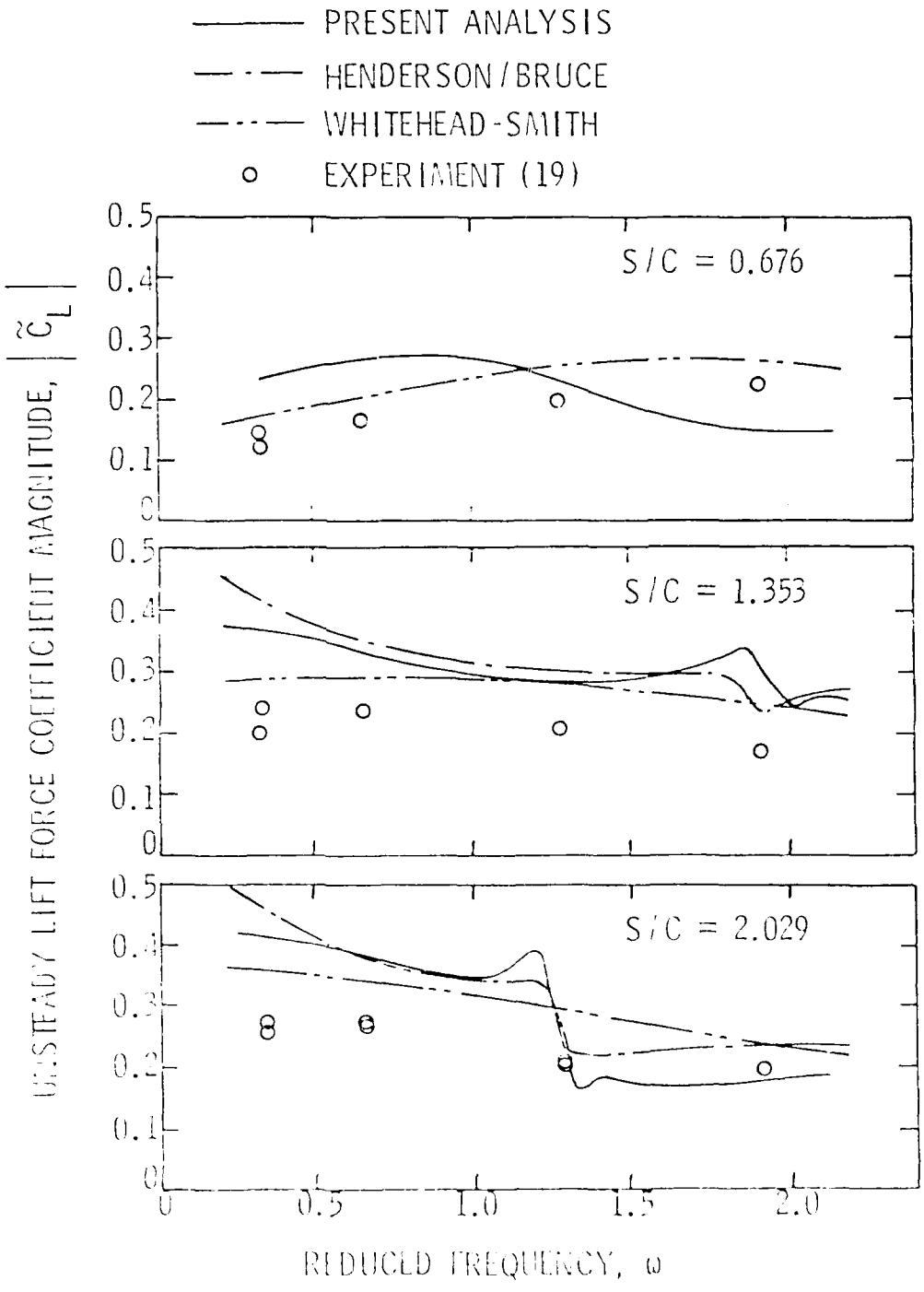
PRESENT ANALYSIS
HENDERSON / BRUCE
WHITEHEAD - SMITH
EXPERIMENT (19)
S/C = 0.676
S/C = 1.353
S/C = 2.029
UNSTEADY LIFT FORCE COEFFICIENT MAGNITUDE, $|\tilde{C}_L|$
REDUCED FREQUENCY, ω
0.5
0.4
0.3
0.2
0.1
0
0.5
1.0
1.5
2.0

AD-A091 173 PENNSYLVANIA STATE UNIV UNIVERSITY PARK APPLIED RESE--ETC F/G 20/4
UNSTEADY PRESSURE DISTRIBUTIONS ON AIRFOILS IN CASCADE.(U)
APR 80 I SHEN N00024-79-C-6043
UNCLASSIFIED ARL/PSU/TM-80-45 NL

2 OF 2
AD
A091173

END
DATE FILMED
12-80
DTIC

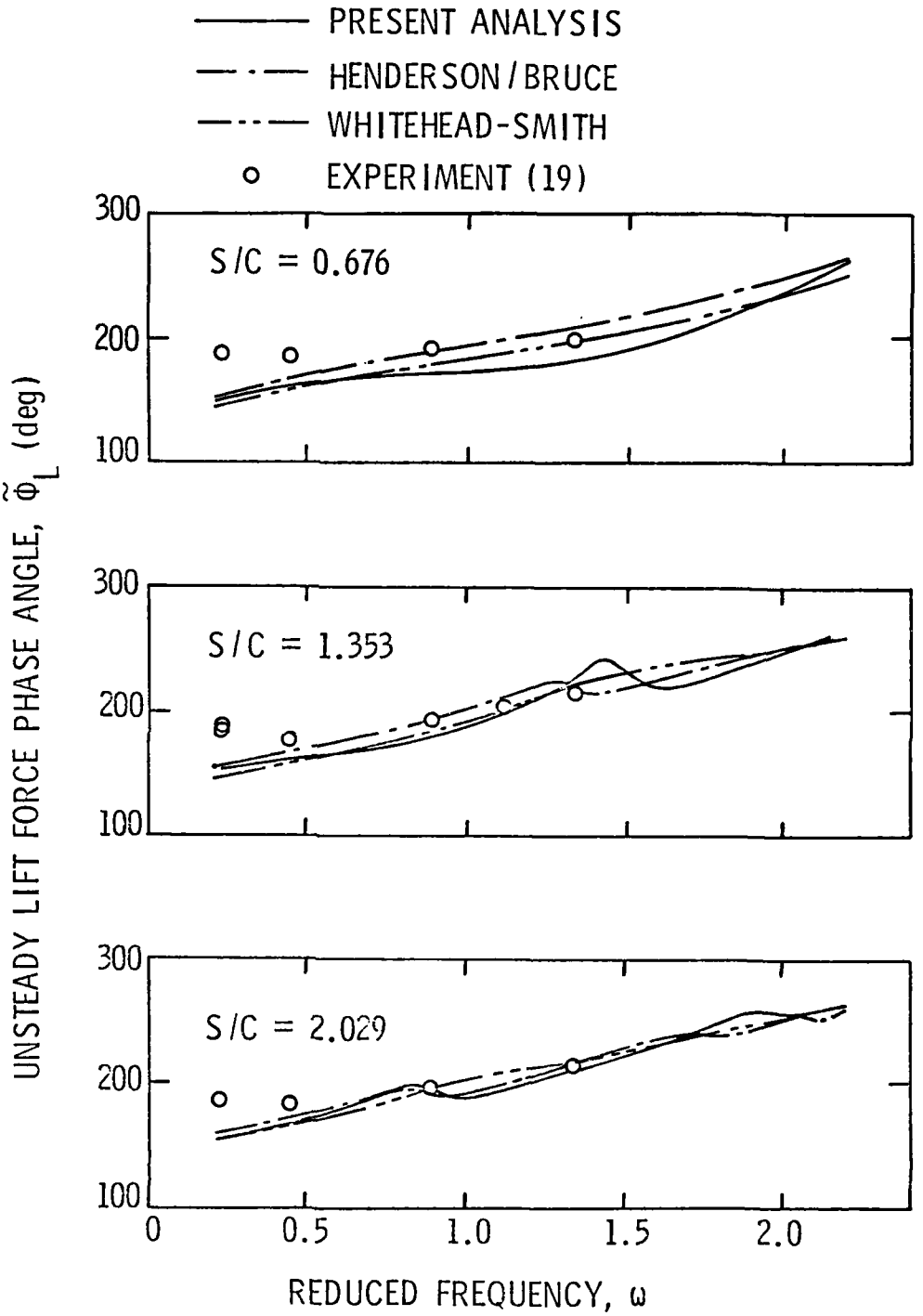

Figure 15. Comparison of Experimental and Theoretical Unsteady Lift Phase Angles with $\alpha_m = y^+_m = 0$ and $\xi = 35^o$.

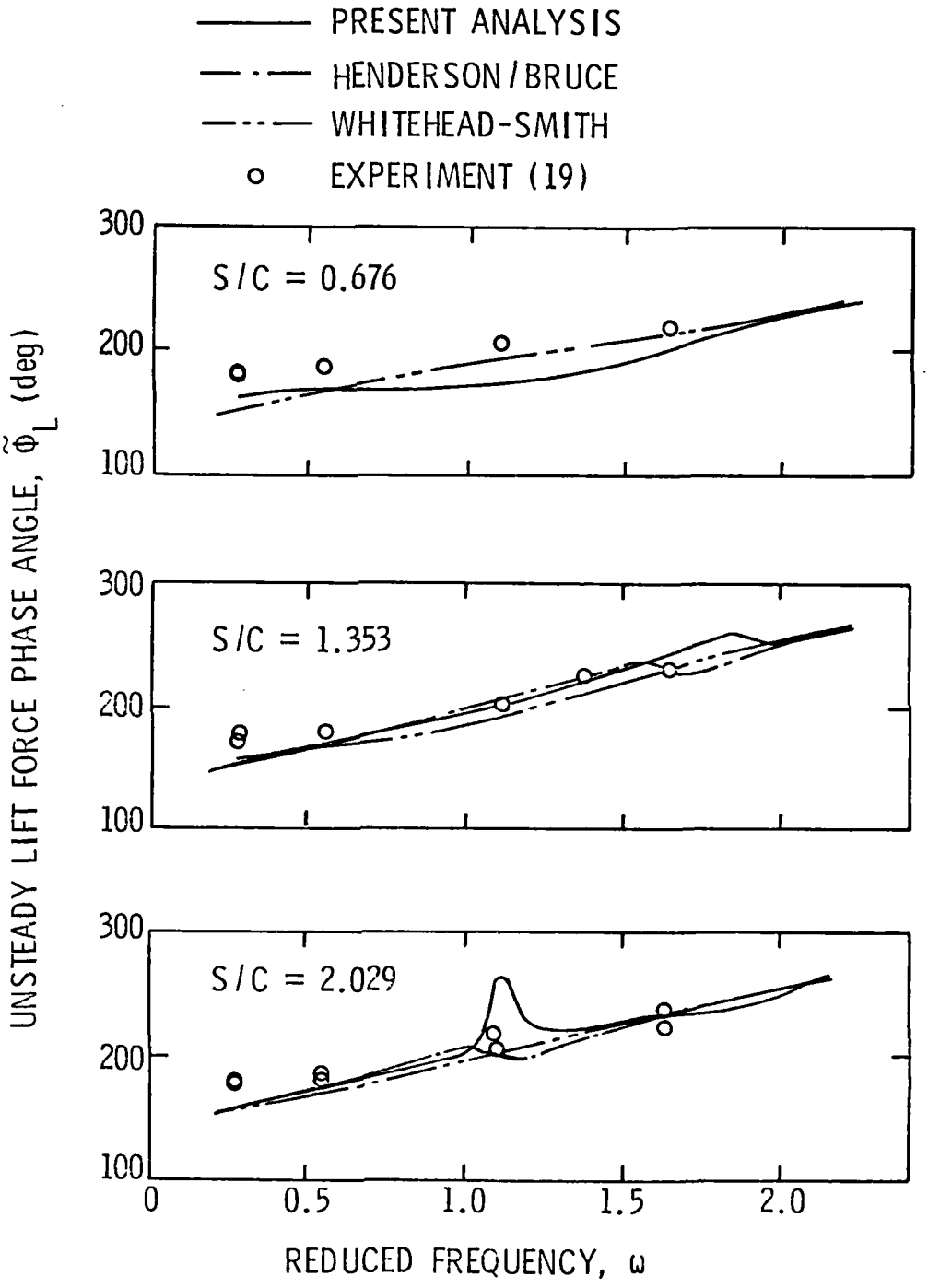

Figure 16. Comparison of Experimental and Theoretical Unsteady Lift Phase Angles with $\epsilon_m = y^+_m = 0$ and $\xi = 45^o$.

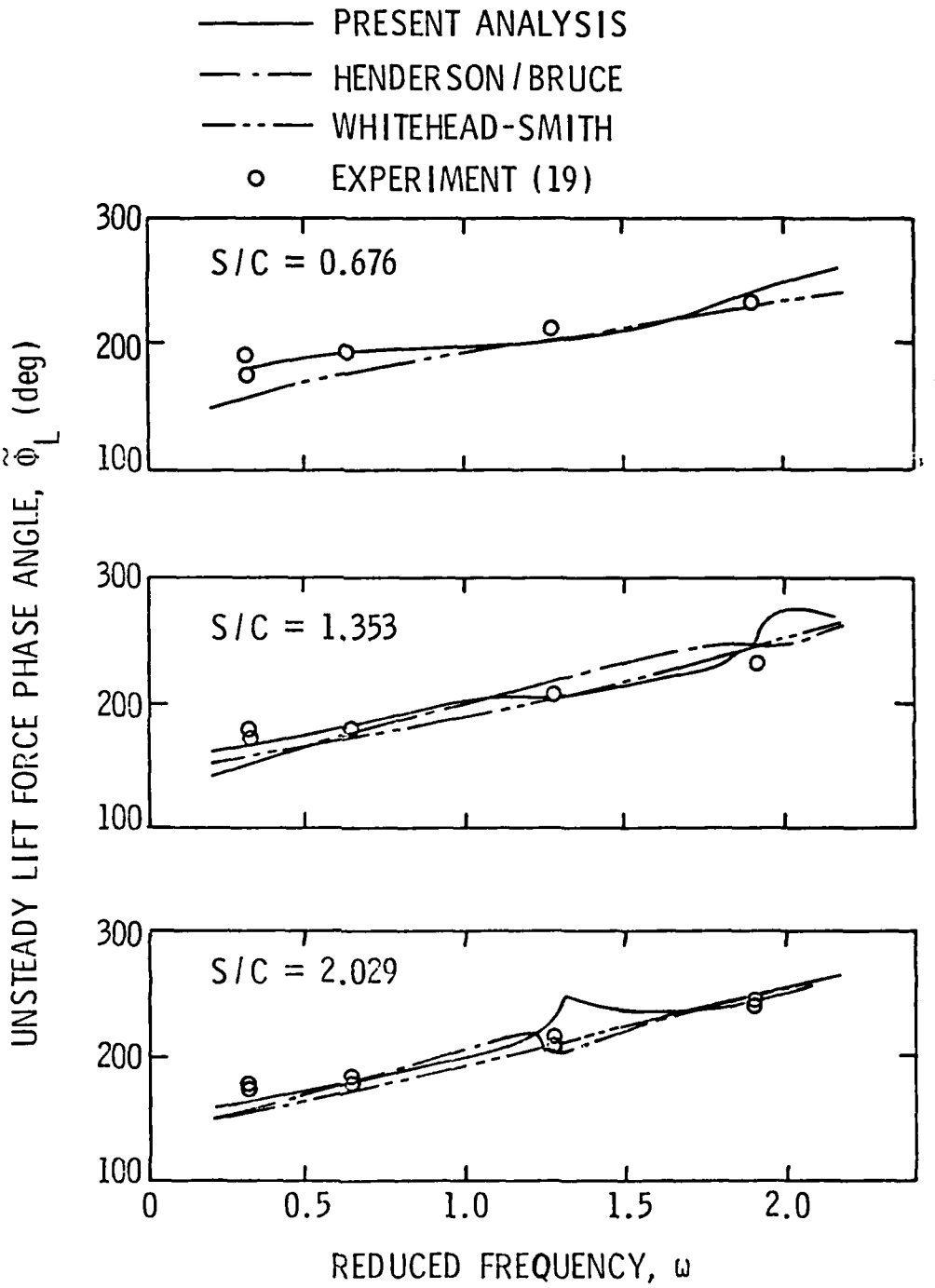

Figure 17. Comparison of Experimental and Theoretical Unsteady Lift Phase Angles with $\epsilon_m = y^+_m = 0$ and $\zeta = 55^o$.

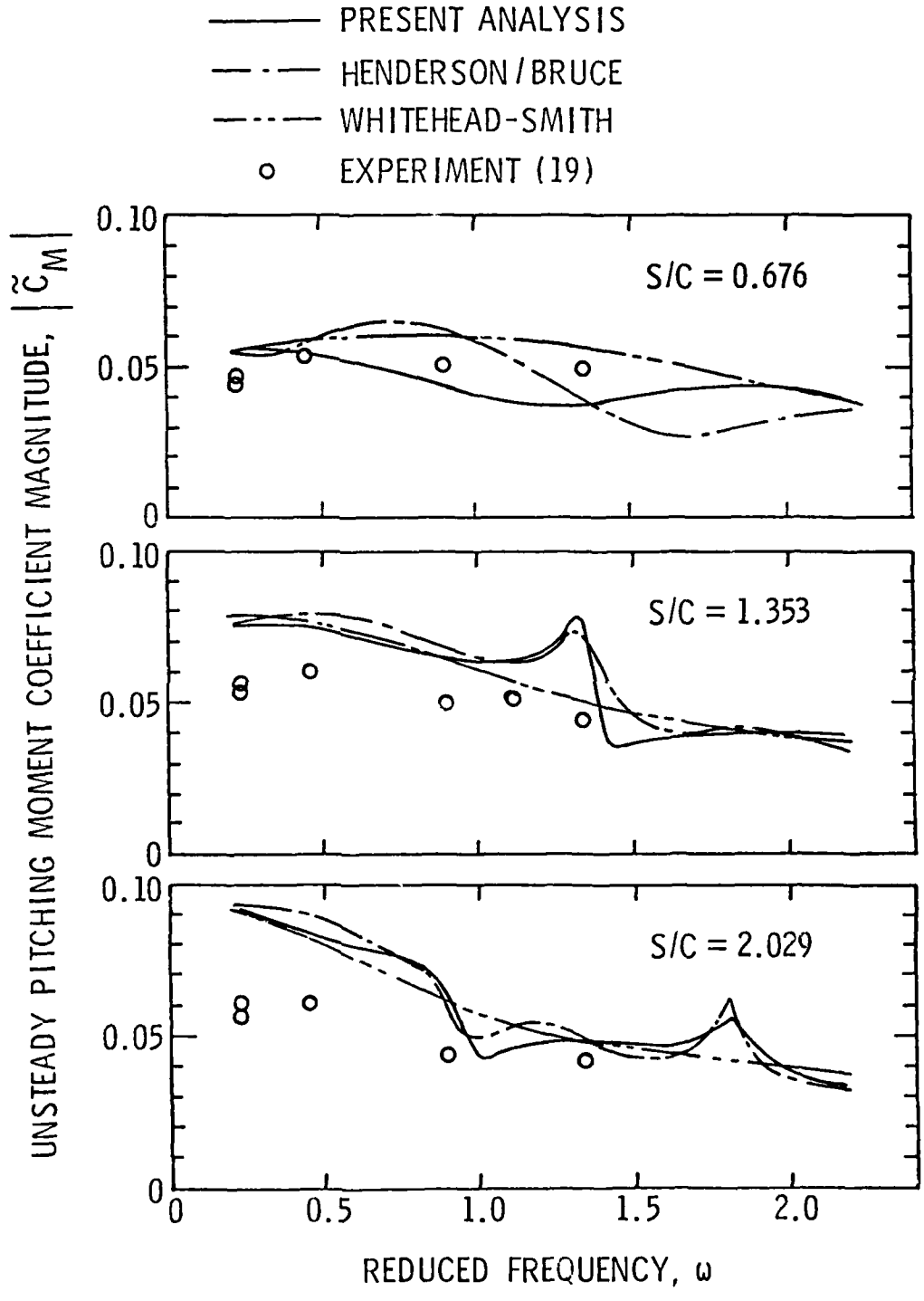

Figure 18. Comparison of Experimental and Theoretical Unsteady Pitching Moment Coefficients with $\epsilon_m = y^+_m = 0$ and $\xi = 35^o$.

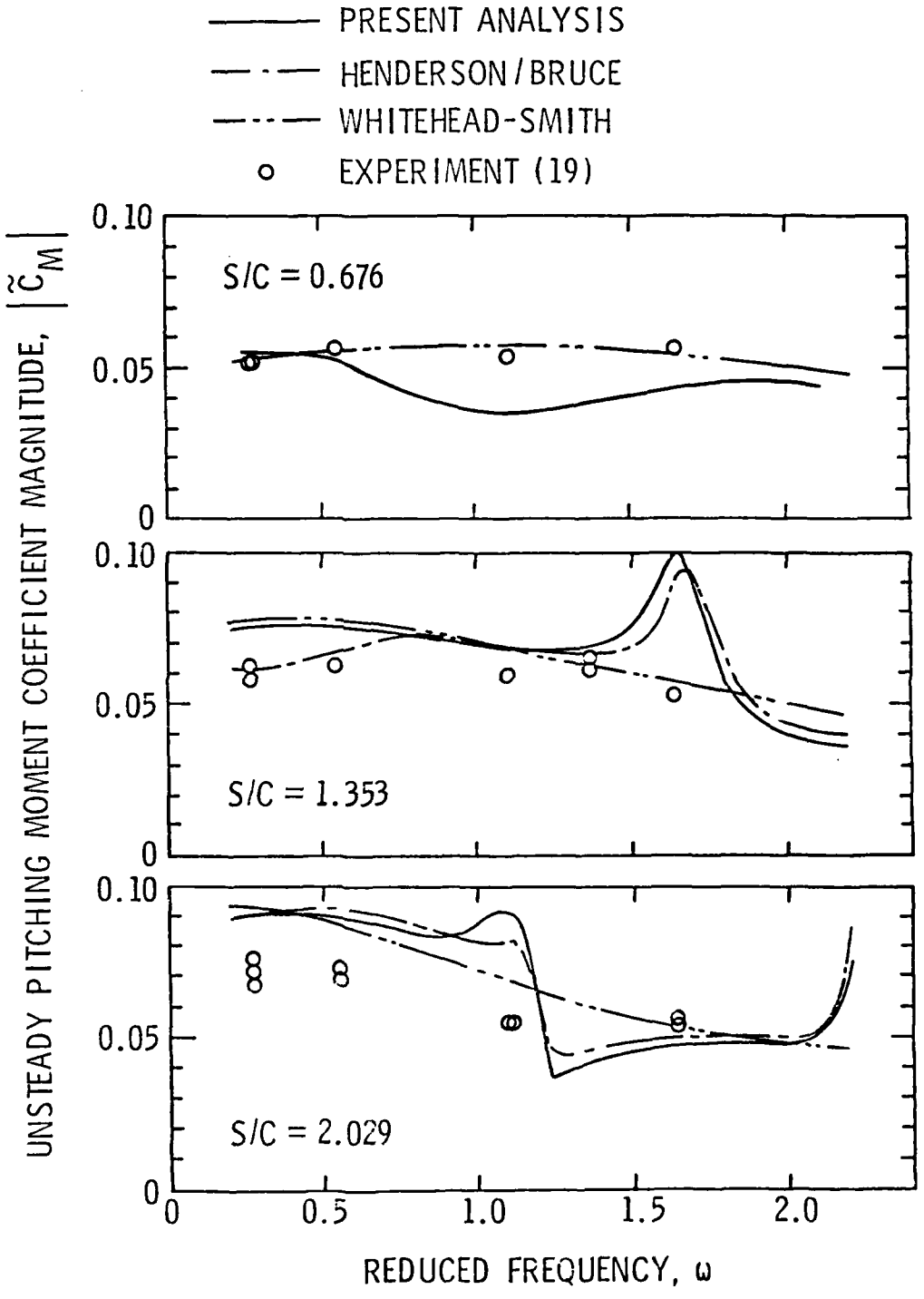

Figure 19. Comparison of Experimental and Theoretical Unsteady Pitching Moment Coefficients with $x_m = y^+_m = 0$ and $\zeta = 45^o$.

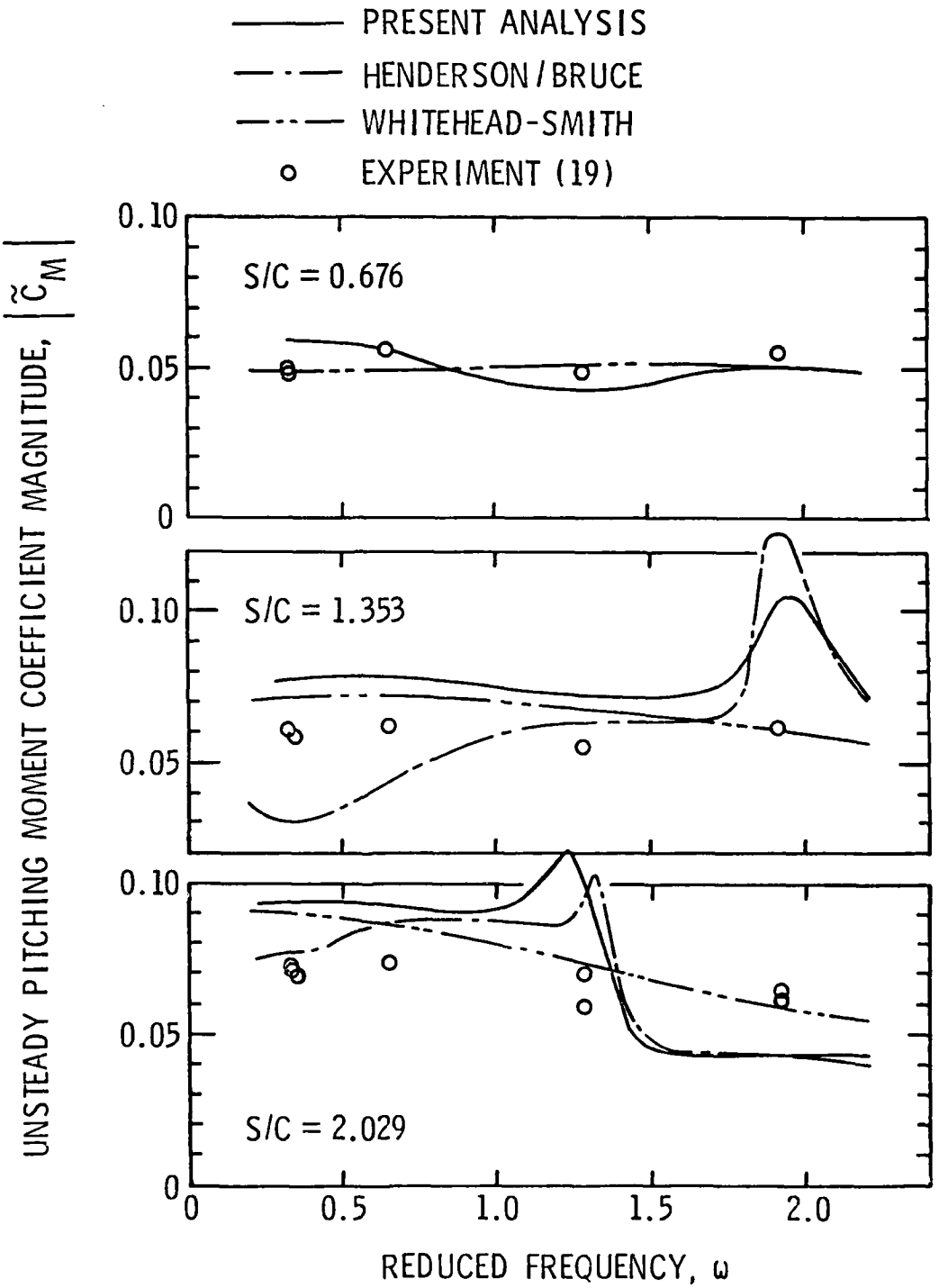

Figure 20. Comparison of Experimental and Theoretical Unsteady Pitching Moment Coefficients with $x_m = y^+_m = 0$ and $\xi = 55^o$.

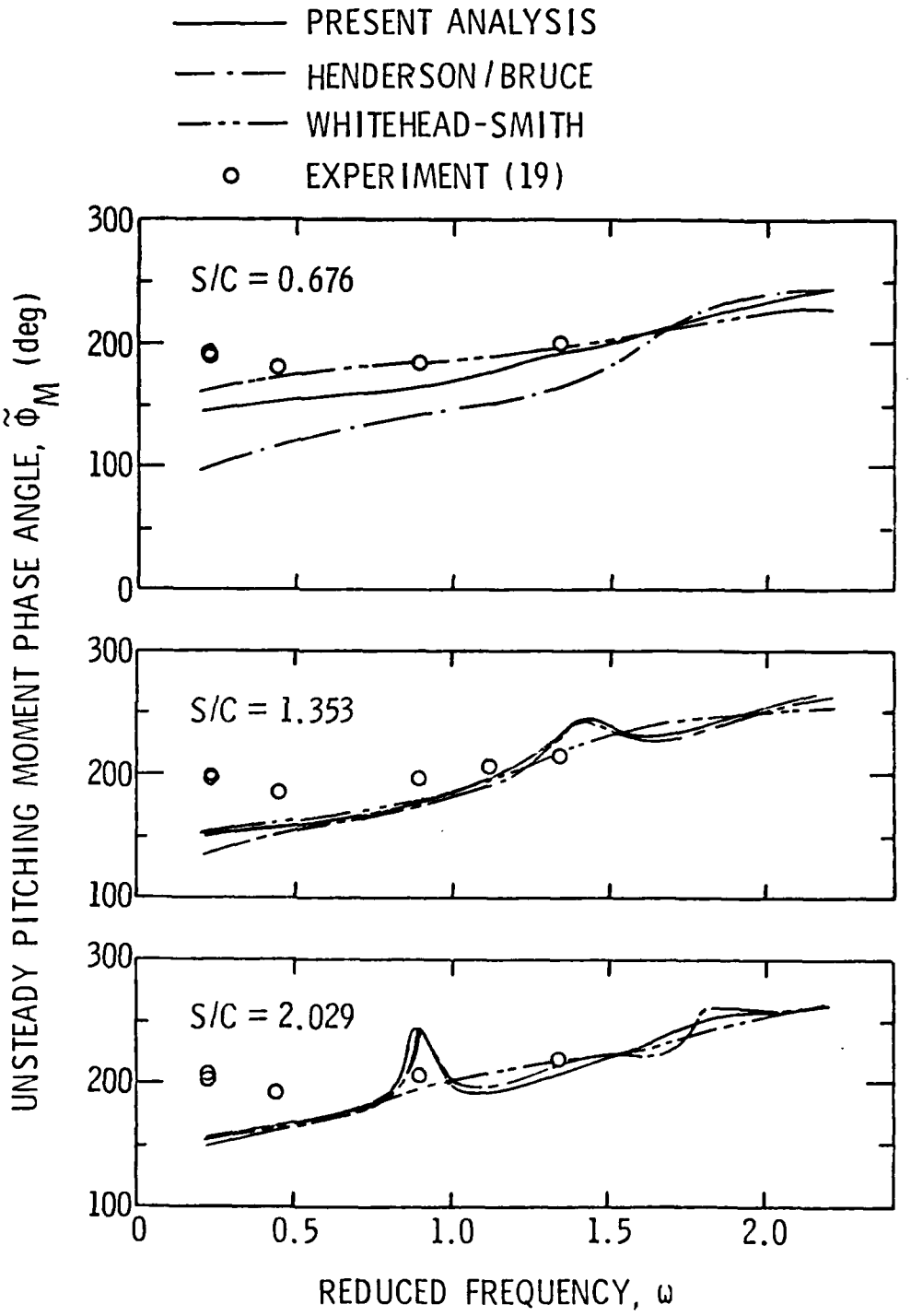

Figure 21. Comparison of Experimental and Theoretical Unsteady Pitching Moment Phase Angles with $x_m + y^+_m = 0$ and $\zeta = 35^o$.

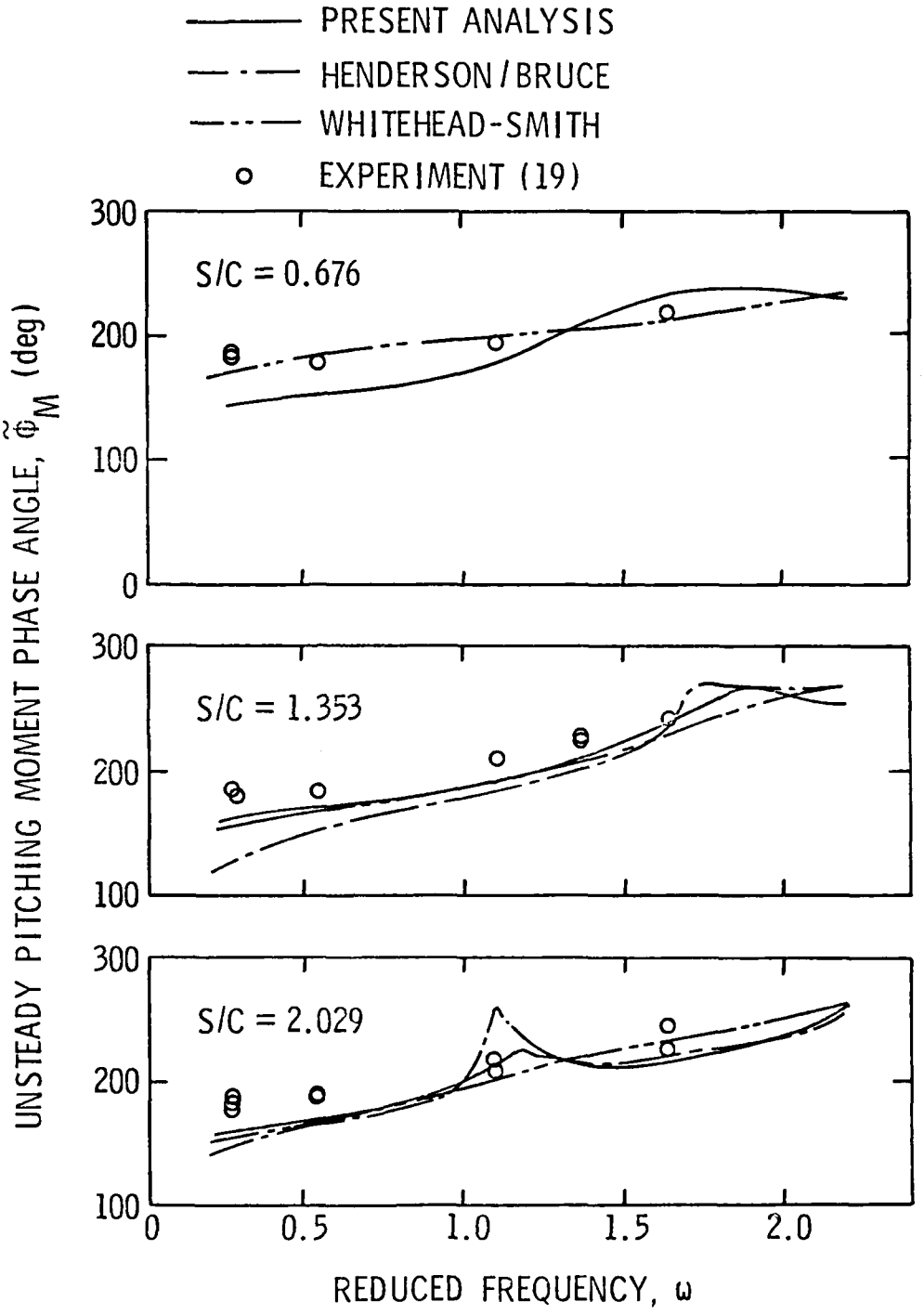

Figure 22. Comparison of Experimental and Theoretical Unsteady Pitching Moment Phase Angles with $\epsilon_m = y^+_m = 0$ and $\gamma = 45^o$.

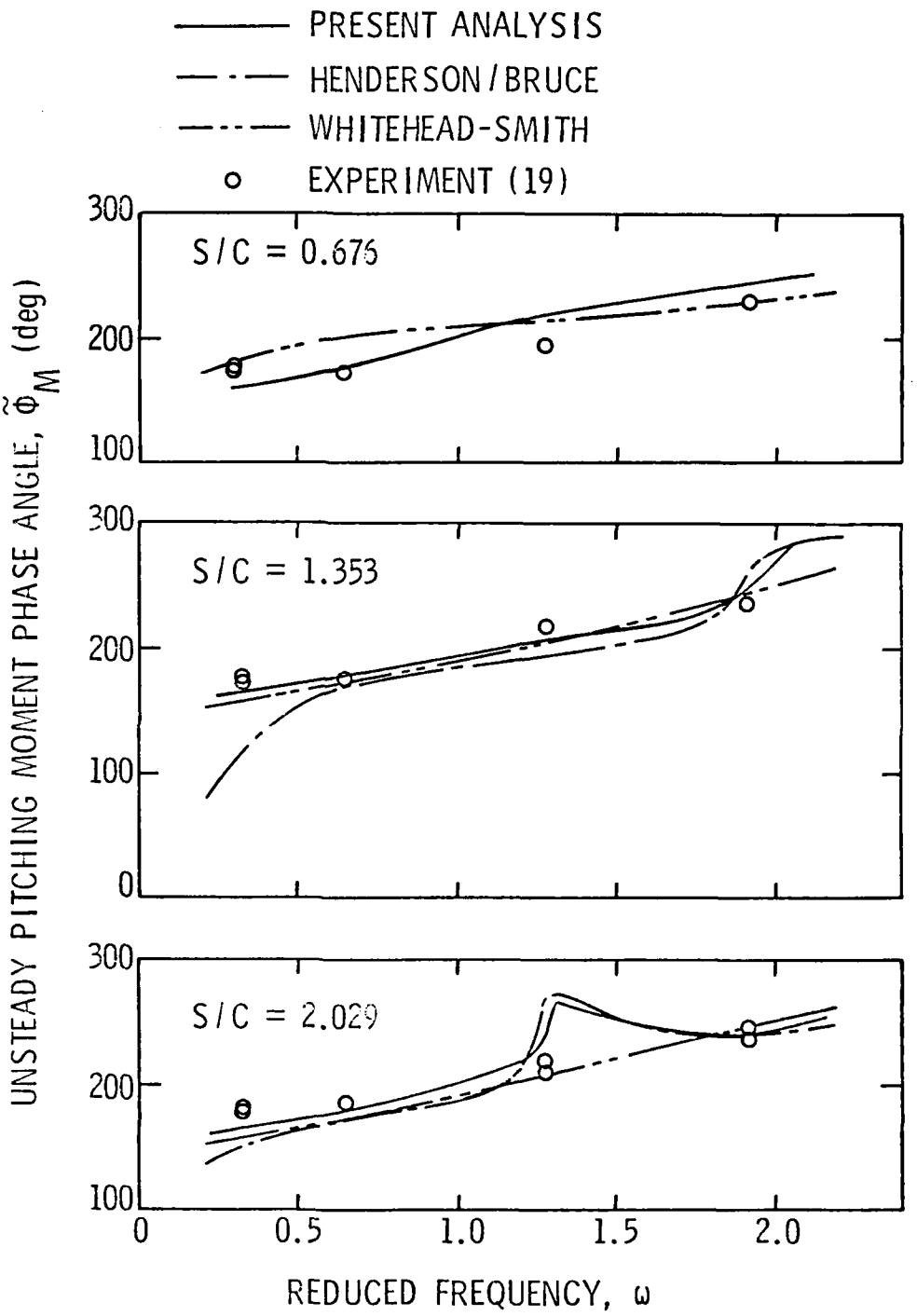

Figure 23. Comparison of Experimental and Theoretical Unsteady Pitching Moment Phase Angles with $\epsilon_m = y^+_m = 0$ and $\zeta = 55^o$.

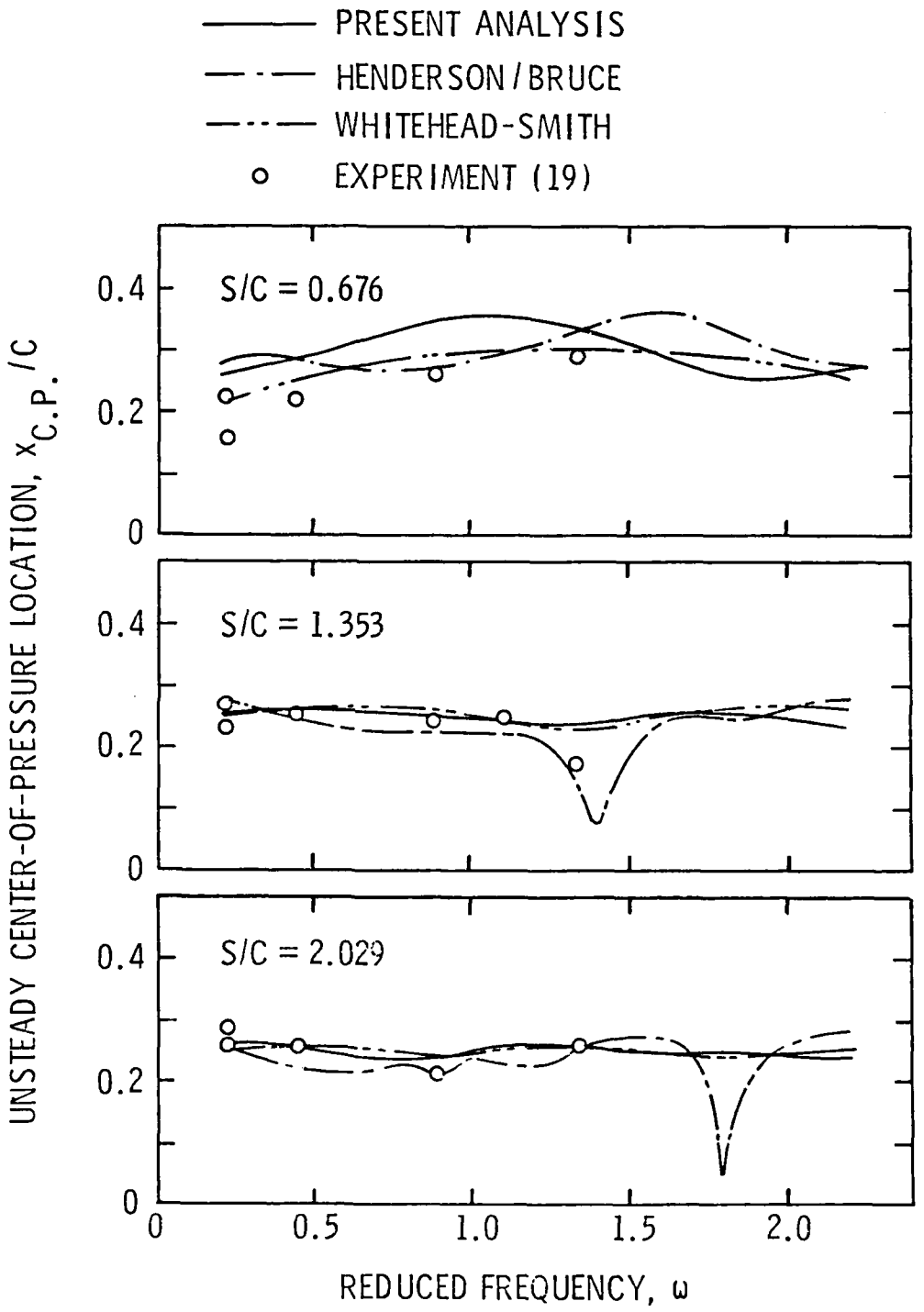

Figure 24. Comparison of Experimental and Theoretical Unsteady Center-of-Pressure Location with $\epsilon_m = y^+_m = 0$ and $\delta = 35^o$.

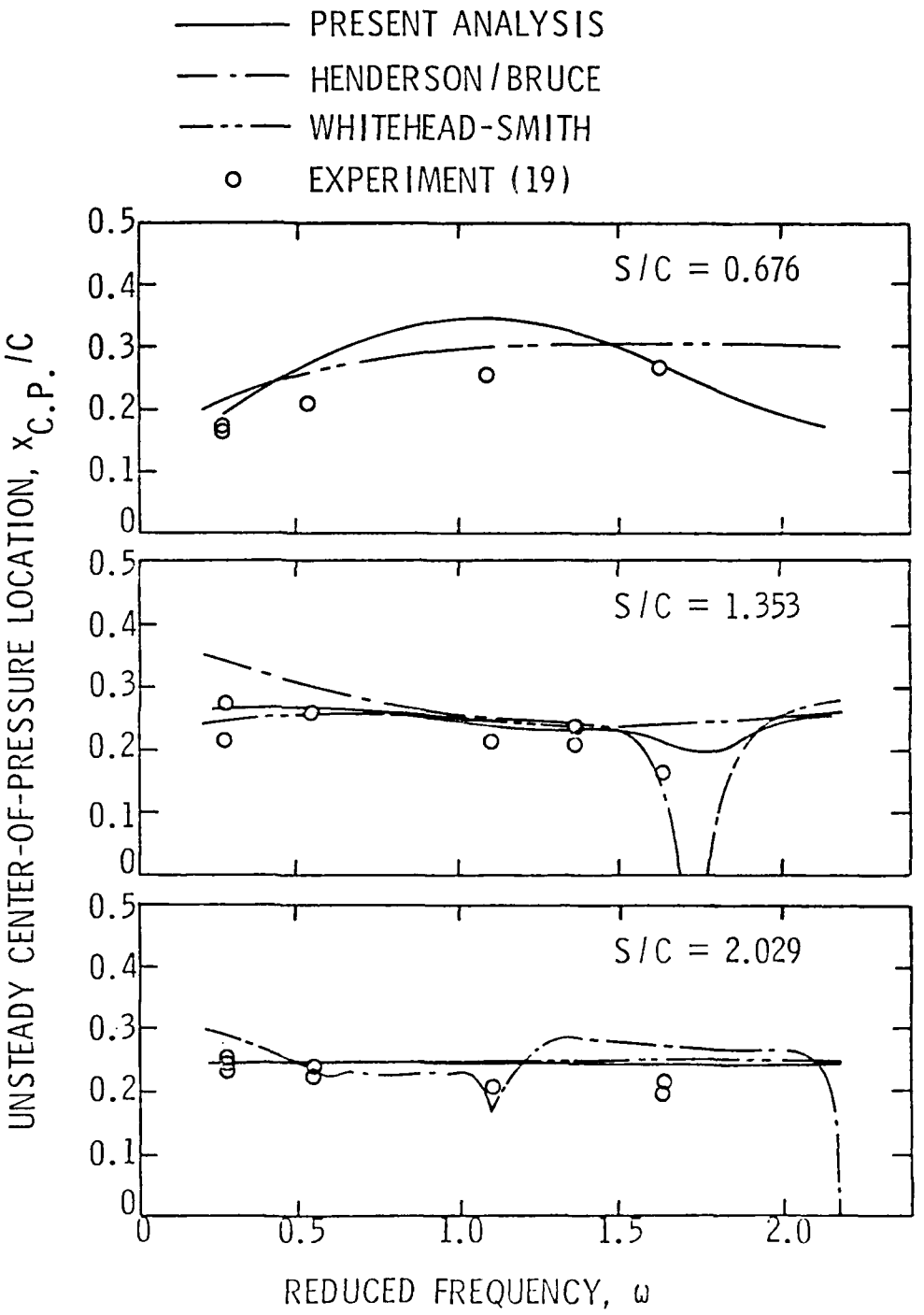

Figure 25. Comparison of Experimental and Theoretical Unsteady Center-of-Pressure Location with $\epsilon_m = y^+_m = 0$ and $\gamma = 45^\circ$.

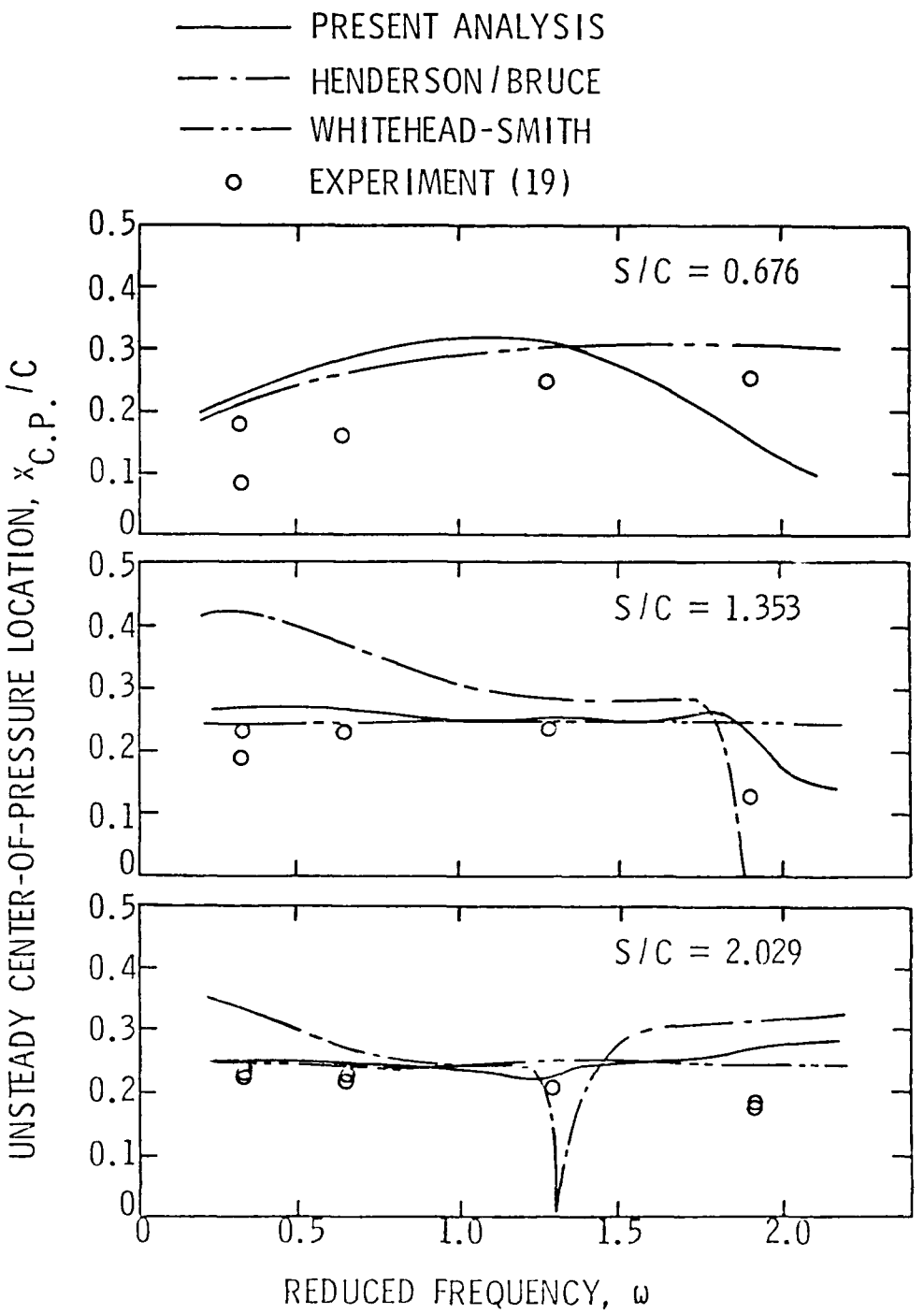

Figure 26. Comparison of Experimental and Theoretical Unsteady Center-of-Pressure Location with $\epsilon_m = \gamma^+_m = 0$ and $\gamma = 55^o$.

reduced frequency ω becomes close to a value of $\omega = 1.642$. Near this value of ω, the present analysis and Henderson's theory indicate significant changes in both the magnitude and phase angle of the unsteady lift coefficients, and a great discrepancy is observed between the present analysis and the Whitehead-Smith theory in the trend of the predicted variations of $\tilde{\phi}_p$.

These critical values of ω occur when the cascade inflow conditions become such that the spacing between blades s is equal to the wavelength of the distorted inflow ξ or an integer multiple of this wavelength, that is, the value of intra-blade frequency τ defined by Equation (11) approaches a multiple of 2π. Henderson (18) has classified these critical values of ω as "resonance" points and suggested a physical interpretation based on the phase-angle difference from blade to blade as follows. A basic assumption is that the vorticity and, as a result, the circulation on the n^{th} blade differs from that on the reference blade by a phase angle $n\tau$. When the "resonance" condition occurs, the vorticity and circulation on all blades and their wakes are in-phase and their contributions to the unsteady response of the reference blade tend to accumulate and, hence, result in significant changes in unsteady cascade performance. The specific values of ω where the resonances occur can be determined from Equation (13) by assuming $\tau = 2k\pi$, k = 1, 2, 3, ... For this cascade geometry of $\xi = 45^{\circ}$ and s/c = 1.353, the corresponding reduced frequencies are $\omega = 1.642k$.

As shown in Figures 12 through 26, the Whitehead-Smith theory does not predict the existence of these resonance conditions. Henderson attributed this to the use of a limit value of τ, $-2\pi < \tau < 0$ in Whitehead-Smith's computation, for the summation of induced velocities

due to all the blades in the cascade. While the Whitehead-Smith analysis computes unsteady response at the resonance points corresponding to $\tau = -2k\pi$, it does not provide a correct mathematical solution.

The values $|\tilde{C}_L|$, $|\tilde{C}_M|$, ϕ_L, and ϕ_M predicted by the present analysis as shown in Figures 12 through 26 are, in general, in good agreement with those calculated by Bruce. Near the "resonance" points, these quantities representing results of both methods undergo significant changes in their levels, but the present analysis predicts a wider range of influence of "resonance" and a greater level of variations. Another difference between these two methods is that in the region of lower values of ω, that is, $\omega < 0.5$, the cascade performance predicted by the present analysis tends to behave as that given by the Whitehead-Smith theory.

Theoretically, for an error-free solution, the results predicted using either the present analysis or Henderson and Bruce's theory should be identical. There is a good reason to believe that these differences can be contributed to computational errors introduced during numerical integrations of the finite summations and are the result of taking only a finite number of terms. However, the similarity between the solutions given by the present analysis and Whitehead-Smith may not be coincidental and should be examined.

The present analysis predicts the resonance, for example, by $|\tilde{C}_L|$ and $|\tilde{C}_M|$ with somewhat of a "lagging" effect as compared to Bruce's calculation. This fact is also demonstrated by the parameter $x_{C.P.}/c$ as shown in Figures 24, 25, and 26 where the present analysis gives a solution similar to that of Whitehead-Smith, although it decreases in

value near resonance points. The abrupt changes in the location of unsteady center-of-pressure obtained by Bruce are not observed.

On the whole, these predictions of unsteady response parameters by the present analysis are in good agreement with predictions based on the expressions of unsteady lift and pitching moment derived by Henderson and Bruce and are similar to the solutions by the Whitehead-Smith theory except in the neighborhood of critical reduced frequencies.

For the comparison of measured and predicted data, conclusions similar to those obtained by Bruce can be drawn. One of these is that the theories, in general, tend to overpredict the magnitude of unsteady response, that is, $|\tilde{C}_L|$ and $|\tilde{C}_M|$. This characteristic is attributed to the flow viscosity and blade thickness effects. Another conclusion is that the Whitehead-Smith model predicts a better overall unsteady cascade performance, especially the trends of variation of $|\tilde{C}_L|$ with ω very small, even though it does not follow the changes in the level of $|\tilde{C}_L|$ shown by the data in the neighborhood of critical reduced frequencies. The most significant agreement in measured and predicted data for $\tilde{\phi}_L$ and $\tilde{\phi}_M$ is observed in Figures 15 through 17 and 21 through 23 where these phase angles obtained using the present analysis show quite accurate predictions. The measured data for $x_{C.P.}/c$ also follows well the predictions by the present analysis as shown in Figures 24, 25, and 26.

As opposed to the Whitehead-Smith model which provides performance prediction based on $\alpha_m = y^+_m = 0$, the theoretical model employed in this analysis can include the effects of mean incidence angle and camber. Bruce obtained measured data for various values of α_m but no experimental information as to the effect of y^+_m. By comparing the measured and predicted data, he showed that the trends of variation of unsteady

response varying with different values of α_m are in agreement. The effects of blade camber were not evaluated because of the lack of experimental data. The effects of mean incidence angle and blade camber predicted by the present analysis will be presented in the next section.

In a recent publication by Gallus et al. [20], the results of measurements of the fluctuating force in an axial flow compressor are presented. A series of dynamic transducers are mounted along the midspan of a stator blade located downstream of a rotor as shown in Figure 27. This is a case in which the stator blade row interacts with moving rotor wakes. Therefore, the theoretical analysis developed in this study can be applied to this flow situation by virtue of relation motion.

The shape of wakes originating from the trailing edge of the rotor blades is measured by the use of a rotating three-hole probe continuously shifted along one spacing behind the rotor as is also shown in Figure 27. It is assumed the velocity distribution in the wake can be described by two parameters h and b/s using the empirical equation

$$\frac{W}{W_{max}} = 1 - h \exp\left(-16\left(\frac{y/s}{b/s}\right)^2\right) \quad . \tag{46}$$

This relationship is shown in Figure 28.

The predicted unsteady pressure coefficient obtained from the present analysis is expressed in terms of pressure difference. A direct comparison of these predictions with the measured data of Reference [20] is not practical, however, because of the staggered chordwise location of the transducers on opposite sides of the stator blade. However, Gallus et al. are able to obtain the unsteady lift by integrating the

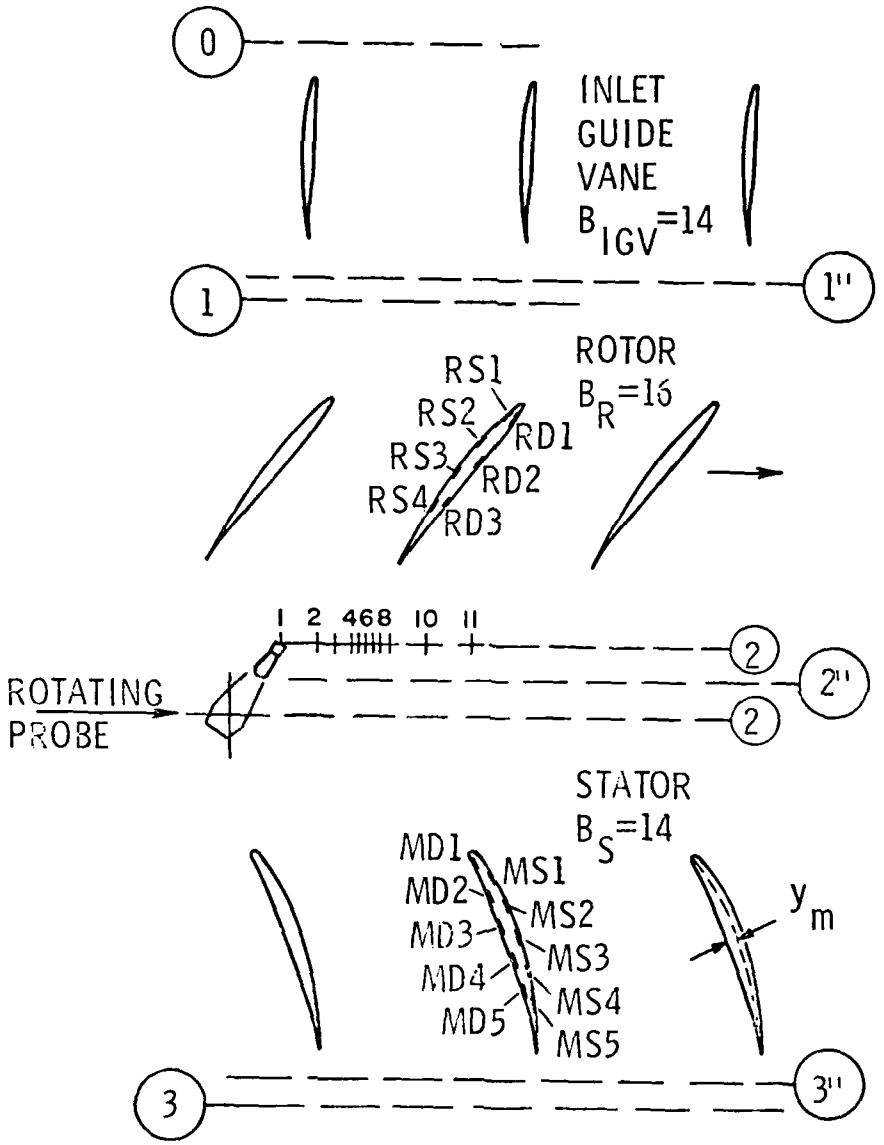

Figure 27. Measuring Positions in the Midspan Section of the Compressor in the Experiment by Gallus et al. (22).

measured pressure distribution, Figure 40 in Reference (20). The present analysis can also determine the unsteady lift for comparison.

At a speed of 6,500 rpm for the rotor and a flow coefficient $\phi = 0.8$ or 0.7, the probe measurement yields the wake shape for which $b/s_R = 0.3$ and 0.4 and $W_{min}/W_{max} = 0.9$ and 0.85, respectively. The flow conditions and cascade geometry tested are listed in Table 2. The flow is incompressible since the Mach number is less than 0.3. The wake profile can then be obtained using Equation (46) and decomposed into harmonic components by the aid of Fourier analysis. Since a cosine series is employed to describe the symmetrical velocity profile for the coordinate system shown in Figure 28, the phase angle of each harmonic component is zero. Thus, for $\phi = 0.8$,

$$\frac{W}{W_{max}} = \frac{\bar{W}}{W_{max}} + \sum_{k=1}^{\infty} A_k \cos\left(2\pi k\left(\frac{y}{s}\right)\right)$$

$$\doteq \left(1 - \frac{\sqrt{\pi}}{4} h\left(\frac{b}{s}\right)\right) - \frac{\sqrt{\pi}}{2} n\left(\frac{b}{s}\right) \sum_{k=1}^{\infty} \exp\left(-\left(\frac{b}{s}\right)^2\left(\frac{\pi}{2}\right)^2 k^2\right) \cos\left(2\pi k\left(\frac{y}{s}\right)\right)$$

$$= 0.9870 - 0.02129 \cos\left(2\pi \frac{y}{s}\right) - 0.01094 \cos\left(4\pi \frac{y}{s}\right)$$

$$- 0.00360 \cos\left(6\pi \frac{y}{s}\right) - 0.00076 \cos\left(8\pi \frac{y}{s}\right)$$

$$- 0.00010 \cos\left(10\pi \frac{y}{s}\right) \ldots .$$

As an approximation, only the first five harmonics are employed to describe the wake profile. The unsteady response caused by each harmonic component is then calculated and summed to find the lift

Table 2

EXPERIMENTAL CONDITIONS OF GALLUS ET AL. (20)

Cascade Geometry
STATOR
$\frac{s}{c}$ = 0.9062 (s = 58.9 mm, c = 65 mm)
ξ = 18.06°
$\frac{y_m}{c/2}$ = 0.13

Operating Conditions	
CASE I	CASE II
$\phi = \frac{\bar{c}_x}{U} = 0.8$	$\phi = 0.7$
$\beta = 33.0^\circ$	$\beta = 35.0^\circ$
$\alpha_m = -3.4^\circ$	$\alpha_m = 1.3^\circ$
$\omega = 3.219$	$\omega = 3.392$

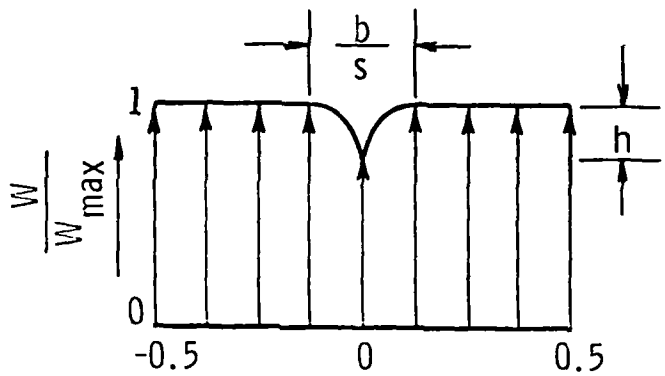

$$h = 1 - \frac{W_{min}}{W_{max}}$$

$$\frac{W}{W_{max}} = 1 - h \exp\left[-16 \left(\frac{y/s}{b/s}\right)^2\right]$$

Figure 28. Mathematical Representation of the Wake Profile.

fluctuation on the stator during one wavelength of the disturbance. The results of these calculations are listed in Table 3 and shown in Figures 29 and 30. Good agreement is observed between the predicted and measured results. This result represents a typical application of the present analysis and, therefore, an indirect verification of this theoretical model.

Satyanarayana (30) has studied the fluctuating lift on cascades at low reduced frequency to verify the validity of thin airfoil theory for cascades. His experiment is conducted in a specially designed gust tunnel which can generate flow disturbance by flexible metal sheets located on the upper and lower surfaces of the test section.

For this special flow situation in the cascade wind tunnel employed by Satyanarayana, the intra-blade frequency τ is related to the reduced frequency ω as $\tau = 2(s/c)\omega \sin \xi$. At the reduced frequency $\omega = 0.10$ and $\lambda = 0.22$, that is, a case where the flow disturbance is nonconvected, the comparison between his measured amplitude of unsteady lift and the values predicted by the present analysis is shown in Figure 31. In contrast to the experiment by Gallus et al. in which high reduced frequencies are considered, this represents data of unsteady lift in the region of low reduced frequency, and good agreement is observed.

4.3 Theoretical Predictions of the Effects of Mean Incidence Angle and Blade Camber on the Unsteady Response

An important feature of the present analysis is that the effects of mean incidence angle ϵ_m and blade camber y^+_m can be predicted. While the factors ϵ_m and y^+_m are second-order contributions to unsteady response as opposed to space-chord ratio s/c and stagger angle ξ, the

Table 3

PREDICTED UNSTEADY LIFT COEFFICIENTS FOR EACH HARMONIC COMPONENT FOR THE EXPERIMENTAL CONDITIONS OF TABLE 2

	k^{th} Harmonic	ω	$\lvert\tilde{C}_L\rvert$	$\tilde{\phi}_L$
CASE I $\phi = 0.8$	1	3.219	0.2624	308.79°
	2	6.438	0.1965	127.72°
	3	9.657	0.1556	307.21°
	4	12.876	0.1255	128.24°
	5	16.095	0.0950	330.50°
CASE II $\phi = 0.7$	1	3.392	0.2244	312.49°
	2	6.784	0.1386	142.93°
	3	10.176	0.1055	346.77°
	4	13.568	0.0963	187.59°
	5	16.960	0.0842	278.60°

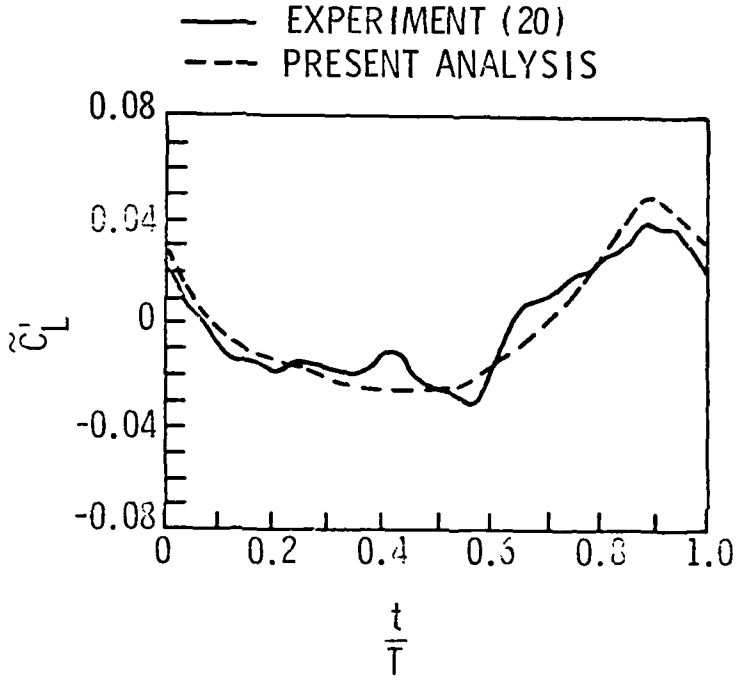

$$\tilde{C}_L' = \frac{\tilde{L}}{1/2\rho V^2 C}$$

Figure 29. Comparison of Predicted Lift Fluctuation with Measured Data for Flow Coefficient ϕ = 0.8 by Gallus et al.

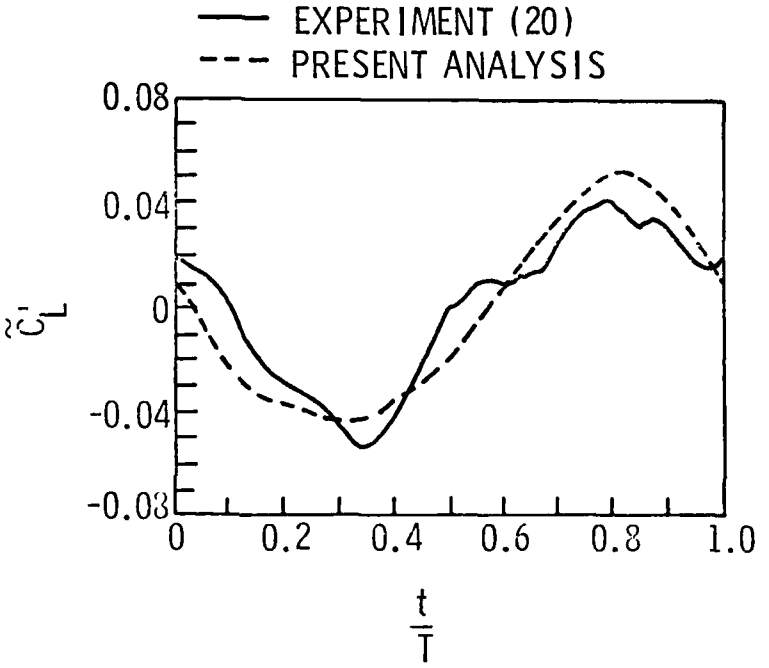

$$\tilde{C}_L' = \frac{\tilde{L}'}{1/2 \rho V^2 C}$$

Figure 30. Comparison of Predicted Lift Fluctuation with Measured Data for Flow Coefficient $\phi = 0.7$ by Gallus et al.

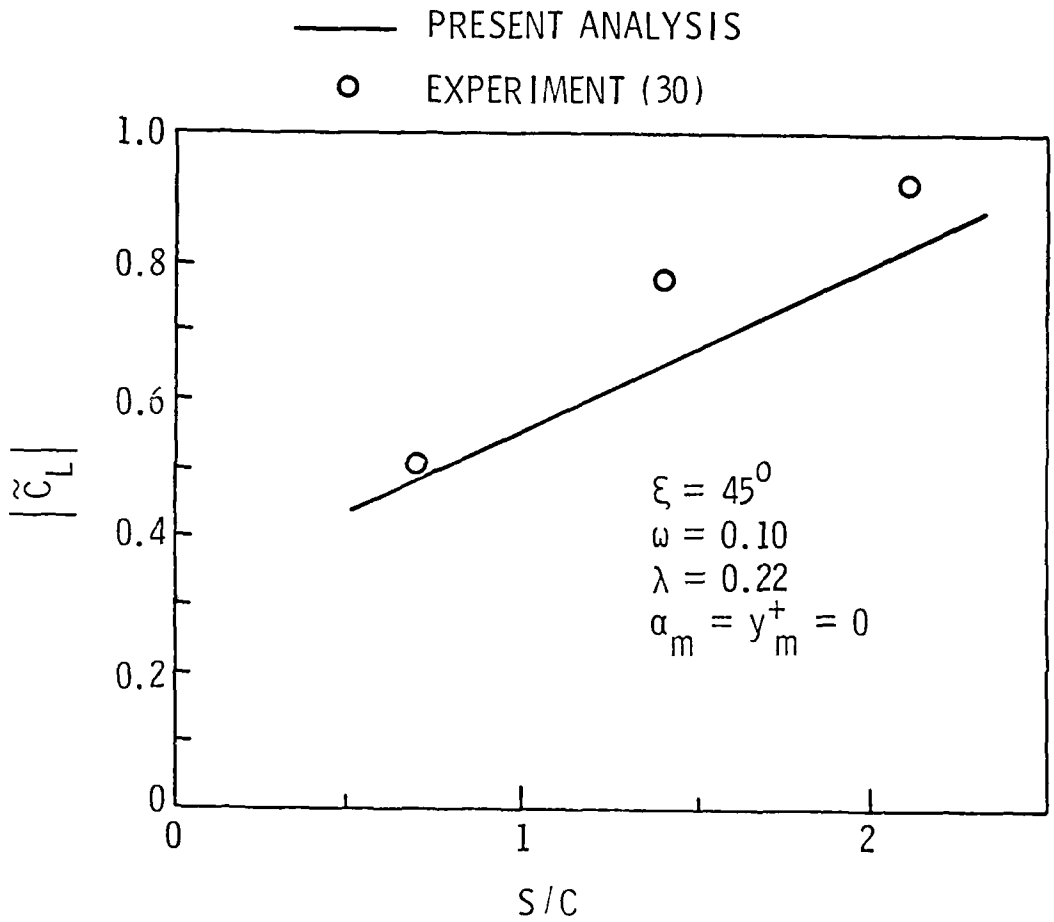

Figure 31. Variation of Unsteady Lift Amplitude with Space-to-Chord Ratio for Nonconvected Disturbance at Low Reduced Frequency.

capability to predict their effects can be of great use to turbomachine designers when estimating the cascade unsteady performance.

The results obtained using the present theory have been presented by Bruce (19) in the form of $\partial|\tilde{C}_L|/\partial\alpha_m$, $\partial|\tilde{C}_L|/\partial y^+_m$, $\partial|\tilde{C}_M|/\partial\alpha_m$, and $\partial|\tilde{C}_M|/\partial y^+_m$. These are useful parameters with which the final coefficients of unsteady lift or pitching moment can be computed using the following relations:

$$|\tilde{C}_L| = |\tilde{C}_{L_{o,o}}| + \frac{\partial|\tilde{C}_L|}{\partial\alpha_m}\alpha_m + \frac{\partial|\tilde{C}_L|}{\partial y^+_m} y^+_m$$

and

$$|\tilde{C}_M| = |\tilde{C}_{M_{o,o}}| + \frac{\partial|\tilde{C}_M|}{\partial\alpha_m}\alpha_m + \frac{\partial|\tilde{C}_M|}{\partial y^+_m} y^+_m \quad ,$$

where $|\tilde{C}_{L_{o,o}}|$ and $|\tilde{C}_{M_{o,o}}|$ represent the basic values of the lift and pitching moment coefficient computed for the case of zero mean incidence angle and zero blade camber.

Values of these derivatives can be obtained by utilizing Equations (39), (37), and (38) which permit the expressions of $\partial\Delta\tilde{C}_p/\partial y^+_m$ and $\partial\Delta\tilde{C}_p/\partial\alpha_m$ to be given as follows:

$$\frac{\partial \Delta \tilde{C}_p}{\partial y_m^+} = -4 \cos \phi \left\{ -\sqrt{\frac{1-\sigma^+}{1+\sigma^+}}\, i J_1(\lambda) - 1 \frac{2\omega}{\lambda^2} Z(\lambda,\sigma) \right.$$

$$\left. + \left(\frac{\omega}{\lambda} - 1\right)\left[2\sigma^+ Z(\lambda,\sigma^+) - \sqrt{1-\sigma^{+2}}\, J_o(\lambda)\right] \right\}$$

$$- 2 \cos \phi\, e^{-i\lambda\sigma^+} \sqrt{\frac{1-\sigma^+}{1+\sigma^+}} \left\{ 2(1+\sigma^+) \right.$$

$$\left. + \frac{\left[\sum_{-\infty}^{-1} + \sum_{1}^{\infty}\right] (E_1 + E_2)}{2 - \left[\sum_{-\infty}^{-1} + \sum_{1}^{\infty}\right] (C_1 + C_2 - 2)} \right\} + \text{... etc.}$$

and

$$\frac{\partial \Delta \tilde{C}_p}{\partial \epsilon_m} = -2 \cos \phi\, e^{-i\lambda\sigma^+} \sqrt{\frac{1-\sigma^+}{1+\sigma^+}} \left\{ 1 + \frac{\left[\sum_{-\infty}^{-1} + \sum_{1}^{\infty}\right] (E_1 + E_2)}{2 - \left[\sum_{-\infty}^{-1} + \sum_{1}^{\infty}\right] (C_1 + C_2 - 2)} \right\}.$$

These derivatives are not functions of y_m^+ and ϵ_m, respectively, that is, they remain constant for various values of y_m^+ or ϵ_m. Thus,

$$\frac{\partial \tilde{C}_L}{\partial \alpha_m} = \frac{\partial}{\partial \alpha_m} \frac{1}{2\pi} \int_{-1}^{1} \Delta \tilde{C}_p(\sigma^+) d\sigma^+ = \frac{1}{2\pi} \int_{-1}^{1} \frac{\partial \Delta \tilde{C}_p}{\partial \alpha_m} d\sigma^+ \quad .$$

Similarly,

$$\frac{\partial \tilde{C}_L}{\partial y^+_m} = \frac{1}{2\pi} \int_{-1}^{1} \frac{\partial \Delta \tilde{C}_p}{\partial y^+_m} d\sigma^+ \quad ,$$

$$\frac{\partial \tilde{C}_M}{\partial \alpha_m} = \frac{1}{4\pi} \int_{-1}^{1} \frac{\partial \Delta \tilde{C}_p}{\partial \alpha_m} \sigma^+ d\sigma^+ \quad ,$$

and

$$\frac{\partial \tilde{C}_M}{\partial y^+_m} = \frac{1}{4\pi} \int_{-1}^{1} \frac{\partial \Delta \tilde{C}_p}{\partial y^+_m} \sigma^+ d\sigma^+ \quad .$$

As an example, results of calculations for $\partial|\tilde{C}_L|/\partial\alpha_m$, $\partial|\tilde{C}_L|/\partial y^+_m$, $\partial|\tilde{C}_M|/\partial\alpha_m$, and $\partial|\tilde{C}_M|/\partial y^+_m$ using the above equations are plotted in Figures 32 through 35 for $\xi = 45^o$ versus ω with s/c = 1.353, 2.029, and 99 and are similar to the results obtained by Bruce. It can be observed that the effects of camber and mean incidence angle are usually of second order but can become significant in some regions of reduced frequency, normally for lower values of ω.

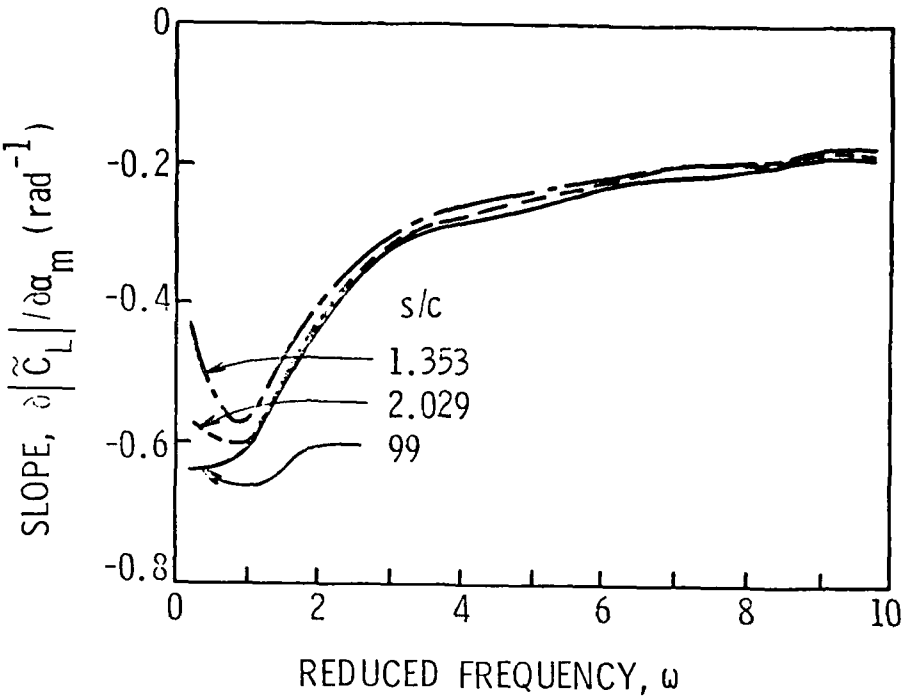

Figure 32. Partial Derivative of the Unsteady Lift Coefficient with Respect to Mean Incidence Angle with $y^+_{max} = 0$ and $\xi = 45^o$.

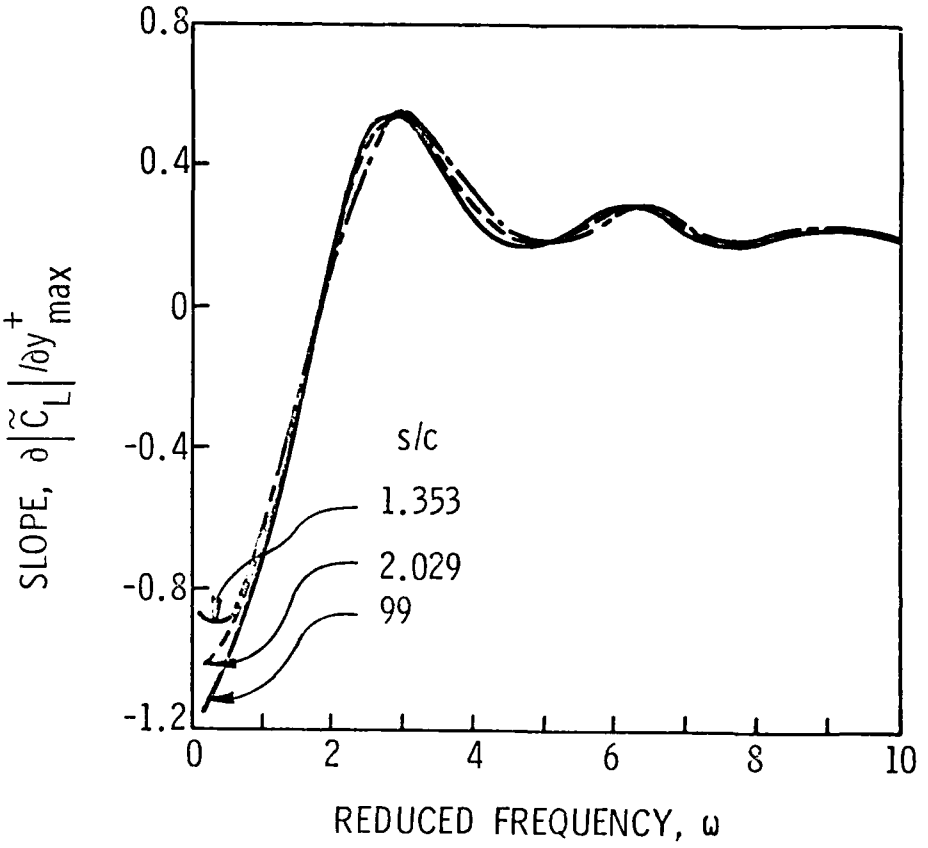

Figure 33. Partial Derivative of the Unsteady Lift Coefficient with Respect to Camber with $\alpha_m = 0$ and $\xi = 45^o$.

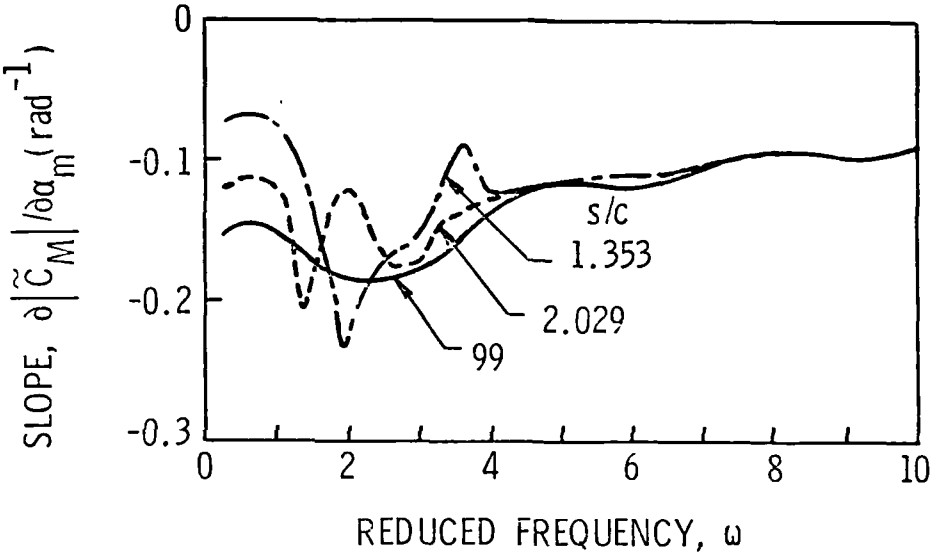

Figure 34. Partial Derivative of the Unsteady Pitching Moment Coefficient with Respect to Mean Incidence Angle with $y^+_{max} = 0$ and $\zeta = 45^\circ$.

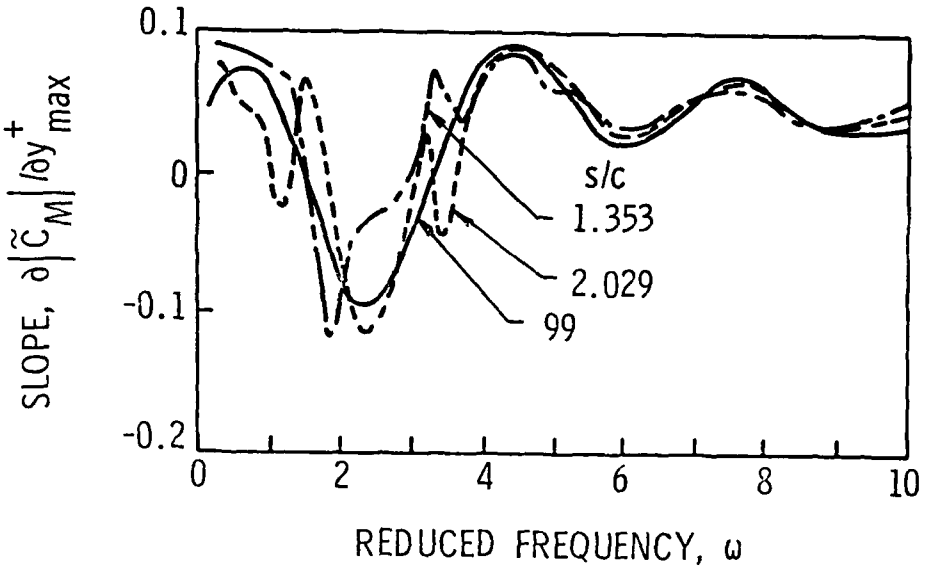

Figure 35. Partial Derivative of the Unsteady Pitching Moment Coefficient with Respect to Camber with $\alpha_m = 0$ and $\xi = 45^o$.

CHAPTER V

CONCLUSIONS AND RECOMMENDATIONS FOR FURTHER RESEARCH

Based on the results obtained in this study regarding the theoretical prediction of the unsteady pressure distribution on a cascade of airfoils, it is concluded that:

(1) The numerical integration of unsteady pressure difference, Equation (39), permits other unsteady response parameters to be calculated. When compared with Bruce's (19) calculation of unsteady lift and moment, the unsteady pressure analysis shows satisfactory agreement except in the regions near the resonance points, Figures 12 through 23. This difference is believed to be a result of the accumulation of computational errors in evaluating the infinite cascade summations and the numerical integrations.

(2) The unsteady pressure difference coefficients $\Delta\tilde{C}_p$ calculated using Equation (39) are compared with the predictions by the Whitehead-Smith theory (14) since suitable experimental data are not available. Comparisons of $|\Delta\tilde{C}_p|$ and $\tilde{\phi}_p$ predicted by the two methods show good agreement except in the neighborhood of critical reduced frequencies or resonance points as presented in Figures 8 through 11. This difference in the predictions by these two theoretical models is also reflected in the comparison of their predicted unsteady

lift and pitching moment, Figures 12 through 23. The Whitehead-Smith theory is formulated in a manner which excludes the critical reduced frequencies. Therefore, agreement between the two methods is not expected at these conditions.

(3) The present analysis provides an unsteady cascade performance prediction similar to the prediction given by the Whitehead-Smith theory, Figures 12 through 26, particularly at low values of reduced frequency, that is, $\omega < 0.5$. This result, however, does not agree well with Bruce's calculations of unsteady lift and moment. Again, these differences appear to be caused by numerical errors which result in the two different computational approaches.

(4) The measured data obtained and presented by Bruce [19], in general, have trends that are in good agreement with the predictions by the present analysis as shown in Figures 12 through 26.

(5) Gallus et al. [20] have conducted measurements of the pressure fluctuations in an axial flow compressor by utilizing a series of dynamic pressure transducers mounted on the midspan surface of a stator blade which experiences rotor wakes. Satyanarayana [30] has also measured the fluctuating lift on a cascade mounted in a specially designed gust tunnel. These two experimental studies consider relatively high and low reduced frequencies, respectively. Good agreement is observed in both cases when the measured unsteady lift is compared with

theoretical predictions by the present analysis as shown in Figures 29, 30, and 31.

Recommendations for the direction of additional experimental and theoretical efforts are as follows:

(1) At the present state of knowledge, it is essential to conduct direct measurements of unsteady pressure differences in an experimental setup similar to that employed in Reference [19] with a rotating blade row and simple sinusoidal spatial distortions. This experimental study should be conducted at intermediate values of reduced frequencies as the high and low values have been considered in References [20] and [30], respectively. Such data are required to complete the verification of the validity of the present analysis.

(2) Once this analysis is verified by measured data, it should be used to generate unsteady design data, which demonstrate the effects of cascade geometry and flow characteristics, in a form similar to the results present in Reference [29].

(3) The present analysis should be used to predict the unsteady forces in a cascade of nonrigid airfoils subjected to a forced vibration by introducing the appropriate boundary conditions into Equation (29).

REFERENCES

1. Dean, R. C., "On the Necessity of Unsteady Flows in Fluid Machines," ASME Transactions, Journal of Basic Engineering, Vol. 81D, 1959, pp. 24-28.

2. Sisto, F., "Review - A Review of the Fluid Mechanics of Aeroelasticity in Turbomachines," Transactions of ASME, Journal of Fluids Engineering, Vol. 99, Series I, No. 1, 1977, pp. 40-44.

3. Morfey, C. L., "Sound Generation in Subsonic Turbomachinery," Transactions of ASME, Journal of Basic Engineering, Vol. 92, Series D, 1970, pp. 450-458.

4. Korn, J. D., "The Effect of Inlet Distortion on the Performance and Stability of the Low-Speed Spool of a Turbofan Engine," presented at AIAA 12th Aerospace Sciences Meeting, Paper No. 74-234, Washington, DC, 1974.

5. Geising, J. P., "Nonlinear Two-Dimensional Unsteady Potential Flow with Lift," AIAA Journal of Aircraft, Vol. 5, No. 2, 1968, pp. 135-143.

6. Taskonas, S., and Jacobs, W. R., "Unsteady Lift Surface for a Marine Propeller of Low Pitch Angle with Chordwise Loading Distribution," Journal of Ship Research, Vol. 9, 1965, pp. 79-101.

7. Von Kármán, T., and Sears, W. R., "Airfoil Theory for Non-Uniform Motion," Journal of Aeronautical Sciences, Vol. 5, 1938, pp. 379-390.

8. Sears, W. R., "Some Aspects of Non-Stationary Airfoil Theory and Its Practical Applications," Journal of Aeronautical Sciences, Vol. 8, 1949, pp. 104-108.

9. Kemp, N. H., and Sears, W. R., "Aerodynamic Interference Between Moving Blade Rows," Journal of Aeronautical Sciences, Vol. 20, 1953, pp. 585-598.

10. Kemp, N. H., and Sears, W. R., "The Unsteady Forces Due to Viscous Wakes in Turbomachines," Journal of Aeronautical Sciences, Vol. 22, 1955, pp. 478-483.

11. Horlock, J. H., "Fluctuating Lift Forces on Aerofoils Moving Through Transverse and Chordwise Gusts," ASME Transactions, Journal of Basic Engineering, Vol. 90D, 1968, pp. 494-500.

12. Holmes, D. H., "Lift Fluctuations on Aerofoils in Transverse and Streamwise Gusts," Ph.D. dissertation, Engineering Department, University of Cambridge, Cambridge, England, October 1972.

13. Naumann, H., and Yeh, H., "Lift and Pressure Fluctuations of a Cambered Airfoil Under Periodic Gusts and Applications in Turbomachinery," presented at ASME Gas Turbine Conference, Paper No. 72-GT-30, San Francisco, CA, March 1972.

14. Whitehead, D. S., "Forces and Moment Coefficients for Vibrating Airfoils in Cascade," Aeronautical Research Council, Great Britain, England, R&M 3254, 1960.

15. Schorr, B., and Reddy, K. C., "Inviscid Flow Through Cascade in Oscillatory and Distorted Flow," AIAA Journal, Vol. 9, No. 10, 1971, pp. 2043-2050.

16. Henderson, R. E., and Daneshyar, H., "Theoretical Analysis of Fluctuating Lift on the Rotor of an Axial Turbomachine," Aeronautical Research Council, Great Britain, England, R&M 3684, 1972.

17. Smith, S., "Discrete Frequency Sound Generation in Axial Flow Turbomachines," Aeronautical Research Council, Great Britain, England, R&M 3709, 1972.

18. Henderson, R. E., "The Unsteady Response of an Axial Flow Turbomachine to an Upstream Disturbance," Ph.D. dissertation, Engineering Department, University of Cambridge, Cambridge, England, 1972.

19. Bruce, E. P., "Axial Flow Rotor Unsteady Performance," Ph.D. Thesis, Department of Aerospace Engineering, The Pennsylvania State University, University Park, PA, 1979.

20. Gallus, H. E., et al., "Blade-Row Interaction in an Axial-Flow Subsonic Compressor Stage," ASME Gas Turbine Conference, San Diego, CA, Paper No. 79-GT-92, March 1979.

21. Tanabe, K., and Horlock, J. H., "A Simple Method for Predicting the Performance of Cascade of Low Solidity," Aeronautical Quarterly, Vol. 18, Part 3, 1967.

22. Blisplinghoff, R. L., Ashley, H., and Halfman, R. L., Aeroelasticity, Addison-Wesley, Reading, MA, 1955.

23. Prandtl, L., and Tietjens, O. G., Fundamentals of Hydro and Aeromechanics, McGraw-Hill, New York, 1934.

24. Söhngen, H., "Die Lösungen der Integralgleichungen

$$g(x) = \frac{1}{2\pi} \int_{-a}^{a} \frac{f(\xi)}{x - \xi} \, d\xi$$

und deren Anwendung in der Tragflügeltheorie," Math. Z, Vol. 45, pp. 245-264, 1939.

25. Gradshteyn, D. S., and Ryzhek, D. M., Tables of Integrals, Series, and Products, Academic Press, New York and London, 1965.

26. Naumann, H., "Unsteady Airfoil Theory Applied to Cambered Blades and to Blade Rows of High Solidity," Ph.D. dissertation, Department of Mechanical Engineering, University of Pennsylvania, Philadelphia, PA, 1971.

27. Shen, I-C, "Documentation of Cascade Unsteady Pressure Difference Program," Applied Research Laboratory, Technical Memorandum File No. 80-10, January 5, 1980.

28. Stroud, A. H., and Secrest, D., Gaussian Quadrature Formulas, Prentice-Hall, 1966.

29. Geising, J. P., Rodden, W. P., and Stahl, B., "Sears Function and Lifting Theory for Harmonic Gust Fields," AIAA Journal of Aircraft, Vol. 7, No. 3, 1970, pp. 252-255.

30. Satyanarayana, B., "Unsteady Flow Past Airfoils and Cascades," Ph.D. dissertation, Engineering Department, University of Cambridge, Cambridge, England, 1975.

31. Van Dyke, M., "Second Order Subsonic Airfoil Theory Including Edge Effects," NACA Report, 1274, 1956.

32. Durand, W. F., Aerodynamic Theory, Vol. 2, Julius Springer, Berlin, 1935.

33. Reissner, E., "Effect of Finite Span on the Airload Distributions for Oscillating Wings, I - Aerodynamic Theory of Oscillating Wings of Finite Span," NACA Technical Note No. 1194, March 1947.

APPENDIX A

DETERMINATION OF UNSTEADY PRESSURE DISTRIBUTION FOR AN ISOLATED AIRFOIL

The determination of unsteady pressure distribution for a cascade of airfoils as written in Equation (29) of Section 2.3 requires that the integral terms be evaluated. For example, the first two terms contributed by the bound vorticity on the reference blade alone can be evaluated by direct substitution of the solutions obtained from the special case of an isolated airfoil, that is, a situation where the space-chord ratio s/c approaches infinity. The solution for the isolated airfoil case, hence, is necessary and can be a good check for the validity of the present analysis.

In the limiting case of an isolated airfoil, it is reasonable that all the effects contributed from blade-to-blade interactions are negligible. As a result, all the terms having infinite summations, that is, terms such as

$$\left(\sum_{-\infty}^{-1} + \sum_{1}^{\infty} \right) (C_1 + C_2 - 2)$$

and

$$\left[\sum_{-\infty}^{-1} + \sum_{1}^{\infty}\right] (B_1 + B_2) \quad ,$$

in the analysis can be shown to vanish mathematically as shown in Appendix C. Thus, Equations (29), (23), and (24) can be reduced to

$$-\frac{\Delta\bar{p}(\sigma^+)}{\rho W_m} = \frac{2}{\pi}\sqrt{\frac{1-\sigma^+}{1+\sigma^+}}\int_{-1}^{1}\sqrt{\frac{1+x^+_1}{1-x^+_1}}\,\frac{\bar{v}_o(x^+_1)}{(\sigma^+ - x^+_1)}\,dx^+_1$$

$$-\frac{2ik}{\pi}\int_{-1}^{1}\bar{v}_o(x^+_1)K(\sigma^+,x^+_1)dx^+_1 - ik\sqrt{\frac{1-\sigma^+}{1+\sigma^+}}\,H_o^{(2)}(\cdot)$$

$$+\frac{\bar{u}_d(\sigma^+)}{W_m}\gamma_{o_s}(\sigma^+) \quad ,$$

$$\Delta = \frac{\bar{\Gamma}_o e^{i\omega}}{c} = \frac{4\int_{-1}^{1}\sqrt{\frac{1+x^+_1}{1-x^+_1}}\,\bar{v}_o(x^+_1)dx^+_1}{ik\pi c\left[H_1^{(2)}(\omega) + iH_o^{(2)}(\omega)\right]} \quad ,$$

and

$$\gamma_{o_s}(\sigma^+) = \frac{2}{\pi}\sqrt{\frac{1-\sigma^+}{1+\sigma^+}}\int_{-1}^{1}\sqrt{\frac{1+x^+_1}{1-x^+_1}}\,\frac{v_{o_s}(x^+_1)}{(\sigma^+ - x^+_1)}\,dx^+_1 \quad .$$

The equation of unsteady pressure distribution therefore contains only the contributions by the bound vorticity representing the reference

blade and by its wake vorticity and is identical to that derived in Reference [22].

For a cambered airfoil with angle of incidence, the induced velocities $\bar{v}_o(x^+_1)$ and $v_{o_s}(x^+_1)$ remain the same as written in Equations (34a) and (34b). For the purpose of solving the problem, several integrals must be evaluated, and their results are listed in Appendix B. Substitution of the boundary conditions and the integral relationships from Equations (8) through (14) of Appendix B gives

$$-\frac{\Delta p(x^+)}{\rho W_m e^{i\lambda t}} = 4y^+_m \hat{u}_d \sqrt{\frac{1-x^+}{1+x^+}} \left\{ (1+x^+)J_o(\lambda) - iJ_1(\lambda) \right.$$

$$\left. + 2i^+ \sqrt{\frac{1+x^+}{1-x^+}} Z(\lambda, x^+) \right\}$$

$$+ 2\hat{v}_d \sqrt{\frac{1-x^+}{1+x^+}} \left\{ J_o(\lambda) - 2 \sqrt{\frac{1-x^+}{1+x^+}} Z(\lambda, x^+) \right\}$$

$$- \frac{4\sigma}{\lambda} y^+_m \hat{u}_d \left\{ \sqrt{1-x^+} J_o(\lambda) - \frac{\pi}{2}(\lambda x^+ + i) Z(\lambda, x^+) \right.$$

$$\left. + \frac{4\sigma}{\lambda} \hat{v}_d Z(\lambda, x^+) + \pi \sqrt{\frac{1-x^+}{1+x^+}} \left[\lambda H_o^{(2)}(\lambda) J_1(\lambda) + i\lambda H_1^{(2)}(\lambda) J_o(\lambda) \right] \right.$$

$$\cdot \left\{ y^+_m \hat{u}_d \left[J_o(\lambda) - J_2(\lambda) - i2J_1(\lambda) \right] + \hat{v}_d \left[J_o(\lambda) - iJ_1(\lambda) \right] \right\}$$

$$+ 2\hat{u}_d e^{-i\lambda\sigma^+} \sqrt{\frac{1-\sigma^+}{1+\sigma^+}} \left(2y^+_m (1+\sigma^+) + z_m \right) \quad . \qquad \text{(A-1)}$$

By utilizing the linear property of the analysis, the unsteady pressure difference can be divided into two parts, namely, the parts due to disturbance velocities u_d and v_d, respectively,

$$-\frac{\tilde{\Delta p}(\sigma^+)}{\rho W_m e^{i\nu t}} = \frac{\tilde{\Delta p}_{u_d}}{\rho W_m e^{i\nu t}} - \frac{\tilde{\Delta p}_{v_d}}{\rho W_m e^{i\nu t}} \quad .$$

Hence,

$$-\frac{\tilde{\Delta p}_{u_d}}{\rho W_m e^{i\nu t}} = 2\hat{u}_d \left\{ y^+_m \sqrt{\frac{1-\sigma^+}{1+\sigma^+}} \left[\frac{H_1^{(2)}(\omega)}{i\left(H_1^{(2)}(\omega) + iH_o^{(2)}(\omega)\right)} \right.\right.$$

$$\left. \cdot \left[J_o(\lambda) - J_2(\lambda) - 2iJ_1(\lambda) \right] - 2iJ_1(\lambda) + \frac{4}{i\omega} \chi(\lambda, \sigma^+) \right]$$

$$\left. + \left[\sqrt{\frac{1-\sigma^+}{1+\sigma^+}} \alpha_m + 2\sqrt{1-\sigma^{+2}}\, y^+_m \right] e^{-i\lambda\sigma^+} \right.$$

$$+ y^{+}_{m}\left(\frac{\omega}{\lambda} - 1\right)\left(4\sigma^{+}Z(\lambda,\sigma^{+}) - 2\sqrt{1 - \sigma^{+2}}\, J_o(\lambda)\right)\Bigg\} \quad .$$

By defining the function

$$F(\omega,\lambda) = T(\omega)\left[J_o(\lambda) - \frac{J_1(\lambda)}{\lambda} - iJ_1(\lambda)\right] - \left[J_o(\lambda) - \frac{J_1(\lambda)}{\lambda} + iJ_1(\lambda)\right] \quad ,$$

where

$$T(\omega) = \frac{H_o^{(2)}(\omega) + iH_1^{(2)}(\omega)}{-H_o^{(2)}(\omega) + iH_1^{(2)}(\omega)}$$

is the Horlock function, the following identity is then derived:

$$F(\omega,\lambda) = \frac{H_1^{(2)}(\omega)}{i\left(H_1^{(2)}(\omega) + iH_o^{(2)}(\omega)\right)}\left(J_o(\lambda) - J_2(\lambda) - i2J_1(\lambda)\right) - i2J_1(\lambda) \quad .$$

The unsteady pressure difference due only to the chordwise disturbance is, therefore,

$$-\frac{\Delta p_{u_d}(\sigma^{+})}{\rho W_m e^{i\omega t}} = 2\hat{u}_d\left\{y^{+}_{m}\sqrt{\frac{1 - \sigma^{+}}{1 + \sigma^{+}}}\left(F(\omega,\lambda) + \frac{4}{i\omega}Z(\lambda,\sigma^{+})\right)\right.$$

$$+ \left\{ {}_{m}\sqrt{\frac{1-\sigma^{+}}{1+\sigma^{+}}} + 2y^{+}_{m} \quad 1-\sigma^{+2} \right\} e^{-i\lambda\sigma^{+}}$$

$$+ y^{+}_{m}\left(\frac{\omega}{\lambda} - 1\right)\left[4\sigma^{+}Z(\lambda,\sigma^{+}) - 2\sqrt{1-\sigma^{+2}}\, J_o(\lambda)\right]\Bigg\} \quad . \tag{A-2}$$

Similarly,

$$-\frac{\Delta p_{v_d}}{W_m} e^{i\omega t} = 2\dot{v}_d \left\{ \sqrt{\frac{1-\sigma^{+}}{1+\sigma^{+}}} \left\{ J_o(\lambda) + \frac{H_o^{(2)}(\omega)}{i\left[H_1^{(2)}(\omega) + iH_o^{(2)}(\omega)\right]} \right.\right.$$

$$\left.\left. \cdot \left[J_o(\lambda) - iJ_1(\lambda)\right] \right\} + 2\left(\frac{\omega}{\lambda} - 1\right) Z(\lambda,\sigma^{+}) \right\} \quad . \tag{A-3}$$

3. Introduction of the Sears' function

$$S(\lambda,\sigma) = C(\omega)\left[J_o(\lambda) - iJ_1(\lambda)\right] + i\,\frac{\omega}{\lambda} J_1(\lambda) \quad ,$$

where $C(\omega)$ is the Theodorsen function

$$C(\omega) = 1 + \frac{H_o^{(2)}(\omega)}{i\left[H_1^{(2)}(\omega) + iH_o^{(2)}(\omega)\right]} \quad ,$$

and by examination of the terms within the brackets in Equation (A-3), the following relationship can be obtained:

$$J_o(\lambda) + \frac{H_o^{(2)}(\omega)}{i\left(H_1^{(2)}(\omega) + iH_o^{(2)}(\omega)\right)}\left(J_o(\lambda) - iJ_1(\lambda)\right)$$

$$= S(\omega,\lambda) - \left(\frac{\omega}{\lambda} - 1\right)iJ_1(\lambda) \quad .$$

The unsteady pressure difference due only to the traverse disturbance is then simplified and becomes

$$-\frac{\Delta\tilde{p}_{v_d}}{\rho W_m e^{i\nu t}} = 2\hat{v}_d \left\{ \sqrt{\frac{1-\sigma^+}{1+\sigma^+}}\, S(\omega,\lambda) + \left(\frac{\omega}{\lambda} - 1\right) \left[2Z(\lambda,\sigma^+) - \sqrt{\frac{1-\sigma^+}{1+\sigma^+}}\, iJ_1(\lambda) \right] \right\} \quad . \tag{A-4}$$

The general expression for the unsteady pressure difference on an isolated airfoil of symmetric parabolic arc operating at a nonzero mean incidence angle in a velocity field that contains both a chordwise and a transverse disturbance is obtained by combining Equations (A-2) and (A-4). Thus,

$$-\frac{\Delta\tilde{p}(\sigma^+)}{\rho W_m e^{i\nu t}} = 2\hat{u}_d \left\{ y^+_m \sqrt{\frac{1-\sigma^+}{1+\sigma^+}} \left[F(\omega,\lambda) + \frac{4}{i\omega} Z(\lambda,\sigma^+) \right] + \left[\alpha_m \sqrt{\frac{1-\sigma^+}{1+\sigma^+}} + 2y^+_m \sqrt{1-\sigma^{+2}} \right] e^{-i\lambda\sigma^+} \right.$$

$$+ y^+_m \left(\frac{\omega}{\lambda} - 1\right)\left(4\sigma^+ Z(\lambda,\sigma^+) - 2\sqrt{1-\sigma^{+2}}\, J_o(\lambda)\right)\Bigg\}$$

$$+ 2\hat{v}_d \left\{\sqrt{\frac{1-\sigma^+}{1+\sigma^+}}\, S(\omega,\lambda)\right.$$

$$\left. + \left(\frac{\omega}{\lambda} - 1\right)\left[2Z(\lambda,\sigma^+) - \sqrt{\frac{1-\sigma^+}{1+\sigma^+}}\, iJ_1(\lambda)\right]\right\} \quad . \qquad \text{(A-5)}$$

As a check for the validity of Equation (A-5), the isolated airfoil case with "convected" disturbances is considered, that is, the disturbance is transported over the airfoil with a velocity W_m. With the substitution of the result $\lambda = \omega$, as discussed in Section 2.2, Equation (A-5) is simplified to

$$-\frac{\Delta\tilde{p}(\sigma^+)}{\rho W_m e^{i\nu t}} = 2\hat{u}_d \left\{y^+_m \sqrt{\frac{1-\sigma^+}{1+\sigma^+}}\left(F(\omega) + \frac{4}{i\omega} Z(\omega,\sigma^+)\right)\right.$$

$$\left. + \left[\sqrt{\frac{1-\sigma^+}{1+\sigma^+}}\,\alpha_m + 2\sqrt{1-\sigma^{+2}}\, y^+_m\right] e^{-i\omega\sigma^+}\right\}$$

$$+ 2\hat{v}_d \sqrt{\frac{1-\sigma^+}{1+\sigma^+}}\, S(\omega) \quad , \qquad \text{(A-6)}$$

where $F(\omega)$ and $S(\omega)$ are complex functions of reduced frequency.

Comparison of Equation (A-6) with that derived by Naumann [26] shows a complete agreement and demonstrates the validity of Equation (A-5) and, hence, the present analysis.

APPENDIX B

TABULATION OF INTEGRALS

Integral Relations in Cascade Analysis

1. $$\int_{-1}^{1} \sqrt{\frac{1 + x_1}{1 - x_1}} \frac{dx_1}{(r - x_1)} = -\pi \text{ for } |r|^2 \leq 1$$ Van Dyke (31)

2. $$\int_{-1}^{1} \sqrt{\frac{1 + x_1}{1 - x_1}} \frac{dx_1}{(r - x_1)} = -\pi \left(1 - \sqrt{\frac{r + 1}{r - 1}}\right) \text{ for } |r|^2 > 1$$

Henderson (18)

3. $$\int_{1}^{\infty} \left(\sqrt{\frac{\lambda^+ + 1}{\lambda^+ - 1}} - 1\right) e^{-i\omega\lambda^+} d\lambda^+ = -\frac{\pi}{2}\left(H_1^{(2)}(\omega) + iH_o^{(2)}(\omega)\right) - \frac{e^{-i\omega}}{i\omega}$$

Durand (32)

4. $$\int_{-1}^{\sigma^+} \sqrt{\frac{1 - x_1}{1 + x_1}} \frac{dx_1}{(r - x_1)} = \frac{\pi}{2} + \sin^{-1}\sigma^+ + \sqrt{\frac{1 - r}{1 + r}}\,\Omega(\sigma^+, x_1)$$

$$\text{for } |r|^2 < 1 \quad ,$$

where

$$\Omega(\sigma,x_1) = \frac{1}{2} \ln \left\{ \frac{1 - \sigma^+ x_1 + \sqrt{1 - x_1^2}\ \sqrt{1 - \sigma^{+2}}}{1 - \sigma^+ x_1 - \sqrt{1 - x_1^2}\ \sqrt{1 - \sigma^{+2}}} \right. \qquad \text{Reissner (33)}$$

$$5. \quad \int_{-1}^{1} \sqrt{\frac{1 - x_1}{1 + x_1}} \frac{dx_1}{(r - x_1)} = \frac{\pi}{2} + \sin^{-1} \sigma^+ + \sqrt{\frac{r - 1}{r + 1}}\ \Lambda(\sigma^+,r)$$

$$\text{for } |r|^2 > 1 \quad ,$$

where

$$\Lambda(\sigma^+,r) = 2 \tan^{-1} \left\{ \sqrt{\frac{1 - \sigma^+}{1 + \sigma^+} \frac{r + 1}{r - 1}} \right\} \qquad \text{Reissner (33)}$$

$$6. \quad \int_1^{\infty} e^{-i\omega\lambda^+} \Lambda(\sigma^+,r) d\lambda^+ = \frac{e^{-i\omega}}{i\omega} \Lambda(\sigma^+,r) \Big|_{\lambda^+ = 1}^{\infty}$$

$$+ \frac{1}{i\omega} \int_1^{\infty} \frac{\partial \Lambda(\sigma^+,r)}{\partial r} e^{-i\omega\lambda} d\lambda^+ \quad ,$$

where $r = \lambda^+$, g_λ, or h_λ

$$7. \quad \int_1^{\infty} \frac{e^{-i\omega\lambda^+}}{\sqrt{\lambda^{+1} - 1}}\ d\lambda^+ = -\frac{i\pi}{2} H_0^{(2)}(\omega) \qquad \text{Durand (32)}$$

Integral Relations for Analysis of Isolated Airfoil

8. $$\int_{-1}^{1} \sqrt{\frac{1+x_1}{1-x_1}} \frac{x_1 e^{-i\lambda x_1} dx_1}{(\sigma^+ - x_1)} = -\pi J_o(\lambda)(1+\sigma^+) + i\pi J_o(\lambda) + 2\pi\sigma^+ \sqrt{\frac{1-\sigma^+}{1+\sigma^+}}\, Z(\lambda,\sigma^+)$$

9. $$\int_{-1}^{1} \sqrt{\frac{1+x_1}{1-x_1}} \frac{e^{-i\lambda x_1} dx_1}{(\sigma^+ - x_1)} = -\pi J_o(\lambda) + 2\pi \sqrt{\frac{1+\sigma^+}{1-\sigma^+}}\, Z(\lambda,\sigma^+)$$

10. $$\int_{-1}^{1} \sqrt{\frac{1+x_1}{1-x_1}} \frac{x_1 dx_1}{(\sigma^+ - x_1)} = -\pi(1+\sigma^+)$$

11. $$\int_{-1}^{1} e^{-i\lambda x_1} \Omega(\sigma^+, x_1) dx_1 = -\frac{i2\pi}{\lambda} Z(\lambda,\sigma^+)$$

12. $$\int_{-1}^{1} x_1 e^{-i\lambda x_1} \Omega(\sigma^+, x_1) dx_1 = \frac{i2\pi}{\lambda^2}\left(\frac{\lambda}{2}\sqrt{1-\sigma^{+2}}\, J_o(\lambda) + (-\lambda\sigma^+ + i) Z(\lambda,\sigma^+)\right)$$

13. $$\int_{-1}^{1} \sqrt{\frac{1+x_1}{1-x_1}} e^{-i\lambda x_1} dx_1 = \pi\left(J_o(\lambda) - iJ_1(\lambda)\right)$$

14. $$\int_{-1}^{1} \sqrt{\frac{1+x_1}{1-x_1}}\, x_1 e^{-i\lambda x_1} dx_1 = \frac{\pi}{2}\left\{J_0(\lambda) - J_2(\lambda) - i2J_1(\lambda)\right\} \quad ,$$

where $-1 \leq o^+ \leq 1$

$J_n(\lambda)$ = Bessel function of the 1st kind, order n

APPENDIX C

UNSTEADY PRESSURE DIFFERENCE EQUATION FOR THE CASE OF INFINITE SPACING

The equation of unsteady pressure difference for a blade in a cascade in a disturbance velocity field is presented in Equation (29). The objective of this appendix is to show that when the spacing between blades becomes infinite this equation reduces to that for an isolated airfoil which was derived by Blisplinghoff et al. [22].

Henderson and Daneshyar [10] have shown that

$$\lim_{s \to \infty} B_1 = \lim_{s \to \infty} B_2 = \lim_{s \to \infty} D_1 = \lim_{s \to \infty} D_2 = 0$$

and

$$\lim_{s \to \infty} C_1 = \lim_{s \to \infty} C_2 = 1 \quad .$$

It can also be shown that

$$\lim_{s \to \infty} E_1 = \lim_{s \to \infty} E_2 = 0$$

in a similar manner.

To determine the limiting value of the term

$$\mathcal{K}(\epsilon^+, x_2) + \mathcal{K}(\epsilon^+, h_2) - \mathcal{K}(\epsilon^+, x_1) - \mathcal{K}(\epsilon^+, h_1) \quad ,$$

express it as

$$A(\sigma^+,r) = 2 \tan^{-1}\left\{\sqrt{\frac{1-\sigma^+}{1+\sigma^+}\frac{r+1}{r-1}}\right\} - \pi \quad ,$$

where r represents g_c, h_c, g_1, and h_1. Then

$$\lim_{s\to\infty} A(\sigma^+,r) = \lim_{s\to\infty}\left\{2 \tan^{-1}\left\{\sqrt{\frac{1-\sigma^+}{1+\sigma^+}\frac{r+1}{r-1}}\right\} - \pi\right\}$$

$$= 2 \tan^{-1}\left\{\lim_{s\to\infty}\sqrt{\frac{1-\sigma^+}{1+\sigma^+}\frac{r+1}{r-1}}\right\} - \pi$$

$$= 2 \tan^{-1}\left\{\sqrt{\frac{1-\sigma^+}{1+\sigma^+}}\lim_{s\to\infty}\sqrt{\frac{r+1}{r-1}}\right\} - \pi$$

$$= 2 \tan^{-1}\left\{\sqrt{\frac{1-\sigma^+}{1+\sigma^+}}\right\} - \pi \quad .$$

Since, by analogy with Henderson and Dameshyar's results that

$$\lim_{s\to\infty} C_1 = \lim_{s\to\infty}\sqrt{\frac{g_c+1}{g_c-1}} = 1 \quad ,$$

$$\lim_{s \to \infty} \sqrt{\frac{g_1 + 1}{g_1 - 1}} = \lim_{s \to \infty} \sqrt{\frac{h_1 + 1}{h_1 - 1}} = 1 \quad .$$

This leads to

$$\lim_{s \to \infty} \left(A(\sigma^+, g_c) + A(\sigma^+, h_c) - A(\sigma^+, g_1) - A(\sigma^+, h_1) \right) = 0 \quad .$$

From the results presented above, it is evident that the infinitive summations as listed in Table 1 and contained in Equations (29), (23), and (24) are all equal to zero when $s = \infty$.

With these results, Equation (29) of Chapter II reduces to

$$-\frac{\Delta \bar{p}(\sigma^+)}{\rho W_m} = \frac{2}{\pi} \sqrt{\frac{1 - \sigma^+}{1 + \sigma^+}} \int_{-1}^{1} \sqrt{\frac{1 + x^+_1}{1 - x^+_1}} \frac{\bar{v}_o(x^+_1)}{(\sigma^+ - x^+_1)} dx^+_1$$

$$- \frac{2i\omega}{\pi} \int_{-1}^{1} \bar{v}_o(x^+_1) K(\sigma^+, x^+_1) dx_1 - \omega A \sqrt{\frac{1 - \sigma^+}{1 + \sigma^+}} H_o^{(2)}(\cdot)$$

$$+ \frac{\bar{u}_d(\sigma^+)}{W_m} \gamma_{o_s}(\sigma^+) \quad ,$$

together with

$$A = \frac{\int_{-1}^{1} \sqrt{\frac{1 - x^+_1}{1 + x^+_1}} \bar{v}_o(x^+_1) dx^+_1}{i\omega\rho \left[H_1^{(2)}(\cdot) + i H_o^{(2)}(\cdot) \right]}$$

and

$$\gamma_{o_s}(\sigma^+) = \frac{2}{\pi}\sqrt{\frac{1-\sigma^+}{1+\sigma^+}}\int_{-1}^{1}\sqrt{\frac{1+x^+_1}{1-x^+_1}}\frac{\bar{v}_o(x^+_1)}{(\sigma^+ - x^+_1)}\,dx^+_1 \quad .$$

This agrees with the equation developed by Blisplinghoff et al. [22] for the isolated airfoil case.

DISTRIBUTION LIST FOR ARL UNCLASSIFIED TM 80-45 by I-Chung Shen dated 1 April 1980.

Commander
Naval Sea Systems Command
Department of the Navy
Washington, DC 20362
Attn: Library
Code NSEA 09G32
(Copy Nos. 1 and 2)

Naval Sea Systems Command
Attn: Code NSEA 0342
(Copy Nos. 3 and 4)

Naval Sea Systems Command
Attn: T. E. Peirce
Code NSEA 63R3
(Copy No. 5)

Naval Sea Systems Command
Attn: A. R. Paladino
Code NSEA 05H1
(Copy No. 6)

Naval Sea Systems Command
Attn: F. Peterson
Code NSEA 52P
(Copy No. 7)

Defense Technical Information Center
5010 Duke Street
Cameron Station
Alexandria, VA 22314
(Copy Nos. 8 through 19)

Commanding Officer
Naval Underwater Systems Center
Newport, RI 02840
Attn: Library
Code 54
(Copy No. 20)

Commanding Officer
Naval Ocean Systems Center
San Diego, CA 92152
Attn: M. Reischman
Code 2542
(Copy No. 21)

Commanding Officer & Director
David W. Taylor Naval Ship R&D Center
Department of the Navy
Bethesda, MD 20084
Attn: W. B. Morgan
Code 15
(Copy No. 22)

David W. Taylor Naval Ship R&D Center
Attn: R. Cumming
Code 1544
(Copy No. 23)

David W. Taylor Naval Ship R&D Center
Attn: J. McCarthy
Code 154
(Copy No. 24)

David W. Taylor Naval Ship R&D Center
Attn: M. Sevik
Code 19
(Copy No. 25)

David W. Taylor Naval Ship R&D Center
Attn: W. K. Blake
Code 1942
(Copy No. 26)

Commanding Officer & Director
David W. Taylor Naval Ship R&D Center
Department of the Navy
Annapolis Laboratory
Annapolis, MD 21402
Attn: J. G. Stricker
Code 2721
(Copy No. 27)

David W. Taylor Naval Ship R&D Center
Attn: Y-F Wang
Code 2740
(Copy No. 28)

Air Force Office of Scientific Research
Bolling Air Force Base, Building 410
Washington, DC 20332
Attn: Dr. Joseph F. Masi
(Copy No. 29)

Office of Naval Research
Power Branch
Department of the Navy
Arlington, VA 22217
Attn: Mr. J. R. Patton
(Copy No. 30)

Office of Naval Research
Fluid Dynamics Branch, Code 438
Department of the Navy
Washington, DC 22217
Attn: Mr. R. D. Cooper
(Copy No. 31)

DISTRIBUTION LIST FOR ARL UNCLASSIFIED TM 80-45 by I-Chung Shen dated 1 April 1980.

General Electric Company
AEG Technical Information Center
Mail Drop N-32, Building 700
Cincinnati, OH 45215
Attn: J. J. Brady
(Copy No. 32)

General Motors Corporation
Detroit Diesel Allison Division
P.O. Box 894
Indianapolis, IN 46206
Attn: Mr. P. C. Tram
(Copy No. 33)

Pratt and Whitney Aircraft
Project Engineer, Advanced
Military System
Engineering Department - 2B
East Hartford, CT 06108
Attn: Mr. Donald S. Rudolph
(Copy No. 34)

United Technologies Research Center
400 Main Street
East Hartford, CT 06108
Attn: Mr. Franklin O. Carta
(Copy No. 35)

Massachusetts Institute of Technology
77 Massachusetts Avenue
Cambridge, MA 02139
Attn: Dr. E. M. Greitzer
(Copy No. 36)

Stevens Institute of Technology
Department of Mechanical Engineering
Castle Point Station
Hoboken, NJ 07030
Attn: Professor F. Sisto
(Copy No. 37)

ONERA
Energie and Propulsion
29 Avenue de la Division Leclure
92 Chatillon sous Bagneux, FRANCE
Attn: Mr J. Fabri
(Copy No. 38)

Virginia Polytechnic Institute and
State University
Mechanical Engineering Department
Blacksburg, VA 24601
Attn: Dr. Walter F. O'Brien, Jr.
(Copy No. 39)

Purdue University
School of Aeronautics and Astronautics
Chaffee Hall
West Lafayette, IN 47907
Attn: Dr. S. N. B. Murthy
(Copy No. 40)

Purdue University
Attn: Dr. S. Fleeter
(Copy No. 41)

University of Salford
Salford, M5 4WT
ENGLAND
Attn: Dr. John H. Horlock
Vice Chancellor
(Copy No. 42)

Netherlands Ship Model Basin
P.O. Box 28
6700 AA Wageningen
THE NETHERLANDS
Attn: Dr. P. van Oossanen
(Copy No. 43)

Mut-Munchen Gmblt
8 Munchen 50
Postfach 50 06 40
GERMANY
Attn: Dr. Hans Mokelke
(Copy No. 44)

Forschungsbeauftrager für Hydroakustik
8012 Ottobrunn B Munchen
Waldparkstr. 41
Munich
GERMANY
Attn: Dr. rer. nat. Horst Merbt
(Copy No. 45)

Admiralty Marine Technology Establishment
Teddington, Middlesex
ENGLAND
Attn: Dr. Allen Moore
(Copy No. 46)

Whittle Turbomachine Laboratory
Madingley Road
Cambridge
ENGLAND
Attn: Dr. D. S. Whitehead
(Copy No. 47)

Whittle Turbomachine Laboratory
Attn: Library
(Copy No. 48)

DISTRIBUTION LIST FOR ARL UNCLASSIFIED TM 80-45 by I-Chung Shen dated 1 April 1980.

Von-Karman Institute for Fluid Dynamics
Turbomachinery Laboratory
Rhode-Saint-Genese
BELGUIM
Attn: Library
(Copy No. 49)

Turbine Research Department
Rolls Royce Ltd.
P.O. Box 31
Derby
ENGLAND
Attn: Dr. D. S. Thompson
(Copy No. 50)

NASA Lewis Research Center
21000 Brookpark Road
Cleveland, OH 44135
Attn: J. Adamczyk
MS 5-9
(Copy No. 51)

NASA Lewis Research Center
Attn: C. Feiler
MS 501-4
(Copy No. 52)

NASA Lewis Research Center
Attn: Dr. M. Goldstein
(Copy No. 53)

NASA Lewis Research Center
Attn: W. M. McNally
MS 5-9
(Copy No. 54)

Cranfield Institute of Technology
School of Mechanical Engineering
Cranfield, Bedford MK430AL
ENGLAND
Attn: Professor R. E. Peacock
(Copy No. 55)

Iowa State University
Mechanical Engineering Department
Ames, IA 50010
Attn: Dr. T. H. Okiishi
(Copy No. 56)

NASA Ames Research Center
Moffett Field, CA 94085
Attn: Dr. S. Bodapati
MA 227-9
(Copy No. 57)

Allis-Chalmers Corporation
Hydro-Turbine Division
Box 712
York PA 17405
Attn: R. K. Fisher
(Copy No. 58)

NSW Institute of Technology
School of Mechanical Engineering
Broadway
Sidney
AUSTRALIA
Attn: Professor J. P. Gostelow
(Copy No. 59)

Naval Post Graduate School
Department of Aeronautics
Monterey, CA 93940
Attn: Dr. M. F. Platzer
(Copy No. 60)

Institute for Turbomachines
Technical University
Templergraben 55
D-5100 Aachen
Federal Republic of Germany
Attn: Dr. H. Gallus
(Copy No. 61)

HSVA Gmblt
Bramfelder Strasse 164
200 Hamburg 60
Postfach 600 929
Federal Republic of Germany
Attn: Dr. E. Weitendorf
(Copy No. 62)

J. M. Voith Gmblt
Hydraulic Department
Postfach 1940
D-7920 Heidenheim
Federal Republic of Germany
Attn: Mr. Eichler
(Copy No. 63)

Notre Dame University
Notre Dame, IN 46554
Attn: Dr. H. Atassi
(Copy No. 64)

Applied Research Laboratory
The Pennsylvania State University
Post Office Box 30
State College, PA 16801
Attn: D. E. Thompson
(Copy No. 65)

DISTRIBUTION LIST FOR ARL UNCLASSIFIED TM 80-45 by I-Chung Shen dated 1 April 1980.

Applied Research Laboratory
Attn: F. S. Archibald
(Copy No. 66)

Applied Research Laboratory
Attn: W. S. Gearhart
(Copy No. 67)


FILM
2-